

**NON-ISOTHERMAL CHARACTERIZATION OF SQUEEZED THIN FILMS IN  
THE PRESENCE OF BIOFLUIDS AND SUSPENDED ULTRAFINE PARTICLES**

DISSERTATION

Presented in Partial Fulfillment of the Requirements for  
the Degree Doctor of Philosophy in the  
Graduate School of the Ohio State University

By

Abdul Rahim A. Khaled, M. S.

\*\*\*\*\*

The Ohio State University

2004

Dissertation Committee:

Professor Kambiz Vafai, Advisor

Professor J. William Rich

Professor Robert H. Essenhight

Approved by

---

Advisor  
Mechanical Engineering Graduate Program

## **ABSTRACT**

Flow and heat transfer inside non-isothermal, incompressible, flat and inclined squeezed thin films are analyzed in this study. Analytical solutions for the flow, temperature distribution and heat transfer under different physical constraints are obtained. For an oscillatory squeezed thin films, the influence of the thermal squeezing parameter, Eckert number, pressure gradient inside the thin film, internal pressure pulsations, the stiffness of the supporting seal, presence of suspended ultrafine particles in the fluid and the motion characteristics of the oscillating boundary of a thin film are determined on the flow and heat transfer process inside thin films.

This study is extended to consider flow inertia, hydromagnetic and buoyancy effects on the flow and heat transfer inside oscillatory squeezed thin films. Also, flow and heat transfer is considered in thin films having the boundary squeezing effects caused by the fluctuation in the applied thermal load. The leakage from thin films and the possibility of fluid slip at the boundaries are investigated on the flow and heat transfer inside squeezed thin films. The present work plays an important role in modeling flow and heat transfer disturbances inside thin film fluidic cells and generates some remedies that can reduce the effects of these disturbances.

**Dictated to my mother, father, sisters and brothers**

## **ACKNOWLEDGMENTS**

First and most, I thank God, the most gracious the most merciful, because nothing can be achieved without his will.

Special thanks are for my Mother and my Father. I do not know how I can compensate them for their support to me until this moment.

Next, I wish to thank my advisor, Professor Kambiz Vafai, for his intellectual support, encouragement, and enthusiasm which made this dissertation possible, and for his patience in correcting both my scientific errors and stylistic.

I wish to thank those who helped me to handle various computer problems especially, Barbara Woodall, John, Andrew and Lorenzo.

Finally, I would like to thank also my friends Khalil, Bader, Ahmad, Mohamad, Wissam, Ali, Magdi, Moustafa, Ashraf, Ihab, Sabri and Amr and many others for their encouragements during my work.

## VITA

April-1969.....	Born- Kuwait City, Kuwait
June-1995.....	B.Sc. in Mechanical Engineering, Kuwait University
Febreuary-1999.....	M.Sc. in Mechanical Engineering, Kuwait University
1996-2000.....	Scientific Assistant, Kuwait University
2000-present.....	Research Associate, the Ohio State University

## PUBLICATIONS

1. Khaled A. –R. A. and Vafai K., Nonisothermal Characterization of Thin Film Oscillating Bearings, Numerical Heat Transfer: A-Appl 41 (5): 451-467, 2002.
2. Khaled A. –R. A. and Vafai K., Non-Isothermal Characterization of Thin Film Oscillating Bearings in The Presence of Ultrafine Particles, Numer Heat Tr A-Appl 42 (6) 549-564, 2002.
3. Khaled A. –R. A. and Vafai K., Flow and Heat Transfer inside Thin Films Supported by Soft Seals in The Presence of Internal and External Pressure Pulsations, Int. J. Heat Mass Transfer 45 (26) 5107-5115, 2002.
4. Khaled A. –R. A. and Vafai K., Flow and Heat Transfer inside Oscillatory Squeezed Thin Films Subject to a Varying Clearance, Int. J. Heat Mass Transfer 46 (4) 631-641, 2003.
5. Khaled A. –R. A. and Vafai K., Heat Transfer and Hydromagnetic Control of Flow Exit Conditions inside Oscillatory Squeezed Thin Films, Numer. Heat Tr A-Appl, 43 (3), 239-258, 2003.

6. Ali A., Vafai K. and Khaled A. –R. A., Comparative Study between Parallel and Counter Flow Configuration between Air and Falling Film Desiccant in The Presence of Nanoparticle Suspensions, *Int. J. of Energy Research*, 27, 725-745, 2003.
7. Khaled A. –R. A., Vafai K., Yang M., Zhang X. and Ozkan C. S., Analysis, Control and Augmentation of Microcantilever Deflections in Bio-Sensing Systems. *Sensors and Actuators B: Chemicals*, 94, 103-115, 2003.
8. Khaled A. –R. A. and Vafai K., Cooling Enhancements Inside Thin Films Supported by Flexible Complex Seals in The Presence of Ultrafine Suspensions, *Journal of Heat Transfer: Transaction of ASME*, 125, 916-925, 2003.
9. Khaled A. –R. A. and Vafai K., The Role of Porous media in Flow and Heat Transfer in Biological Tissues, *International Journal of Heat and Mass Transfer*, 46, 4989-5003, 2003.
10. Khaled A. –R. A. and Vafai K., Heat Transfer and Flow Induced by Both Natural Convection and Vibrations Inside an Open-End Vertical Channels, *Heat and Mass Transfer*, in Press.

## **FIELDS OF STUDY**

Major Field: Mechanical Engineering

## TABLE OF CONTENTS

<b>ABSTRACT</b> .....	ii
<b>ACKNOWLEDGMENT</b> .....	iv
<b>VITA</b> .....	v
<b>TABLE OF CONTENTS</b> .....	vii
<b>LIST OF TABLES</b> .....	xii
<b>LIST OF FIGURES</b> .....	xiii
<b>NOMENCLATURE</b> .....	xvii
<b>CHAPTERS:</b>	<b>Page</b>
<b>1. INTRODUCTION</b> .....	<b>1</b>
1.1 Significance of the Problem.....	1
1.2 Literature Review.....	1
1.3 Scope and the Objective.....	7
1.3.1 Objectives.....	7
<b>2. PROBLEM FORMULATION</b> .....	<b>9</b>
2.1 Problem Definition.....	9
2.2 General Model.....	11
2.3 The Model for Low Reynolds Number.....	13
2.3.1 Effects of Ultrafine Particles Suspensions in the Working Fluid.....	17
2.3.2 Assumptions.....	20
2.4 Large Squeezing Reynolds Numbers.....	20
2.5 Coordinate Transformation.....	22
2.6 Dimensionless Heat Transfer Parameters.....	25
2.7 Mass Transfer.....	27
2.10 applications.....	28

<b>3. ANALYTICAL AND SIMILARITY SOLUTIONS.....</b>	<b>29</b>
3.1 Scale Analysis.....	29
3.2 Small Thermal Squeezing Parameter in the Absence of Viscous Dissipation.....	30
3.3 Small Thermal Squeezing Parameter in the Presence of Viscous Dissipation.....	31
3.4 One Dimensional Steady State with Fixed and Permeable Boundaries.....	32
3.5 Transient Solution of Thin Film with Oscillating Boundaries.....	33
3.5.1 Sinusoidal Squeezing Velocity.....	35
3.6 Hydromagnetic Squeezed Flow and Heat Transfer over a Sensor Surface.....	36
3.6.1 Governing Equations.....	37
3.6.2 Results and Discussions.....	40
3.6.3 Correlations.....	42
<b>4. NUMERICAL METHODS.....</b>	<b>43</b>
4.1 Introduction.....	43
4.2 The Simple Implicit Method.....	43
4.3 The Alternating Direction Implicit Method (ADI).....	44
4.3.1 Finite Differencing in $\xi$ -Sweep.....	46
4.3.2 Finite Differencing in $\eta$ -Sweep.....	47
4.4 Solution to the Stream Function Formulation.....	48
4.5 Validations of Numerical Results.....	49
<b>5. HEAT TRANSFER INSIDE THIN FILMS SUBJECT TO PURE OSCILLATORY SQUEEZING FLOW.....</b>	<b>51</b>
5.1 Effects of Thermal Squeezing Parameter and Dimensionless Motion Amplitudes.....	51
5.2 Effects of Viscous Dissipation and the Presence of Suspended Ultrafine Particles.....	55
5.3 Comments.....	59
<b>6. ANALYSIS OF HEAT TRANSFER CHARACTERISTICS INSIDE OSCILLATORY SQUEEZED THIN FILMS SUBJECT TO A VARYING CLEARANCE .....</b>	<b>61</b>
6.1 Controlling Parameters.....	61
6.2 Effects of the Squeezing and the Thermal Squeezing Numbers.....	62
6.3 Effects of Dimensionless Slope of the Thin Film $\kappa$ .....	64
6.4 Effects of Viscous Dissipation and Thermal Dispersion Effects.....	67

6.5 Effects of Dimensionless Amplitude of the Upper Plate Motion $\beta$ ...	68
6.6 Correlations.....	69
6.7 An Approximate Correlation for the Exit Thermal Boundary Condition.....	72
6.8 Effects of Inlet Axial Velocity Conditions on Nusselt Numbers....	73
6.9 Comments.....	74
<b>7. ANALYSIS OF FLOW AND HEAT TRANSFER INSIDE OSCILLATORY SQUEEZED THIN FILMS WITH LARGE INERTIA EFFECTS.....</b>	<b>76</b>
7.1 Controlling Parameters.....	76
7.2 Effects of the Varying the Squeezing Reynolds Number.....	77
7.3 Effects of Varying the Squeezing Frequency.....	81
7.4 Effects of Varying the Inlet Velocity.....	83
7.5 Effects of Varying the Dimensionless Slope.....	86
7.6 Comments.....	91
<b>8. HYDROMAGNETIC CONTROL OF FLOW AND THERMAL EXIT CONDITIONS INSIDE OSCILLATORY SQUEEZED THIN FILM.....</b>	<b>93</b>
8.1 Mathematical Model for the Magnetic Field Effects.....	93
8.1.1 Effects of the Magnetic Field on the Flow inside Squeezed thin films.....	94
8.1.2 Effects of the Magnetic Field on the Heat Transfer inside Squeezed Thin films.....	96
8.2 Comments.....	99
<b>9. EFFECTS OF INTERNAL PRESSURE PULSATIONS ON FLOW AND HEAT TRANSFER INSIDE OSCILLATORY SQUEEZED FLAT THIN FILMS .....</b>	<b>100</b>
9.1 Problem Formulation.....	100
9.2 Numerical Methods.....	106
9.3 Effects of Pressure Pulsations on the Dimensionless Film Thickness.....	106
9.4 Effects of Pressure Pulsations on Heat Transfer Characteristics of Thin Films.....	109
9.5 Comments.....	113
<b>10. FLOW AND HEAT TRANSFER INDUCED BY NATURAL CONVECTIONS INSIDE AN OSCILLATORY SQUEEZED OPEN-ENDVERTICAL CHAMBER.....</b>	<b>114</b>

10.1 Mathematical Model.....	114
10.2 Analytical Solution for a Special Case.....	116
10.3 Contours of Stream lines and Isotherms.....	118
10.4 Effects of $R_S$ and $Gr$ on Average Nusselt Numbers.....	122
10.5 Effects of $R_S$ and $Gr$ on Flow inside Vertical Chambers.....	122
10.6 Correlations.....	125
<b>11. ANALYSIS OF OSCILLATORY FLOW TURBULENCES AND THERMAL CHARACTERISTICS INSIDE FLUIDIC CELLS DUE TO FLUID LEAKAGE AND WALL SLIP CONDITIONS.....</b>	<b>128</b>
11.1 Analysis.....	129
11.1.1 Fluid Leakage in the Presence of Internal Pressure Pulsations.....	130
11.1.2 Slip Effects and non-Newtonian Effects in the Presence of External Squeezing.....	134
11.1.3 Thermal Boundary Conditions.....	136
11.2 Numerical Methods.....	136
11.3 Discussion of the Results.....	136
11.3.1 Leakage and Slippage Effects on Flow Dynamics inside Thin Films.....	137
11.3.2 Effects of Leakage on Thermal Characteristics of the Thin Film.....	141
11.4 Recommendations.....	142
<b>12. COOLING ENHANCEMENTS IN THIN FILMS SUPPORTED BY FLEXIBLE COMPLEX SEALS IN THE PRESENCE OF ULTRAFINE SUSPENSIONS.....</b>	<b>144</b>
12.1 Analysis.....	145
12.1.1 Thermal Boundary Condition.....	153
12.2 Numerical Procedure.....	153
12.3 Discussions of the Results.....	155
12.3.1 Effects of Dimensionless Coefficient of Thermal Expansion.....	155
12.3.2 Effects of Dimensionless Thermal Dispersion Parameter.....	157
12.3.3 Effects of Thermal Squeezing Parameter and the Squeezing Number.....	160
12.3.4 Effects of the Fixation Parameter and the Amplitude of the Thermal Load.....	162
12.3.5 Effects of Coefficient of Thermal Expansion on Average Pressure.....	163
<b>13. CONCLUSIONS.....</b>	<b>165</b>

<b>REFERENCES.....</b>	<b>168</b>
------------------------	------------

## LIST OF TABLES

<u>Table</u>	<u>Page</u>
3.1 Correlations for Local wall Shear Stress and Local Nusselt Number.....	42
6.1 Correlations for mean Nusselt numbers and Fluctuations in Nusselt numbers.....	71
11.1 Correlations for Nusselt Numbers and their Corresponding Fluctuations...	126

## LIST OF FIGURES

<u>Figure</u>	Page
2.1 Figure 2.1: (a) Schematic Diagram, (b) Coordinate systems and, (c) Boundary conditions.....	10
3.1 Transient Behavior for $\Theta$ .....	36
3.2 Schematic Diagram.....	37
3.3 Effects of $N$ on $f'$ and $\theta$ .....	40
3.4 Effects of $Pr$ on $\theta$ .....	40
3.5 Effects of $f_0$ on $f'$ and $\theta$ .....	41
4.1 (a) Physical Domain, (b) Computational Domain.....	45
4.2 Implicit versus ADI.....	50
4.3 Analytical versus Implicit.....	50
5.1 Effects of $P_S$ on Average $\Theta$ (1).....	52
5.2 Effects of $P_S$ on Average $\Theta$ (2).....	52
5.3 Effects of $\beta$ on Average $\Theta$ (1).....	54
5.4 Effects of $\beta$ on Average $\Theta$ (2).....	54
5.5 Effects of Perturbation Parameter $\varepsilon$ on Average $\Theta$ .....	55
5.6 Effects of $E_S$ on $Q_R$ .....	56
5.7 Effects of $E_S$ on Average $\Theta$ (1).....	56
5.8 Effects of $E_S$ on Average $\Theta$ (2).....	57
5.9 Effects of $\lambda$ on $Q_R$ .....	57
5.10 Effects of $\lambda$ on Average $\Theta$ (1).....	58
5.11 Effects of $\lambda$ on Average $\Theta$ (2).....	58
5.12 Effects of $\beta$ on Average $\Theta$ ( $E_S$ and $\lambda$ are none zeros).....	59
6.1 Effects of $\sigma$ on Average $\Theta$ .....	63
6.2 Effects of $\sigma$ on Average $\theta_w$ .....	63
6.3 Effects of $\sigma$ on $Nu_L$ (UHF).....	64
6.4 Effects of $P_S$ on $\theta_m$ (UHF).....	64
6.5 Effects of $\kappa$ on $Nu$ (CWT).....	65
6.6 Effects of $\kappa$ on $Nu_L$ (UHF).....	65
6.7 $Nu_L$ Distribution (CWT).....	66

6.8	$Nu_L$ Distribution (UHF).....	66
6.9	Effects of $\kappa$ on $\theta_m$ (CWT).....	67
6.10	Effects of $\kappa$ on $\theta_w$ (UHF).....	67
6.11	Effects of $E_S$ on Average $\Theta$ (CWT).....	68
6.12	Effects of $\lambda$ on $\theta_w$ (UHF).....	68
6.13	Effects of $\beta$ on $Nu_L$ (CWT).....	69
6.14	Effects of $\beta$ on $\theta_w$ (UHF).....	69
6.15	Temperature Development(UHF).....	72
6.16	Validation for Eq. (6.4)(CWT).....	72
6.17	Inlet Flow Conditions versus Nusselt: (a) CWT and (b) UHF.....	74
7.1	Effects of $R_S$ on U: (a) Low $R_S$ and (b) High $R_S$ .....	78
7.2	U for Divergent Film (High $R_S$ ).....	79
7.3	Effects of $R_S$ on Nu (CWT, 1).....	79
7.4	Effects of $R_S$ on Nu (CWT, 2).....	80
7.5	Effects of $R_S$ on $Nu_L$ (UHF).....	80
7.6	Effects of $R_S$ on $\theta_m$ (CWT).....	81
7.7	Effects of $\omega$ on Average $\Theta$ .....	82
7.8	Effects of $\omega$ on Average $\theta_w$ .....	82
7.9	Effects of $\omega$ on $\Delta\Theta$ (CWT).....	83
7.10	Effects of $\gamma$ on $\Delta\theta_w$ (UHF).....	83
7.11	Stream lines: (a) $\tau^*=3\pi/2$ and (b) $\tau^*=11\pi/6$ ( $Pr=3.0, R_S=1.0, \beta=0.3, \varepsilon=0.1, \gamma=3.0, \kappa=0.0, \sigma=9.0$ ).....	84
7.12	Effects of (a) $V_o$ and (b) Inlet Flow Conditions on $\theta_m$ (CWT).....	85
7.13	Isotherms: (a) $\tau^*=3\pi/2$ and (b) $\tau^*=11\pi/6$ ( $Pr=3.0, R_S=1.0, \beta=0.3, \varepsilon=0.1, \gamma=3.0, \kappa=0.0, \sigma=9.0$ , CWT).....	86
7.14	Effects of $\kappa$ on U Profiles.....	87
7.15	Effects of $\kappa$ on V Profiles.....	87
7.16	Effects of $\kappa$ on $\theta_m$ (CWT).....	88
7.17	Effects of $\kappa$ on $\theta_w$ (UHF).....	88
7.18	Isotherms: (a) $\tau^*=3\pi/2$ and (b) $\tau^*=11\pi/6$ ( $Pr=3.0, R_S=1.0, \beta=0.3, \varepsilon=0.1, \gamma=3.0, \kappa=0.0, \sigma=5.14$ , UHF).....	89
7.19	Inertia effects on $Nu_L$ ( $P_S=const.$ , UHF).....	90
8.1	Effects of Ha on U.....	95
8.2	Effects of Ha on V.....	95
8.3	Effects of Ha on U (high $R_S$ ).....	96
8.4	Effects of Ha on $\Omega^*(\xi, 1)$ .....	96
8.5	Effects of Ha on $Nu_L$ (CWT).....	97
8.6	Effects of Ha on $Nu_L$ (UHF).....	97
8.7	Effects of Ha on $\theta$ (CWT).....	98
8.8	Effects of Ha on $\theta_m$ (CWT).....	98
8.9	Effects of Ha on $\theta_w$ (UHF).....	98

9.1	(a) Schematic Diagram for a Thin Film and, (b) Coordinate system.....	102
9.2	Effects of $F_n$ on $H$ .....	107
9.3	Effects of $F_n$ on $V(X,H,\tau)$ .....	107
9.4	Effects of $\gamma_p$ on $V(X,H,\tau)$ .....	108
9.5	Effects of $\sigma$ on $H$ .....	108
9.6	Effects of $\sigma$ on $V(X,H,\tau)$ .....	109
9.7	Effects of $\phi_p$ on $H$ .....	109
9.8	Effects of $F_n$ and $P_S$ on $\theta_m$ .....	110
9.9	Effects of $F_n$ and $P_S$ on $\theta_w$ (UHF).....	110
9.10	Effects of $F_n$ on $Nu_L$ (CWT).....	111
9.11	Effects of $F_n$ on $Nu_L$ (UHF).....	111
9.12	$Nu_L$ versus $\xi$ and $F_n$ (UHF).....	111
9.13	Effects of $\gamma_p$ on Average $\Theta$ .....	111
9.14	Effects of $\gamma_p$ on Average $\theta_w$ .....	112
9.15	Effects of $\gamma_p$ on $\delta\Theta$ and $\delta\theta_w$ .....	112
10.1	Schematic Diagram.....	115
10.2	Validation for Numerical Results.....	118
10.3	Dimensionless Stream Lines.....	119
10.4	Dimensionless Isotherms.....	121
10.5	Effects of $Gr$ on $Nu_{AVG}$ : (a) $R_S=1.0$ and (b) $R_S=10$ .....	123
10.6	Effects of $\frac{Gr}{R_S}$ on $U$ at Different Times.....	124
10.7	Effects of $\frac{Gr}{R_S}$ on $\Omega^*(\xi,0)$ : (a) $R_S=1.0$ and (b) $R_S=10$ .....	125
11.1	Schematic Diagram for a Thin Film Fluidic Cell.....	130
11.2	Effects of $M_L$ on (a) $H$ , and (b) Inlet Pressure Gradient.....	138
11.3	Effects of $F_n$ on $dH/d\tau$ .....	139
11.4	Effects of $\sigma$ on $dH/d\tau$ .....	139
11.5	Effects of $\beta_P/h_o$ on (a) wall slip velocity $U_{slip}$ , and (b) normal velocity $V$ ..	140
11.6	Effects of $n$ on (a) wall slip velocity $U_{slip}$ , and (b) normal velocity $V$ .....	140
11.7	Effects of $M_L$ on Average $\theta_w$ .....	141
11.8	Effects of $F_n$ on Average $\theta_w$ .....	141
11.9	Effects of $\sigma$ on Average $\theta_w$ .....	142
12.1	Schematic diagram for a thin film with flexible complex seal and the corresponding coordinate system: (a) front view, (b) side view, and (c) a three dimensional diagram.....	146
12.2	Effects of the dimensionless thermal expansion paramter $F_T$ on (a) dimensionless thin film thickness $H$ , (b) dimensionless average lower plate temperature $(\theta_w)_{AVG}$ , (c) $dH/d\tau$ , and (d) exit Nusselt number $Nu_L$ ...	156

12.3	Effects of the dimensionless thermal dispersion parameter $\lambda$ on (a) dimensionless average lower plate temperature $(\theta_w)_{AVG}$ , (b) dimensionless thickness $H$ , (c) temperature Profile, and (d) exit Nusselt number $Nu_L$ .....	158
12.4	Effects of the dimensionless dispersion parameter $\lambda$ on the time variation of the dimensionless thin film thickness $dH/d\tau$ .....	160
12.5	Effects of the thermal squeezing parameter $P_s$ and the squeezing number $\sigma$ on (a) dimensionless average lower plate temperature $(\theta_w)_{AVG}$ , (b) dimensionless thin film thickness $H$ , and (c) $dH/d\tau$ .....	161
12.6	Effects of the fixation parameter $F_n$ and the dimensionless thermal load amplitude $\beta_q$ on (a) dimensionless average lower plate temperature $(\theta_w)_{AVG}$ , and (b) dimensionless thin film thickness $H$ .....	163
12.7	Effects of the dimensionless thermal expansion parameter $F_T$ on the average dimensionless pressure inside the thin film $\Pi_{AVG}$ .....	164

## NOMENCLATURE

$B$	thin film length
$C$	concentration
$c_p$	specific heat of the fluid
$D$	width of the thin film
$D_{AB}$	mass diffusivity
$d_s$	effective diameter of the seal
$E$	modulus of elasticity for the seal's material
$F_n, F_T$	Fixation number and dimensionless coefficient of thermal expansion
$H, h$	dimensionless and dimensional thin film thickness
$h_c$	convective heat transfer coefficient
$h_o$	reference thin film thickness
$K^*$	elastic contribution factor for the upper plate
$k$	thermal conductivity of the fluid
$L_S$	squeezing mass transfer paramtes
$M_L$	dimensionless mass leakage parameter
$Nu$	local Nusselt number
$n$	power law index
$Pr$	Prandtl number

$P_S$	thermal squeezing parameter
$p$	fluid pressure
$q$	heat flux at the lower plate (UHF)
$R_L, R_S$	lateral and squeezing Reynolds numbers
$T$	temperature in fluid
$T_1$	fluid inlet temperature
$T_2$	temperature at upper plate or at both lower and upper plates (CWT)
$t$	time
$U, u$	dimensionless and dimensional axial velocities
$V, v$	dimensionless and dimensional normal velocities
$X, x$	dimensionless and dimensional horizontal coordinates
$Y, y$	dimensionless and dimensional vertical coordinates
$Z, z$	dimensionless and dimensional lateral coordinates

### **Greek Symbols**

$\Omega, \Omega^*$	vorticity and dimensionless vorticity
$\Psi, \Psi^*$	stream function and dimensionless stream function
$\beta, \beta_0$	dimensionless squeezing motion amplitude and coefficient of thermal expansion
$\beta_p$	dimensionless internal pressure pulsation or thermal load amplitudes
$\beta_s, \beta_T$	wall slip coefficient and coefficient of thermal expansion
$\varepsilon$	perturbation parameter
$\gamma, \gamma_p$	dimensionless squeezing motion and pressure pulsation frequencies
$\eta$	variable transformation for Y-coordinate

$\kappa$	dimensionless slope of the upper plate
$\mu$	dynamic viscosity of the fluid
$\theta$	dimensionless temperature in flow field
$\rho$	density of the fluid
$\sigma$	squeezing number
$\tau, \tau^*$	dimensionless time
$\nu$	kinematic viscosity
$\omega$	reciprocal of a reference time (reference squeezing frequency)
$\xi$	variable transformation for the dimensionless x-coordinate
$\Pi$	dimensionless pressure
$\Pi_i, \Pi_o$	dimensionless inlet pressure and dimensionless mean pressure
$\Lambda$	reference lateral to normal velocity ratio
$\chi$	dimensionless concentration

### **Subscripts**

L	lower plate
m	average value for velocity and mean bulk value for temperature
U	upper plate
W	lower plate for temperature (UHF)

## **CHAPTER 1**

### **INTRODUCTION**

#### **1.1 Significance of the Problem**

The study of flow and heat transfer inside thin films has received a lot of attention in recent years because they are widely used in engineering applications such as in lubrication, heat pipes used in cooling of electronic components, microchannels and in recent biological sensors. In certain applications, external disturbances such as unbalances in rotating machines and increased noise levels from the surroundings can result in an oscillatory motion at the boundary. Even small oscillating motion can have a substantial impact as the thickness of thin films is very small. Accordingly, the dynamics and thermal characterization of thin films will be altered. As a result, the present study establishes how both thermal and dynamical characteristics of flat or inclined thin films are affected by external or internal disturbances in the presence of various effects such as viscous dissipation, the presence of ultrafine suspensions, hydromagnetic and other effects. Also, the flow and thermal characteristics will be analyzed in the presence of non-Newtonian effects as in highly viscous oils and blood at low shear rates.

#### **1.2 Literature Review**

Thin films are widely used in lubrication. When these thicknesses are filled with fluid, they are said to have fluid-film lubrication. Lubrication usually occurs when the

plates of a bearing starts to move. Accordingly, the fluid will move by its viscous effect. At the same time, the fluid will be compressed due to the load on the bearing. The movement of the fluid creates a self-pumping effect as well as prevents contact between the plates of the bearing. This kind of lubrications is called hydrodynamic lubrication (Sezri, 1980). Hydrodynamic lubrication can be found in hydrodynamic journal and thrust bearings. It also can be used in high load capacity applications as discussed by Gross et al. (1980).

Self-lubrication in fluid films, like hydrodynamic lubrication, can also be generated by reciprocating or oscillating motions of at least one of the plates of the bearing. These motions in certain intervals will have squeezing effects on the fluid. These will result in pressurizing the fluid due to its viscosity. Accordingly, the fluid will support the load. In the interval when the load is being removed and the plates of the bearing move apart, the fluid will be sucked in and will recover its thickness for the next application. These phenomena are repeated as oscillating motions of the bearing plates continue with no requirement for any external pumping.

Thin films are also used in cooling of electronic devices. These devices use thin films in their cooling systems as in flat heat pipes (Moon et. al., 2000) or microchannel heat sink (Fedorov, 2000). External noise from a transformer, fan and others tends to vibrate the boundaries of the thin films. The resulting squeezing motion will affect the thermal characteristics of these components.

Another important application for thin films is related to chambers for chemical and biological detection systems such as fluidic cells for chemical or biological microcantilever probes (Lavrik et. al., 2001). Microcantilever probes are based on

measuring the deflection of the microcantilever tip resulting from the reaction of the target molecules with one side of the microcantilever which has a special receptor coating. The integration of different microcantilever probes in one fluidic cell can form a biochip which can be used for detection of hundreds of DNA mismatches or proteins. This will result in better screening for diseases such as cancer. A special design for the fluidic cell of the biochip is needed in order to transport the target proteins to the probes with minimum effects of flow or thermal disturbances as discussed later.

Fluidic cells can have large length to thickness ratios. Accordingly, external or internal noises may produce relatively large squeezing motions at the boundaries of the fluidic cells. In addition to the dynamical effects due to squeezing which can alter the deflection measurements, the thermal behavior inside the cell as a result of squeezing will also increase the bimaterial effects of the microcantilever. These bimaterial effects are due to the fact that the used microcantilever is composed of two layers having different thermal expansion coefficient: silicon substrate and gold coating. Further, the bimaterial effect is the second major problem after the effect of flow disturbances in microcantilever probes (Fritz et. al., 2001).

Biofluids such as blood contain different molecules. These molecules could be proteins, lipids, minerals, vitamins and others. These suspensions will increase the effective thermal conductivity of the fluid as will be discussed later. They also increase the apparent viscosity of the biofluid as shown in the works of Eckmann et. al. (2000) and Saundres and Patel (1998), respectively. Further, biofluids behave like non-Newtonian fluid only at small shear rates because red-blood-cell deformability is negligible at small shear rates. As the deformation in red-blood-cell increases, the blood will behave like

Newtonian fluid having constant viscosity. This fact is demonstrated for the human blood and blood of turtles in the works of Eckmann et. al. (2000) and Saundres and Patel (1998), respectively.

Heat transfer can be enhanced inside thin films by several methods (Huang and Vafai; 1993 and 1994, Lee and Vafai; 1999). Among these methods is the introduction of suspended ultrafine particles in the working fluid. This causes an enhancement in the effective thermal conductivity of the fluid as seen in the works of Xuan and Li (2000) and Eastman et. al. (2001). This is because ultrafine particles tend to increase the exposed heat transfer surface area. Further, the presence of ultrafine particles in fluids increases the mixing within the fluid which causes an additional increase in the fluid's thermal conductivity due to thermal dispersion effects as discussed by Xuan and Li (2000).

The relation between the geometry of the surfaces of a thin film, the properties of the fluid and the pressure inside the thin film was first derived by Reynolds (1886). Although, he did not include the compressibility effects of the fluid, his derived differential equation was the basic foundation for the fluid film lubrication theory.

There are several studies that have analyzed flow in squeezed thin films like Langlois (1962) who solved the momentum equations analytically for hydrodynamic pressure in isothermal squeeze films with fluid density varying according to the pressure. He considered in his analytical work the possibility of having sinusoidal squeezing at one of the boundaries. His work can be used to describe the effects of external vibrations on the hydrodynamic pressure inside thin films.

Later studies consider the effects of boundary squeezing on the temperature distribution inside the thin film like Hamza (1992) and Bhattacharyya et. al. (1996).

Although they considered thermal aspects in their analysis, their works were very restricted. For example, Hamza (1992) considered a specific squeezing velocity in order to have similarity solutions, also considered a one dimensional temperature field. Bhattacharyya et. al. (1996) considered a constant squeezing velocity at one boundary as well as they assumed that the temperature field is one dimensional. Moreover, both works were concerned with flow between two parallel disks and this simplified their flow formulations as the reduced transformed momentum equations ended to be one-dimensional.

Further studies considered two dimensional effects in non-isothermal squeezed thin films like Radakovic and Khonsari (1997) who studied the influence of heat transfer on the dynamic behavior of a thin film bearing when the fluid viscosity varies with temperature. Wang et. al. (2001) performed a thermodynamic analysis on journal bearings lubricated with fluids having couple stresses. However, these studies did not consider the heat transfer aspects of the squeezed thin films. Further, Radakovic and Khonsari (1997) and others such as Tashtoush et. al. (2001) ignored in their analysis transient terms associated with flow accelerations and fluid thermal capacitance. Those terms are important in our analysis especially at large squeezing frequencies or large thermal capacitance.

Recently, Khaled and Vafai (2002) considered heat transfer in incompressible squeezed thin films with sinusoidal squeezing but they did not include effects of viscous dissipation or the possibility of presence of ultrafine particles in the fluid. It is clear that external disturbances such as vibrations will change the dynamic and thermal behavior of the fluid inside thin films. Accordingly, they may be considered to be important in

designing the cooling systems in lubrications and electronic cooling. Heat transfer aspects are also important in biosensors because it determines the optimum location of the probe from the inlet of the fluidic cell to avoid measuring alterations by the bimaterial effects. In this work, the effect of these disturbances will be analyzed to determine whether they can produce significant effects on the dynamic and thermal characteristics inside thin films.

In the literature, there are many studies that consider hydromagnetic effects on the flow and heat transfer inside channels such as Chamkha (2001) yet few of them considered the hydromagnetic effects inside squeezed thin films as that by Bhattacharyya et. al. (1997). As such, hydromagnetic effects on both flow and heat transfer are discussed in this study. Another effect that will be considered is the effect of wall slip conditions. In certain situations, the fluid may slip at the boundary of a surface when the size of the fluidic cell is relatively small (Shiping and Ameen, 2001). Also, wall slip occurs when the fluid contains suspensions (Soltani and Yilmazer, 1998) or when the flow is over a hydrophobic surface (Tretheway et. al., 2002). In these cases, the slip velocity is assumed to be proportional to the local shear stress at the surface (Navier, 1823).

Natural convection inside vertical channels can represent a good candidate for fluidic chambers, and has received increased attention in the past decade (Dyko et. al.; 1999, Dyko and Vafai; 2002). Conjugate conductive and porous medium effects are considered as in the works of Morrone (2001) and Paul et. al. (1999), respectively. Further, the presence of internal sources, mass species and variable properties effects have been taken into account in various works concerning natural convection inside

cavities and vertical channels as in the work of Barozzi and Corticelli (2000), Kuan-Tzon (1999) and the work of Zamora and Hernandez (1997), respectively. In addition, turbulent, thermal radiation and two phase flow effects have been encountered recently in the study of natural convection inside vertical channels as in the works of Bessaih and Kadja (2000), Hall et. al. (1999) and Dalal et. al. (1999), respectively.

There are only few works that have dealt with laminar heat transfer and flow induced by natural convection inside vibrating geometries. As an example, Fu and Shieh (1993) studied the effects of the buoyancy and vertical vibrations at the four walls of a square closed cavity. Further, Kwak (1998) discussed the effects of having vibrations on the temperature of one plate of a closed cavity on the natural convection inside the cavity. Although natural convection inside different geometries have been investigated for many effects as shown before, the literature lacks investigations that relate the behavior of vertical channels in a vibrated media with both horizontal and vertical vibrations.

### **1.3 Scope and Objectives**

The purpose of the present work is to study the effects of pressure squeezing boundary conditions on the flow and heat transfer inside laminar flat or inclined thin films filled with Newtonian or non-Newtonian fluids.

#### **1.3.1 Objectives**

- 1- Derive analytical solutions for velocity and temperature fields as well as heat transfer characteristics for certain limiting cases.
- 2- Develop a two dimensional model for laminar flat or inclined squeezed thin films with small Reynolds numbers.
- 3- Study for the previous model the effects of

- Thermal squeezing parameter, squeezing amplitudes and the perturbation parameter on heat transfer inside oscillating thin films.
  - Viscous dissipation and squeezing amplitudes on heat transfer inside oscillating thin films.
  - Pressure gradient in the thin film and squeezing amplitudes on heat transfer inside oscillating thin films.
  - Presence of suspended ultrafine particles on heat transfer inside oscillating thin films.
- 4- Develop a two-dimensional model for laminar squeezed thin films with large Reynolds numbers including hydromagnetic effects.
  - 5- Develop a two dimensional model for squeezed thin films supported by soft seals that accounts for the presence of internal pressure pulsations.
  - 6- Develop a model for thin films that have flows induced by both boundary squeezing and natural convection effects.
  - 7- Developing a two-dimensional model that accounts for non-Newtonian fluids.
  - 8- Develop analytical solutions that involve slip applications inside disturbed thin films.
  - 9- Develop a model for squeezed thin films having a complex flexible sealing. That is, the clearance of the thin film depends on both pressure and temperature.

## CHAPTER 2

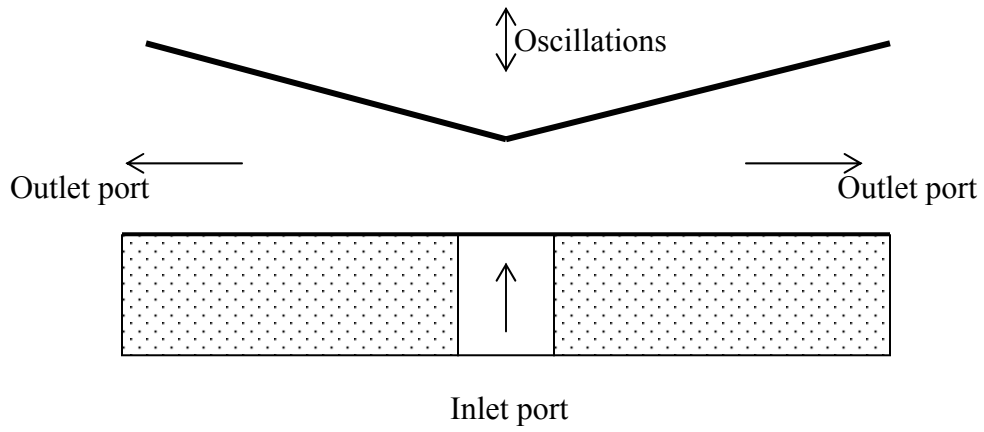
### PROBLEM FORMULATION

#### 2.1 Problem Definition

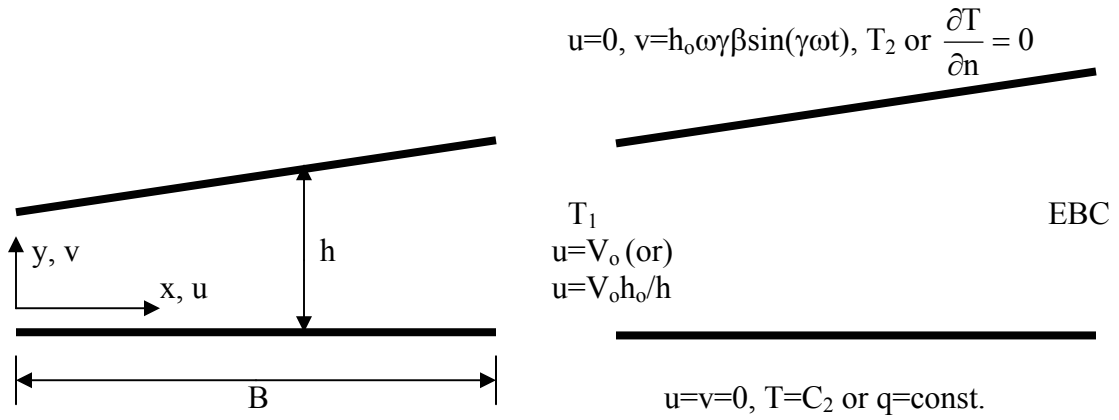
Consider a two dimensional symmetrical thin film, Figure 2.1(a), that has a small thickness  $h$  compared to its length  $B$ . The  $x$ -axis is taken in the direction of the length of the thin film while  $y$ -axis is taken along its thickness as shown in Figure 2.1(b). The lower plate of the thin film is fixed while the vertical motion of the upper plate can have the following generic sinusoidal behavior under uniform external oscillating conditions:

$$h = h_0 \left( 1 - \beta \cos(\gamma \omega t) + \kappa \frac{x}{B} \right) \quad (2.1)$$

where  $\kappa$ ,  $\beta$  and  $\omega$  are the dimensionless slope of the thin film, upper plate motion amplitude and a reference frequency, respectively. The quantity  $\gamma$  is the dimensionless frequency. It is assumed at this stage that the fluid is Newtonian and having constant properties except for the thermal conductivity.



(a)



(b)

(c)

Figure 2.1: (a) Schematic Diagram, (b) Coordinate systems and, (c) Boundary conditions

## 2.2 General Model

The general two-dimensional continuity, momentum and energy equations for the laminar thin film are given as

$$\frac{\partial u}{\partial x} + \frac{\partial v}{\partial y} = 0 \quad (2.2)$$

$$\rho \left( \frac{\partial u}{\partial t} + u \frac{\partial u}{\partial x} + v \frac{\partial u}{\partial y} \right) = -\frac{\partial p}{\partial x} + \mu \left( \frac{\partial^2 u}{\partial x^2} + \frac{\partial^2 u}{\partial y^2} \right) \quad (2.3)$$

$$\rho \left( \frac{\partial v}{\partial t} + u \frac{\partial v}{\partial x} + v \frac{\partial v}{\partial y} \right) = -\frac{\partial p}{\partial y} + \mu \left( \frac{\partial^2 v}{\partial x^2} + \frac{\partial^2 v}{\partial y^2} \right) \quad (2.4)$$

$$\begin{aligned} \rho c_p \left( \frac{\partial T}{\partial t} + u \frac{\partial T}{\partial x} + v \frac{\partial T}{\partial y} \right) &= \frac{\partial}{\partial x} \left( k \frac{\partial T}{\partial x} \right) + \frac{\partial}{\partial y} \left( k \frac{\partial T}{\partial y} \right) \\ &+ \mu \left( \left( \frac{\partial u}{\partial y} \right)^2 + 2 \left( \left( \frac{\partial u}{\partial x} \right)^2 + \left( \frac{\partial v}{\partial y} \right)^2 \right) \right) \end{aligned} \quad (2.5)$$

where  $T$ ,  $\rho$ ,  $p$ ,  $\mu$ ,  $c_p$  and  $k$  are the fluid temperature, density, pressure, dynamic viscosity, specific heat and the thermal conductivity of the fluid, respectively.

A generalized set of initial and boundary conditions for this problem are, some of them are listed on Figure 2.1(c):

$$\begin{aligned} u(x,0,t) = 0, \quad u(x,h,t) = 0, \quad v(x,0,t) = 0, \quad v(x,h,t) = h_0 \omega \gamma \beta \sin(\gamma \omega t) \\ \frac{\partial p(0,y,t)}{\partial x} = C_1, \quad p(B,y,t) = p_e \\ T(x,0,t) = C_2 \\ T(x,h,t) = T_2, \quad T(0,y,t) = T_1, \quad \frac{\partial T(B,y,t)}{\partial x} = 0, \quad T(x,y,0) = T_1 \end{aligned} \quad (2.6(a))$$

where  $p_i$ ,  $p_e$ ,  $T_1$  and  $T_2$  are application specified constants.  $C_2$  is taken to be either  $T_1$  or  $T_2$  for more generic conditions. If the value of  $C_1$  is set to zero, there will be no flow

entering the thin film at  $x=0$ . These cases will be studied in chapters 5 and 10. On the other hand, negative values of  $C_1$  insure that flow is always entering the thin film. The constant  $C_1$  can be function of time and will be determined later based on the assumption that either the average velocity at the inlet or the inlet flow rate is constant. The condition of constant inlet flow rate can be satisfied in applications where the fluid is pumped to the thin film using mechanical pumps while constant inlet average velocity can find its applications in thin films driven by gravitational effects such as in the fluidic cells used by Raiteri et. al. (2000) when the existing valve is automatically controlled. Constant average inlet velocity condition is preferable over constant inlet flow rate condition in fluidic cells to keep uniform detection since the reaction on the sensor surface is related to the rolling velocity (Pritchard et. al., 1995) rather than the inlet flow rate. Other values of  $C_1$  will be considered in chapters 10, 13 and 14.

Another set of thermal boundary conditions that assumes the boundaries of the thin film are subject to uniform heat flux conditions are

$$T(x, y, 0) = T_1, \quad T(0, y, t) = T_1, \quad -k \frac{\partial T(x, 0, t)}{\partial y} = q, \quad \frac{\partial T(x, h, t)}{\partial S_n} = 0 \quad 2.6(b)$$

$$\frac{\partial T(B, y, t)}{\partial x} = \frac{q}{\rho c_p u_m(B, t) h(B, t)} - \frac{1}{u_m(B, t)} \frac{\partial T(B, y/h, t)}{\partial t}$$

where  $q$ ,  $u_m$  and  $S_n$  are a constant represents the heat flux applied at the lower plate, the mean axial velocity at the exit and the direction normal to the plate, respectively. It is assumed that the upper plate is insulated as in thin films used in biological sensing applications since the upper plate is usually made from glass, to allow laser beams to pass to probes inside the thin film, subjected from outside to a non-convective medium. In order to obtain the exit thermal boundary condition shown in conditions 2.6(b), integral

energy balance is utilized at the exit noticing that the axial mean bulk temperature gradient as well as time change of average temperature at the exit are approximated as equal to axial temperature gradients and time change of temperatures there for flat thin films, respectively. Also, it is assumed that convection at the exit is the main mechanism of heat transfer.

### 2.3 The Model for Low Reynolds Numbers

Equations (2.2)-(2.5) are non-dimensionalized using the following dimensionless variables:

$$X = \frac{x}{B}, \quad Y = \frac{y}{h_o} \quad 2.7(a, b)$$

$$\tau = \omega t \quad 2.7(c)$$

$$U = \frac{u}{(\omega B + V_o)}, \quad V = \frac{v}{h_o \omega} \quad 2.7(d, e)$$

$$\Pi = \frac{p}{\mu \left( \omega + \frac{V_o}{B} \right) \epsilon^{-2}} \quad 2.7(f)$$

$$\theta = \frac{T - T_1}{\Delta T} \quad 2.7(g)$$

where  $T_1$  and  $V_o$  are the temperature at the inlet of the thin film and a constant representing a reference inlet velocity, respectively.  $\Delta T$  is equal to  $T_2 - T_1$  for constant wall temperature conditions (CWT) and it is equal to  $\frac{qh_o}{k}$  for uniform wall heat flux conditions (UHF). The variables  $X$ ,  $Y$ ,  $\tau$ ,  $U$ ,  $V$ ,  $\Pi$  and  $\theta$  are the dimensionless forms of  $x$ ,  $y$ ,  $t$ ,  $u$ ,  $v$ ,  $p$  and  $T$  variables, respectively. The above transformations except for

dimensionless temperature have been used by Langlois (1962) along with the following perturbation parameter:

$$\varepsilon = \frac{h_o}{B} \quad (2.8)$$

where that  $h_o$  is a reference thin film thickness.

Substituting the variables (2.7) through (2.8) in equations (2.1) through (2.4) and then, eliminating the terms that contain  $\varepsilon$  raised to the power greater than one leads to the following set of non-dimensionalized governing equations

$$\frac{\partial U}{\partial X} + \frac{\sigma}{12} \frac{\partial V}{\partial Y} = 0 \quad (2.9)$$

$$\frac{\partial \Pi}{\partial X} = \frac{\partial^2 U}{\partial Y^2} - R_s \frac{\partial U}{\partial \tau} - (R_s + R_L) \left[ U \frac{\partial U}{\partial X} \right] - R_s V \frac{\partial U}{\partial Y} \quad (2.10)$$

$$\frac{\partial \Pi}{\partial Y} = 0 \quad (2.11)$$

where  $R_s$  and  $R_L$  are squeezing and lateral modified Reynolds numbers, respectively.

They are given as:

$$R_s = \frac{\rho h_o^2 \omega}{\mu}, \quad R_L = \frac{\rho V_o h_o}{\mu} \left( \frac{h_o}{B} \right) \quad 2.12(a, b)$$

Both  $R_s$  and  $R_L$  are very small (much less than 1) for most of the applications of thin films. The dimensionless  $h$  value is

$$H = \frac{h}{h_o} \quad (2.13)$$

The corresponding dimensionless boundary conditions for flat thin films with constant wall temperature conditions (CWT) will be

$$\begin{aligned}
U(X,0,\tau) = 0, \quad U(X,H,\tau) = 0 \\
V(X,0,\tau) = 0, \quad V(X,H,\tau) = \gamma\beta \sin(\gamma\tau) \\
\frac{\partial \Pi(0,Y,\tau)}{\partial X} = C_1^*, \quad \Pi(B,Y,\tau) = \Pi_e \\
\theta(X,0,\tau) = C_2^* \\
\theta(X,H,\tau) = 1, \quad \theta(0,Y,\tau) = 0, \quad \frac{\partial \theta(1.0,Y,\tau)}{\partial X} = 0, \quad \theta(X,Y,0) = 0
\end{aligned} \tag{2.14(a)}$$

The values of  $C_2^*$  will be taken to be either 0 or 1. It is clear that this value is selected to be 1 in inclined thin films to satisfy the exit thermal boundary condition. In the subsequent chapters, new exit thermal boundary will be proposed for cases where the above one can not be satisfied as in highly convective applications. Moreover, these dimensionless thermal boundary conditions for thin films with uniform wall heat flux conditions (UHF) will be

$$\begin{aligned}
\frac{\partial \theta(X,0,\tau)}{\partial Y} = -1, \quad \frac{\partial \theta(X,H,\tau)}{\partial S_n} = 0 \\
\theta(X,Y,0) = 0, \quad \theta(0,Y,\tau) = 0 \\
\frac{\partial \theta(1,Y,\tau)}{\partial X} \cong \frac{\sigma}{12U_m} \left( \frac{1}{P_s H} - \frac{\partial \theta(1,Y/H,\tau)}{\partial \tau} \right)
\end{aligned} \tag{2.14(b)}$$

where  $\sigma$  will be called the squeezing number and it is equal to

$$\sigma = \frac{12}{1 + (V_o/\omega B)} \tag{2.15}$$

Errors associated with the exit thermal boundary condition are proportional to the ratio of axial conductions to axial convections which is of order of  $(\sigma \varepsilon^2)/(12P_s U)$ . Accordingly, cases where convections are high and/or where axial conductions are low as for cases having lower values of  $\varepsilon$  are found to be less affected by the assumptions that are used to

set up this boundary condition. These assumptions are: (1)  $\frac{\partial \theta_m(1, \tau)}{\partial X} \approx \frac{\partial \theta(1, Y, \tau)}{\partial X}$  and (2)

$\frac{\partial \theta_{AVG}(1, \tau)}{\partial \tau} \approx \frac{\partial \theta(1, Y/H, \tau)}{\partial \tau}$  where they are satisfied for thin films having relatively low

flow rates. In cases where the last parameter is low or having negative values when back flows are present, singularity will be introduced at the exit boundary condition when back flows are present. Thus, another exit thermal boundary condition will be proposed in the subsequent chapters.

Solving equations (2.10) and (2.11) for low Reynolds numbers results in

$$U = \frac{1}{2} \frac{\partial \Pi}{\partial X} (Y)(Y - H) \quad (2.16)$$

If Equation (2.16) is substituted in Equation (2.9), the result will be the Reynolds equation, derived by Reynolds (1886)

$$\frac{\partial}{\partial X} \left( H^3 \frac{\partial \Pi}{\partial X} \right) = \sigma \frac{\partial H}{\partial \tau} \quad (2.17)$$

Equation (2.16) reduces to the following after solving Equation (2.17):

$$U(X, Y, \tau) = \frac{1}{2} \left[ \frac{\sigma \beta \gamma \sin(\gamma \tau) X}{H} + \frac{C_1^*}{H} \right] \left( \frac{Y}{H} \right) \left( \frac{Y}{H} - 1 \right) \quad 2.18(a)$$

The corresponding normal velocities will be

$$V(X, Y, \tau) = \beta \gamma \sin(\gamma \tau) \left[ -2 \left( 1 - \frac{3\kappa X}{H} \right) \left( \frac{Y}{H} \right)^3 + 3 \left( 1 - \frac{2\kappa X}{H} \right) \left( \frac{Y}{H} \right)^2 \right] \\ + \frac{6C_1^* \kappa}{\sigma H} \left[ \left( \frac{Y}{H} \right)^3 - \left( \frac{Y}{H} \right)^2 \right] \quad 2.19(a)$$

The constant  $C_1^*$  can be obtained by equating the flow rate at the inlet calculated by integrating equation (2.16) to that the average velocity at the inlet which is assumed to be

constant, reference axial velocity  $V_o$ , multiplied by inlet film thickness.  $C_1^*$  is found to equal to  $-(12 - \sigma)H(0, \tau)$ . Accordingly, Equations 2.18(a) and 2.19(a) are reduced to the following:

$$U(X, Y, \tau) = \frac{1}{2H} [\sigma\beta\gamma X \sin(\gamma\tau) - (12 - \sigma)H(0, \tau)] \left(\frac{Y}{H}\right) \left(\frac{Y}{H} - 1\right) \quad 2.18(b)$$

$$V(X, Y, \tau) = \beta\gamma \sin(\gamma\tau) \left[ 3 \left(1 - \frac{2\kappa X}{H}\right) \left(\frac{Y}{H}\right)^2 - 2 \left(1 - \frac{3\kappa X}{H}\right) \left(\frac{Y}{H}\right)^3 \right] - 6 \left(\frac{12}{\sigma} - 1\right) \frac{\kappa H(0, \tau)}{H} \left[ \left(\frac{Y}{H}\right)^3 - \left(\frac{Y}{H}\right)^2 \right] \quad 2.19(b)$$

In the case where the inlet flow rate is kept constant when the flow inside thin films is driven by variable head pumps, Equations 2.18(b) and 2.19(b) reduces to the following:

$$U(X, Y, \tau) = \frac{1}{2H} [\sigma\beta\gamma X \sin(\gamma\tau) - (12 - \sigma)] \left(\frac{Y}{H}\right) \left(\frac{Y}{H} - 1\right) \quad 2.18(c)$$

$$V(X, Y, \tau) = \beta\gamma \sin(\gamma\tau) \left[ 3 \left(1 - \frac{2\kappa X}{H}\right) \left(\frac{Y}{H}\right)^2 - 2 \left(1 - \frac{3\kappa X}{H}\right) \left(\frac{Y}{H}\right)^3 \right] - 6 \left(\frac{12}{\sigma} - 1\right) \frac{\kappa}{H} \left[ \left(\frac{Y}{H}\right)^3 - \left(\frac{Y}{H}\right)^2 \right] \quad 2.19(c)$$

### 2.3.1 Effects of Ultrafine Particles Suspensions in the Working Fluid:

The thermal conductivity of the fluid is considered to be variable since the existence of ultrafine particles in the working fluids in certain applications is expected to enhance the heat transfer to these fluids. These enhancements can be shown with metallic ultrafine particles in the works of Eastman et. al. (2001) and Xuan and Li (2000). Further, the work of Adams et. al. (1999) shows that heat transfer enhancements also occur in the presence of dissolved air molecules in fluids. These ultrafine particles at large velocities

tend to increase the thermal conductivity due to thermal dispersion effects (Xuan and Roetzel (2000)).

The following is a model suggested by Xuan and Roetzel (2000) in order to account for enhancements in the thermal conductivity due to the presence of suspended ultrafine particles.

$$k_{nf} = k_{eff} + k_d \quad (2.20)$$

where  $k_{nf}$ ,  $k_{eff}$ ,  $k_d$  are the resulting thermal conductivity of the nanofluid (a term used to describe the continuum mixture composed of the fluid and the suspended ultrafine particles), effective flow thermal conductivity of the nanofluid at stagnant conditions and the thermal conductivity due dispersion effects. The effective thermal conductivity of the nanofluid at stagnant conditions needs to be determined experimentally and may be approximated using correlations derived for relatively large suspensions. The following represents an example of these correlations determined by Wasp (1977)

$$\frac{k_{eff}}{k_f} = \frac{k_p + 2k_f - 2\phi(k_f - k_p)}{k_p + 2k_f + \phi(k_f - k_p)} \quad (2.21)$$

where  $k_p$ ,  $k_f$  and  $\phi$  are the thermal conductivity of the solid particles, the thermal conductivity of the pure fluid and the volume fraction of the solid particles, respectively.

The thermal conductivity due to dispersion effects inside pipes is suggested by Xuan and Roetzel (2000) to be linearly proportional to the fluid speed.

$$k_d = C^* (\rho c_p)_{nf} Ru \quad (2.22)$$

where  $R$  and  $u$  are the radius of the pipe and the speed of fluid, respectively.

It is worth noting that the other fluid-ultrafine mixture properties vary with the ultrafine particles volume fraction and their corresponding relationships are found in the works of Xuan and Roetzel (2000). Therefore, the fluid properties appearing in Equations (2.2-2.5) will be for the mixture properties when ultrafine suspensions are included. The previous model is utilized in the present work and the corresponding thermal conductivity of the fluid with suspended ultrafine particles is calculated from

$$k(X, Y, \tau) = k_o \left( 1 + \lambda \sqrt{U^2(X, Y, \tau) + \Lambda^2 V^2(X, Y, \tau)} \right) = k_o \phi(X, Y, \tau) \quad (2.23)$$

where  $\lambda$  and  $\Lambda$  are the dimensionless thermal dispersion coefficient and dimensionless reference squeezing to lateral velocity ratio. They are

$$\lambda = C^* (\rho c_p)_{nf} h_o (V_o + \omega B) \quad \Lambda = \frac{\varepsilon \sigma}{12} \quad 2.24(a, b)$$

where  $C^*$  is constant depends on the diameter of the ultrafine particles, its volume fraction and both fluid and the ultrafine particles properties.  $k_o$  is a reference thermal conductivity of the working fluid that contains ultra fine particles. This reference thermal conductivity is usually greater than the thermal conductivity of the pure fluid (Eastman (2001)).

Equation (2.5) is reduced to the following when dimensionless variables (2.7) and (2.8) are used

$$\begin{aligned} P_s \left( \frac{\partial \theta}{\partial \tau} + \frac{12}{\sigma} U \frac{\partial \theta}{\partial X} + V \frac{\partial \theta}{\partial Y} \right) = \varepsilon^2 \frac{\partial}{\partial X} \left( \phi \frac{\partial \theta}{\partial X} \right) + \frac{\partial}{\partial Y} \left( \phi \frac{\partial \theta}{\partial Y} \right) \\ + E_s \left[ \left( \frac{\partial U}{\partial Y} \right)^2 + 2 \left[ \varepsilon^2 \left( \frac{\partial U}{\partial X} \right)^2 + \Lambda^2 \left( \frac{\partial V}{\partial Y} \right)^2 \right] \right] \end{aligned} \quad (2.25)$$

where  $P_S$  is a new parameter that contains the fluid properties as well as the oscillating characteristics of the thin film. It is therefore named thermal squeezing parameter.  $E_S$  is the Eckert number. They are

$$P_S = R_S Pr \quad E_S = \frac{\mu(V_o + \omega B)^2}{k_o \Delta T} \quad 2.26(a, b)$$

where  $Pr = \frac{\rho c_p \nu}{k_o}$  and it is the Prandtl number of the fluid.

### 2.3.2 Assumptions:

The following assumptions were utilized in the previous derivations:

- 1- The variation of the pressure across the film is small and negligible.
- 2- The rate of change of the U component of the velocity along the film is small when compared to the rate of change of this same velocity component across the film. Therefore, it can be neglected.
- 3- The flow of the fluid in the film is predominantly two-dimensional.
- 4- Flow Reynolds numbers are small.
- 5- In the energy equation, the term  $\varepsilon^2$  is not eliminated because axial conduction near inlet is not small.

### 2.4 Large Squeezing Reynolds Numbers

It is convenient to solve the vorticity equation and stream function formulations for cases with large squeezing Reynolds numbers. These equations are listed below in dimensional form:

$$\frac{\partial \Omega}{\partial t} + u \frac{\partial \Omega}{\partial x} + v \frac{\partial \Omega}{\partial y} = \nu \left( \frac{\partial^2 \Omega}{\partial x^2} + \frac{\partial^2 \Omega}{\partial y^2} \right) \quad (2.27)$$

$$\frac{\partial^2 \Psi}{\partial x^2} + \frac{\partial^2 \Psi}{\partial y^2} = -\Omega \quad (2.28)$$

where  $\Omega$  and  $\Psi$  are the dimensional vorticity and stream functions, respectively. The vorticity and stream functions are related the velocity components through the following:

$$\Omega = \frac{\partial v}{\partial x} - \frac{\partial u}{\partial y} \quad (2.29)$$

$$u = \frac{\partial \Psi}{\partial y} \quad v = -\frac{\partial \Psi}{\partial x} \quad 2.30 \text{ (a, b)}$$

The following set of dimensionless variables is suggested

$$X = \frac{x}{B}, \quad Y = \frac{y}{h_0} \quad 2.31 \text{ (a, b)}$$

$$\tau = \omega t \quad 2.31 \text{ (c)}$$

$$\Omega^* = \frac{\Omega}{(V_0 + \omega B)/h_0}, \quad \Psi^* = \frac{\Psi}{h_0(V_0 + \omega B)} \quad 2.31 \text{ (d, e)}$$

$$\theta = \frac{T - T_1}{\Delta T} \quad 2.31 \text{ (f)}$$

where  $\Omega^*$  and  $\Psi^*$  are the corresponding dimensionless values of  $\Omega$  and  $\Psi$ , respectively. The introduction of variable 2.31(e) in equations 2.30(a, b) results in the following dimensionless velocity components:

$$U = \frac{u}{V_0 + \omega B}, \quad V = \frac{v}{\varepsilon(V_0 + \omega B)} \quad 2.32 \text{ (a, b)}$$

The dimensionless vorticity-stream function formulations for the flow inside the thin film and the dimensionless energy equation are

$$\left( \frac{\partial \Omega^*}{\partial \tau} + \left( 1 + \frac{R_L}{R_s} \right) \left( \frac{\partial \Psi^*}{\partial Y} \frac{\partial \Omega^*}{\partial X} - \frac{\partial \Psi^*}{\partial X} \frac{\partial \Omega^*}{\partial Y} \right) \right) = \frac{1}{R_s} \left( \varepsilon^2 \frac{\partial^2 \Omega^*}{\partial X^2} + \frac{\partial^2 \Omega^*}{\partial Y^2} \right) \quad (2.33)$$

$$\left( \varepsilon^2 \frac{\partial^2 \Psi^*}{\partial X^2} + \frac{\partial^2 \Psi^*}{\partial Y^2} \right) = -\Omega^* \quad (2.34)$$

$$\begin{aligned} P_s \left( \frac{\partial \theta}{\partial \tau} + \left( 1 + \frac{R_L}{R_s} \right) \left( \frac{\partial \Psi^*}{\partial Y} \frac{\partial \theta}{\partial X} - \frac{\partial \Psi^*}{\partial X} \frac{\partial \theta}{\partial Y} \right) \right) &= \varepsilon^2 \frac{\partial}{\partial X} \left( \phi \frac{\partial \theta}{\partial X} \right) + \frac{\partial}{\partial Y} \left( \phi \frac{\partial \theta}{\partial Y} \right) \\ &+ E_s \left[ \left( \frac{\partial^2 \Psi}{\partial Y^2} \right)^2 + 4\varepsilon^2 \left[ \left( \frac{\partial^2 \Psi}{\partial Y \partial X} \right)^2 \right] \right] \end{aligned} \quad (2.35)$$

The dimensionless boundary conditions for flat thin film that will be implemented are

$$\begin{aligned} \Psi^*(0, Y, \tau) &= \left( 1 - \frac{\sigma}{12} \right) C_3 Y, \quad \frac{\partial^2 \Psi^*(1, Y, \tau)}{\partial X^2} = 0 \\ \Psi^*(X, 0, \tau) &= 0, \quad \Psi^*(X, H, \tau) = \left( 1 - \frac{\sigma}{12} \right) C_4 - \left( \frac{\sigma}{12} \right) X \beta \gamma \sin(\gamma \tau) \\ U(0, Y, \tau) &= 1 - \frac{\sigma}{12}, \quad U(X, 0, \tau) = 0, \quad U(X, H, \tau) = 0 \\ V(X, 0, \tau) &= 0, \quad V(X, H, \tau) = \left( \frac{\sigma}{12} \right) \gamma \beta \sin(\gamma \tau) \end{aligned} \quad (2.36)$$

$$\begin{aligned} \Omega^*(0, Y, \tau) &= -\varepsilon^2 \frac{\partial^2 \Psi^*(0, Y, \tau)}{\partial X^2}, \quad \frac{\partial^2 \Omega^*(1, Y, \tau)}{\partial X^2} = 0 \\ \Omega^*(X, 0, \tau) &= -\frac{\partial U(X, 0, \tau)}{\partial Y}, \quad \Omega^*(X, H, \tau) = \varepsilon^2 \frac{\partial V(X, H, \tau)}{\partial X} - \frac{\partial U(X, H, \tau)}{\partial Y} \end{aligned} \quad (2.37)$$

where  $C_3$  and  $C_4$  are equal to one and  $H(0, \tau)$  if inlet average velocity is kept constant (CIV condition) and they are equal to  $1/H(0, \tau)$  and one if inlet flow rate is kept constant (CIF condition). For the last case, inlet flow rate is always kept at the value  $V_0 h_0$ .

## 2.5 Coordinate Transformation:

The following transformations are suggested in order to avoid time and spatial dependent grid points:

$$\tau^* = \tau, \quad \xi = X \quad 2.38(a, b)$$

$$\eta = \frac{Y}{H(X, \tau)} \quad 2.38(c)$$

Accordingly, the transformed dimensionless energy and vorticity equations will have the following forms:

$$\begin{aligned} a \frac{\partial f(\xi, \eta, \tau^*)}{\partial \tau^*} + b \frac{\partial f(\xi, \eta, \tau^*)}{\partial \xi} + c \frac{\partial f(\xi, \eta, \tau^*)}{\partial \eta} = & d \frac{\partial^2 f(\xi, \eta, \tau^*)}{\partial \xi^2} + d_1 \frac{\partial^2 f(\xi, \eta, \tau^*)}{\partial \xi \partial \eta} \\ & + e \frac{\partial^2 f(\xi, \eta, \tau^*)}{\partial \eta^2} + g \end{aligned} \quad (2.39)$$

where a, b, c, d, d<sub>1</sub> and e are

$$a = R_s H^2, \quad b = R_s \left(1 + \frac{R_L}{R_s}\right) U H^2, \quad g = 0 \quad 2.40(a, b, c)$$

$$c = R_s H \left[ \left(1 + \frac{R_L}{R_s}\right) (V - \eta \kappa U) - \eta \beta \gamma \sin(\gamma \tau) \right] - 2\eta \varepsilon^2 \kappa^2 \quad 2.40(d)$$

$$d = (\varepsilon H)^2, \quad d_1 = -2\eta \kappa \varepsilon^2 H, \quad e = 1 + (\varepsilon \eta \kappa)^2 \quad 2.40(e, f, g)$$

when f is set to be the dimensionless vorticity  $\Omega^*$ . When f is taken to be the dimensionless temperature, the constants changes to the following:

$$a = P_s H^2, \quad b = H^2 \left( P_s \left(1 + \frac{R_L}{R_s}\right) U - \varepsilon^2 \frac{\partial \phi}{\partial \xi} \right) \quad 2.41(a, b)$$

$$c = P_s H \left[ \left( V - \eta \kappa U \left(1 + \frac{R_L}{R_s}\right) \right) - \eta \beta \gamma \sin(\gamma \tau) \right] + \varepsilon^2 \eta \kappa H \frac{\partial \phi}{\partial X} - 2\eta \varepsilon^2 \kappa^2 \phi - \frac{\partial \phi}{\partial \eta} \quad 2.41(c)$$

$$d = \phi (\varepsilon H)^2, \quad d_1 = -2\eta \kappa \varepsilon^2 H \phi, \quad e = (1 + (\varepsilon \eta \kappa)^2) \phi \quad 2.41$$

(d, e, f)

$$g = E_s \left[ \left( \frac{\partial U}{\partial \eta} \right)^2 + 2 \left[ \varepsilon^2 H^2 \left( \frac{\partial U}{\partial \xi} \right)^2 + \Lambda^2 \left( \frac{\partial V}{\partial \eta} \right)^2 \right] \right] \quad 2.41(g)$$

where the constant 2.41(c) changes to the following when large squeezing Reynolds numbers are considered

$$c = R_s H \left[ \left( 1 + \frac{R_L}{R_s} \right) (V - \eta \kappa U) - \eta \beta \gamma \sin(\gamma \tau) \right] + \varepsilon^2 \eta \kappa H \frac{\partial \phi}{\partial X} - 2 \eta \varepsilon^2 \kappa^2 \phi - \frac{\partial \phi}{\partial \eta} \quad 2.42$$

The transformed boundary conditions in terms of the squeezing number are

$$\Psi^*(0, \eta, \tau^*) = \left( 1 - \frac{\sigma}{12} \right) C_5 \eta, \quad \frac{\partial^2 \Psi^*(1, \eta, \tau^*)}{\partial \xi^2} \cong 0 \quad 2.43(a, b)$$

$$\Psi^*(\xi, 0, \tau^*) = 0, \quad \Psi^*(\xi, 1, \tau^*) = \left( 1 - \frac{\sigma}{12} \right) C_6 - \left( \frac{\sigma}{12} \right) \xi \beta \gamma \sin(\gamma \tau^*) \quad 2.43(c, d)$$

$$\Omega^*(0, \eta, \tau^*) = -\varepsilon^2 \left( \frac{\partial^2 \Psi^*(0, \eta, \tau^*)}{\partial \xi^2} + \frac{2 \eta \kappa^2}{H^2(0, \tau^*)} \frac{\partial^2 \Psi^*(0, \eta, \tau^*)}{\partial \xi} - \frac{2 \eta \kappa}{H(0, \tau^*)} \frac{\partial^2 \Psi^*(0, \eta, \tau^*)}{\partial \xi \partial \eta} \right) \quad 2.44(a)$$

$$\frac{\partial \Omega^*(1, \eta, \tau^*)}{\partial \xi} \cong \frac{C_4(1 - \beta \cos(\gamma \tau^*) - \kappa) - 2C_3 \kappa}{(C_3 + C_4)(1 - \beta \cos(\gamma \tau^*) + \kappa)} \Omega^*(1, \eta, \tau^*) \quad 2.44(b)$$

$$\Omega^*(\xi, 0, \tau^*) = -\frac{\partial U(\xi, 0, \tau^*)}{H \partial \eta} \quad 2.44(c)$$

$$\Omega^*(\xi, 1, \tau^*) = \frac{\eta \kappa \varepsilon^2}{H} \frac{\partial V(\xi, 1, \tau^*)}{\partial \eta} - \frac{\partial U(\xi, 1, \tau^*)}{H \partial \eta} \quad 2.44(d)$$

where both  $C_5$  and  $C_6$  are equal to  $H(0, \tau)$  for CIV condition and to one for CIF condition.

Boundary conditions 2.43(b) and 2.44(b) are derived from the knowledge that velocity profiles are fully developed at the exit and it is approximated as follows

$$U = \frac{C_7 + C_8 \xi}{H} p(\eta) \quad 2.45$$

where  $p(\eta)$  is an unknown function of  $\eta$ , the parameters  $C_7$  and  $C_8$  are

$$C_7 = \left(1 - \frac{\sigma}{12}\right) C_6 \quad C_8 = -\left(\frac{\sigma}{12}\right) \beta \gamma \sin(\gamma \tau^*) \quad 2.46(a, b)$$

The thermal boundary conditions for plates having constant wall temperatures are

$$\theta(\xi, 0, \tau^*) = 1 \quad \theta(\xi, 1, \tau^*) = 1 \quad 2.47(a, b)$$

$$\theta(0, \eta, \tau^*) = 0 \quad \frac{\partial \theta(1, \eta, \tau^*)}{\partial \xi} = \frac{\kappa \eta}{H} \frac{\partial \theta(1, \eta, \tau^*)}{\partial \eta} \quad 2.47(c, d)$$

The corresponding thermal boundary conditions for uniform heat flux conditions are

$$\frac{\partial \theta(\xi, 0, \tau^*)}{H \partial \eta} = -1 \quad \frac{\partial \theta(\xi, 1, \tau^*)}{\partial \eta} = \frac{\varepsilon^2 \kappa H}{1 + (\varepsilon \kappa)^2} \frac{\partial \theta(\xi, 1, \tau^*)}{\partial \xi} \quad 2.48(a, b)$$

$$\theta(0, \eta, \tau^*) = 0 \quad 2.48(c)$$

$$\frac{\partial \theta(1, \eta, \tau^*)}{\partial \xi} = \frac{\sigma}{12 U_m} \left( \frac{1}{P_s H} - \frac{\partial \theta(1, \eta, \tau^*)}{\partial \tau^*} \right) + \frac{\kappa \eta}{H} \frac{\partial \theta(1, \eta, \tau^*)}{\partial \eta} \quad 2.48(d)$$

## 2.6 Dimensionless Heat Transfer Parameters

From energy balance at the lower or upper surfaces of the thin film

$$\begin{aligned} k \frac{\partial T}{\partial S_n} \Big|_h &= h_c (T_u - T_m) \\ -k \frac{\partial T}{\partial S_n} \Big|_0 &= h_c (T_l - T_m) \end{aligned} \quad (2.49)$$

where  $h_c$ ,  $T_l$ ,  $T_u$  and  $T_m$  are the local convective heat transfer coefficient, lower plate temperature, upper plate temperature and the mean bulk temperature at a given section,

respectively, The Nusselt number ( $Nu = (h_c h_o)/k_o$ ) evaluated at the upper ( $Nu_U$ ) or lower ( $Nu_L$ ) surfaces of a thin film and the total Nusselt number can be calculated from:

$$\begin{aligned} Nu_U(X, \tau) &= \frac{1}{1 - \theta_m(X, \tau)} \frac{k_u}{k_o} \left( \left( \frac{\partial \theta(X, H, \tau)}{\partial Y} \right)^2 + \varepsilon^2 \left( \frac{\partial \theta(X, H, \tau)}{\partial X} \right)^2 \right)^{1/2} \\ Nu_L(X, \tau) &= \frac{-1}{1 - \theta_m(X, \tau)} \frac{\partial \theta(X, 0, \tau)}{\partial Y} \\ Nu(X, \tau) &= Nu_U + Nu_L \end{aligned} \quad (2.50)$$

where  $\theta_m$  is the dimensionless mean bulk temperature. It is defined as follows

$$\begin{aligned} \theta_m(X, \tau) &= \frac{1}{U_m(X, \tau)H} \int_0^H U(X, Y, \tau) \theta(X, Y, \tau) dY \\ U_m(X, \tau) &= \frac{1}{H} \int_0^H U(X, Y, \tau) dY \end{aligned} \quad (2.51)$$

The net local dimensionless heat transferred to the fluid for thin films  $\Theta$  is

$$\Theta(X, \tau) \equiv \frac{q(X, \tau)h_o}{k_o(T_2 - T_1)} \quad 2.52(a)$$

$$\Theta(X, \tau) = \pm \left( \frac{k_u}{k_o} \left( \left( \frac{\partial \theta(X, H, \tau)}{\partial Y} \right)^2 + \varepsilon^2 \left( \frac{\partial \theta(X, H, \tau)}{\partial X} \right)^2 \right)^{1/2} - \frac{\partial \theta(X, 0, \tau)}{\partial Y} \right) \quad 2.52(b)$$

where  $k_u$  is the fluid thermal conductivity at the upper plate.  $k_u$  is usually greater than  $k_o$  if dispersion effects exist when ultrafine particles are suspended in the fluid. The positive sign for equation 2.52(b) is taken when both plates are kept at a similar temperature while the negative sign is used when the upper plate is kept at a temperature higher than that for the lower plate as in chapter 5. When the lower plate is kept under uniform wall heat flux condition as described by condition 2.6(b), the appropriate

dimensionless heat transfer parameter is the local Nusselt number defined at the lower plate which is defined as follows:

$$Nu_L(X, \tau) = \frac{1}{\theta(X, 0, \tau) - \theta_m(X, \tau)} \quad (2.53)$$

## 2.7 Mass Transfer

Disturbances in the concentration of species at the inlet of a thin film propagate to down stream until they diminish far from the inlet because of both mass convections and mass diffusions. The following equation is the dimensional governing equation for the concentration of certain species:

$$\frac{\partial C}{\partial t} + u \frac{\partial C}{\partial x} + v \frac{\partial C}{\partial y} = D_{AB} \left( \frac{\partial^2 C}{\partial x^2} + \frac{\partial^2 C}{\partial y^2} \right) \quad (2.54)$$

where  $C$  and  $D_{AB}$  are the concentration of species and the mass diffusivity constant, respectively. Define  $\chi$  as the dimensionless concentration as follows

$$\chi = \frac{C - C_i}{\Delta C} \quad (2.55)$$

where  $C_i$  and  $\Delta C$  are the reference concentration and a reference differential value, respectively, Equation (2.54) reduces to the following equation after applying dimensionless variables (2.7) and (2.8):

$$L_s \left( \frac{\partial \chi}{\partial \tau} + \frac{12}{\sigma} U \frac{\partial \chi}{\partial X} + V \frac{\partial \chi}{\partial Y} \right) = \varepsilon^2 \frac{\partial^2 \chi}{\partial X^2} + \frac{\partial^2 \chi}{\partial Y^2} \quad (2.56)$$

where  $L_s$  is referred as to the squeezing mass transfer parameter and it is equal to

$$L_s = \frac{h_o^2 \omega}{D} \quad (2.57)$$

According to Equation (2.56), there is an analogy between heat transfer equation, Equation (2.25), and mass transfer equation. Thus the generated results from the heat transfer equation are applicable for the mass transfer within the thin film by replacing  $P_S$  with  $L_S$  and the temperature with the concentration.

## **2.8 Applications**

In chapters 8-12, different applications to the pressure squeezed problem inside thin films are investigated. One of these applications is concerned with hydromagnetic flow and heat transfer inside oscillatory squeezed thin films which will be modeled and discussed in chapter 8. Another study is conducted in chapter 9 is about flow and heat transfer inside thin films supported by soft seals in the presence of internal pressure pulsations. Chapter 10 models and analyzes numerically heat transfer and flow induced by natural convection inside oscillatory squeezed thin films. Non-Newtonian effects and effect of side leakage on flow and heat transfer inside disturbed thin films are considered in chapter 11 while chapter 12 analyzes the squeezing effects that can be caused by variations in the thermal load.

## CHAPTER 3

### ANALYTICAL AND SIMILARITY SOLUTIONS

#### 3.1 Scale Analysis

Consider a two dimensional infinite oscillating thin film where the film thickness  $h$  is much greater than the thermal boundary layer thickness  $\delta_t$ . After the initial squeezing stage, the thermal boundary layer starts to develop during the first stage of the upper plate motion from the midsection of the thin film outward to both left and right sections. For this boundary layer problem and assuming slug flow conditions inside the thin film, the application of the scale analysis for the continuity equation inside the thermal boundary layer reveals that the order of magnitude of the dimensional velocity  $u$  is  $(\bar{v}B)/h$  where  $\bar{v}$  is the wall dimensional squeezing velocity. Note that the order of magnitude of squeezing velocities inside the thermal boundary layer is  $(\bar{v}\delta_t)/h$ . Utilizing this result along with a scale analysis for the energy equation results

$$\rho c_p \left( \frac{\partial T}{\partial t} + u \frac{\partial T}{\partial x} + v \frac{\partial T}{\partial y} \right) = k \left( \frac{\partial^2 T}{\partial y^2} \right) \quad (3.1)$$

This result is obtained by noting that both  $v \frac{\partial T}{\partial y}$  and  $u \frac{\partial T}{\partial x}$  are of order  $\bar{v} \frac{\Delta T}{h}$ . Further, the

term  $\frac{\partial^2 T}{\partial y^2}$  which is of order  $\frac{\Delta T}{\delta_t^2}$  is greater than  $\frac{\partial^2 T}{\partial x^2}$  which is of order  $\frac{\Delta T}{B^2}$ . Accordingly,

Equation (2.25) in chapter 2 reduces to

$$\frac{\partial^2 \theta}{\partial Y^2} = P_s \left[ \frac{\partial \theta}{\partial \tau} + U \frac{\partial \theta}{\partial X} + V \frac{\partial \theta}{\partial Y} \right] \quad (3.2)$$

Note that the above analysis shows that the thermal boundary layer thickness is almost independent on the thin film length B and it is valid when  $\left( \frac{\delta_t}{h} \right)^2 \approx \frac{k}{\rho c_p \bar{v} h} \ll 1$ .

This is applicable for thin films having large squeezing velocities and operating at relatively large thicknesses as well as for situations where the working fluid has a low thermal diffusivity. That is, it is applicable for thin films having large a thermal squeezing parameter.

### 3.2 Small Thermal Squeezing Parameter in the Absence of Viscous Dissipation

For small thermal squeezing parameters and in the absence of thermal dispersion and viscous dissipation, Equation (2.25) in chapter 2 reduces to

$$\varepsilon^2 \frac{\partial^2 \theta}{\partial X^2} + \frac{\partial^2 \theta}{\partial Y^2} = 0 \quad (3.3)$$

This case represents a pure conduction problem. The solution to Equation (3.3) for flat thin film having its lower and upper plate temperatures equal to  $T_1$  and  $T_2$ , respectively, is

$$\theta(\xi, \eta, \tau^*) = \eta + 2 \sum_{n=1}^{\infty} \frac{(-1)^n}{n\pi} \sin(n\pi\eta) \left[ \cosh\left(\frac{n\pi\xi}{\varepsilon H}\right) - \tanh\left(\frac{n\pi}{\varepsilon H}\right) \sinh\left(\frac{n\pi\xi}{\varepsilon H}\right) \right] \quad (3.4)$$

The corresponding average dimensionless heat transfer to the fluid will be

$$\Theta_{\text{AVG}}(\tau^*) = -\frac{4\varepsilon}{\pi} \sum_{n=1,3,5}^{\infty} \frac{1}{n} \left[ \frac{\sinh\left(\frac{n\pi}{\varepsilon H}(1-\xi^*)\right)}{\cosh\left(\frac{n\pi}{\varepsilon H}\right)} \right] \quad (3.5)$$

where  $\Theta_{\text{AVG}}$  is the average dimensionless heat transferred to the fluid from the upper and lower plates of the thin film between  $\xi = \xi^*$  to  $\xi = 1$ .

### 3.3 Small Thermal Squeezing Parameter in the Presence of Viscous Dissipation

For thin films having small thermal squeezing parameters, zero values of  $C_1^*$  and in the presence of viscous dissipation, Equation (2.25) in chapter 2 reduces to

$$\frac{\partial^2 \theta}{\partial \eta^2} + E_s \left( \frac{\partial U}{\partial \eta} \right)^2 = 0 \quad (3.6)$$

The solution to Equation (3.23) for flat thin film having its lower and upper plate temperatures equal to  $T_1$  and  $T_2$ , respectively, is

$$\theta(\xi, \eta, \tau^*) = \eta + \frac{36E_s\beta^2\gamma^2 \sin^2(\gamma\tau^*)\xi^2}{H^2} \left( \frac{1}{3}\eta^4 - \frac{2}{3}\eta^3 + \frac{1}{2}\eta^2 - \frac{1}{6}\eta \right) \quad (3.7)$$

The corresponding dimensionless heat transfer to the fluid will be

$$\Theta(\xi, \tau^*) = 12 \frac{E_s\beta^2\gamma^2 \sin^2(\gamma\tau^*)\xi^2}{H^3} \quad (3.8)$$

If  $Q_R$  is defined as the ratio of heat conduction at the upper plate to heat conduction at the lower plate of the thin film, That is

$$Q_R = \left( k_u \frac{\partial \theta}{\partial \eta} \right) \Big|_{\eta=1} / \left( k_l \frac{\partial \theta}{\partial \eta} \right) \Big|_{\eta=0} \quad (3.9)$$

This will result in the following heat ratio for the present case

$$Q_R = \frac{\left(1 - \beta \cos(\gamma \tau^*)\right)^2 - 6E_s \beta^2 \gamma^2 \xi^2 \sin^2(\gamma \tau^*)}{\left(1 - \beta \cos(\gamma \tau^*)\right)^2 + 6E_s \beta^2 \gamma^2 \xi^2 \sin^2(\gamma \tau^*)} \quad (3.10)$$

### 3.4 One Dimensional Steady State with Fixed and Permeable Boundaries

For the case where the plates of a thin film are fixed, infinite and permeable leading to a constant permeable velocity as follows

$$V(\bar{S}_1) = V(\bar{S}_2) = -a \quad (3.11)$$

Under steady state conditions, energy equation reduces to the following

$$\frac{\partial^2 \theta}{\partial Y^2} + P_s a \frac{\partial \theta}{\partial Y} = 0 \quad (3.12)$$

where  $a$  is a constant. Further, the term  $P_s a$  is equal to  $\frac{h_o w_o}{\alpha}$  where  $w_o$  is the negative of the dimensional permeable vertical velocity at the bearing's plates. Equation (3.12) prescribes a temperature distribution given by

$$\theta(Y) = \frac{e^{-P_s a Y} - 1}{e^{-P_s a} - 1} \quad (3.13)$$

where  $\bar{S}_1$  and  $\bar{S}_2$  are taken to be 0 and 1, respectively. Accordingly, the dimensionless heat parameter will be

$$\Theta = P_s a \quad (3.14)$$

The values of  $\Theta$  are positive when more heat is conducted from the fluid to the lower plate than that conducted from the upper plate to the fluid. This is for the values of  $T_2$  and initial fluid temperatures that are larger than or equal to  $T_1$  and in the absence of any heat source or sink in the fluid. On the other hand, negative  $\Theta$  values mean that the heat conducted to the fluid from the upper plate is more than the heat transferred from the fluid to the lower plate under the same previous conditions.

### 3.5 Transient Solution of Thin Films with Oscillating Boundaries

Energy equation, Equation (2.25) in chapter 2 can be approximated by the following equation at dimensionless  $X$  values that result in either  $U = 0$  or  $\frac{\partial \theta}{\partial X} = 0$ , at the exit of thin films or at the center section for infinite thin films.

$$\frac{\partial^2 \theta}{\partial Y^2} = P_s \left[ \frac{\partial \theta}{\partial \tau} + \frac{Y}{H} \frac{dH}{d\tau} \frac{\partial \theta}{\partial Y} \right] \quad (3.15)$$

where  $\frac{Y}{H} \frac{dH}{d\tau}$  is used to approximate the fluid normal velocity  $V$  at the given sections.

In the presence of ultrafine particles suspensions inside the working fluid, fluid average thermal conductivity can be expressed by the following equation, see Equation (2.23) in chapter 2.

$$k(\tau) = k_o \left( 1 + \lambda |\bar{V}(\tau)| \right) \quad (3.16)$$

where  $\bar{V}$  is the average of fluid dimensionless normal velocity. Accordingly, Equation (3.15) changes to

$$\left( 1 + \lambda |\bar{V}(\tau)| \right) \frac{\partial^2 \theta}{\partial Y^2} = P_s \left[ \frac{\partial \theta}{\partial \tau} + V \frac{\partial \theta}{\partial Y} \right] \quad (3.17)$$

Equation (3.17) reduces, for large squeezing velocities, to

$$\frac{\partial^2 \theta}{\partial Y^2} = \frac{P_s}{\lambda} \left[ \frac{1}{|\bar{V}(\tau)|} \frac{\partial \theta}{\partial \tau} \pm 2 \frac{Y}{H} \frac{\partial \theta}{\partial Y} \right] \quad (3.18)$$

The positive sign is when the thin film is in its relief stage while the negative is when it is in the squeezing stage. Transferring the domain into  $\xi, \eta, \tau^*$  domain, defined in the last chapter, results in

$$\frac{\partial^2 \theta}{\partial \eta^2} = 2 \frac{P_s}{\lambda} \frac{H^2}{\left| \frac{dH}{d\tau} \right|} \frac{\partial \theta}{\partial \tau^*} \quad (3.19)$$

The solution to the above equation based on the following initial thermal condition  $\theta(0, \eta, 0) = 0$  is

$$\theta(\eta, \tau^*) = 2 \left[ \sum_{n=1}^{\infty} \frac{(-1)^n}{n\pi} \sin(n\pi\eta) e^{\frac{\pm n^2 \pi^2 \lambda}{2P_s} \left[ \frac{1}{H} - \frac{1}{H_0} \right]} \right] + \eta \quad (3.20)$$

where the positive sign is when the thin film is in its relief stage while the negative is when it is in the squeezing stage. Accordingly, the values of  $\Theta$  can be approximated using the first term of the series

$$\Theta(\tau) = -\frac{4}{H(\tau^*)} e^{\frac{\pm \pi^2 \lambda}{2P_s} \left[ \frac{1}{H(\tau^*)} - \frac{1}{H_0} \right]} \quad (3.21)$$

The previous solution is valid only in the first stage of the upper plate motion because  $V(\tau^*)$  and the second term on the right side of equation (3.18) change their sign in the second stage resulting in a new partial differential equation. In order to solve this new equation, the initial fluid temperature can be replaced by the final temperature from the

previous stage and the result of solving the new equation will have similar terms as in Equations (3.20) and (3.21) with different coefficients.

### 3.5.1 Sinusoidal Squeezing Velocity

Assuming the upper plate is moving only in z-direction according to  $\bar{S}_2 = H(\tau)$  where

$$H(\tau) = 1 - \beta \cos(\gamma\tau) \quad (3.22)$$

The dimensionless heat transfer parameter obtained from equation (3.21) can be written as

$$\Theta(\tau) = -4 \frac{e^{\frac{\pi^2 \beta \lambda}{2P_s} \left( \frac{\cos(\gamma\tau) - 1}{(1-\beta)(1-\beta \cos(\gamma\tau))} \right)}}{1 - \beta \cos(\gamma\tau)} \quad (3.23)$$

This is valid for  $0 < \gamma\tau < \pi$ . Since it will results in  $V > 0$ . The negative values of  $\Theta$  indicate that heat conduction at the upper plate is larger than that at the lower plate.

Figure 3.1 represents the behavior of the proposed oscillating thin film described by Equation (3.19) under conditions where the fluid encounters dispersion effects. The results of solving Equation (3.18), considering the exact normal velocity profile for the values of  $\Theta$  shown in Figure 3.1, It is noticed that both the approximate analytical and numerical solution are in excellent agreement. Further, it is noticed that the dimensionless heat transfer parameter is always negative and decreasing asymptotically to zero. This can be noticed from Equation (3.23).

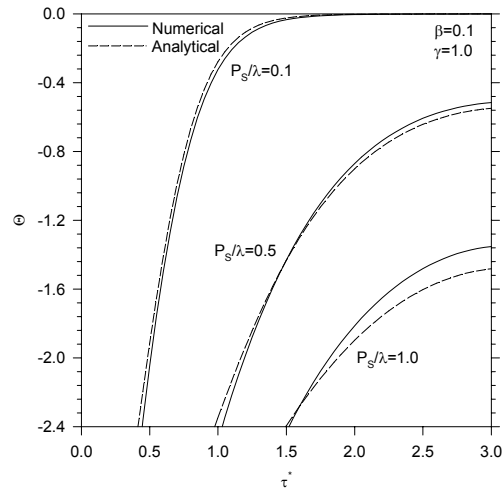


Figure 3.1: Transient Behavior for  $\Theta$

### 3.6 Hydromagnetic Squeezed Flow and Heat Transfer over a Sensor Surface

Consider flow over a horizontal surface. The surface is assumed to have a length  $L$ . The  $x$ -axis is taken along the length of the surface starting from its free end while the  $y$ -axis is taken normal to the upper surface as shown in Figure 3.2. The surface is enclosed inside a squeezed channel such that the height  $h(t)$  is much greater than the boundary layer thickness and the squeezing in the free stream is assumed to start from the tip of the surface as illustrated in Figure 3.2. This problem can find its application in flow over microcantilever sensor caused by an external squeezing at the boundaries of the fluidic cell.

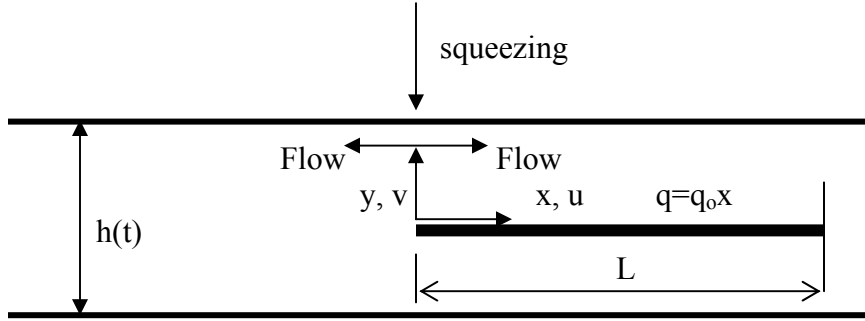


Figure 3.2: Schematic Diagram

### 3.6.1 Governing Equations

The working fluid is taken as Newtonian and electrically conducting with  $\sigma_m$  as its electrical conductance. It is assumed that a magnetic field of strength  $B_m$  is applied normal to the flow in the  $y$ -direction and that the induced magnetic Reynolds number is negligible. The continuity, momentum and energy governing equations are

$$\frac{\partial u}{\partial x} + \frac{\partial v}{\partial y} = 0 \quad (3.24)$$

$$\frac{\partial u}{\partial t} + u \frac{\partial u}{\partial x} + v \frac{\partial u}{\partial y} = -\frac{1}{\rho} \frac{\partial p}{\partial x} + \nu \frac{\partial^2 u}{\partial y^2} - \frac{\sigma_m B_m^2}{\rho} u \quad (3.25)$$

$$\frac{\partial U}{\partial t} + U \frac{\partial U}{\partial x} = -\frac{1}{\rho} \frac{\partial p}{\partial x} - \frac{\sigma_m B_m^2}{\rho} U \quad (3.26)$$

$$\frac{\partial T}{\partial t} + u \frac{\partial T}{\partial x} + v \frac{\partial T}{\partial y} = \alpha \frac{\partial^2 T}{\partial y^2} \quad (3.27)$$

where  $u$ ,  $v$ ,  $U$ ,  $T$ ,  $t$  and  $\alpha$  are the axial component of the velocity, normal component of the velocity, axial free stream velocity, temperature, time and thermal diffusivity of the working fluid, respectively. Equations (3.25) and (3.27) are applicable within the

boundary layer while Equation (3.26) governs the outer stream flow which is assumed to be uniform with respect to the normal coordinate. Equation (3.25) is transferred to the following after eliminating the pressure gradient using Equation (3.26):

$$\frac{\partial u}{\partial t} + u \frac{\partial u}{\partial x} + v \frac{\partial u}{\partial y} = \frac{\partial U}{\partial t} + U \frac{\partial U}{\partial x} + v \frac{\partial^2 u}{\partial y^2} + \frac{\sigma_m B_m^2}{\rho} (U - u) \quad (3.28)$$

A generalized set of boundary conditions are imposed

$$u(x, 0, t) = 0 \quad v(x, 0, t) = v_o(t) \quad u(x, \infty, t) = U(x, t) \quad 3.29(a, b, c)$$

$$-k \frac{\partial T(x, 0, t)}{\partial y} = q(x) \quad T(x, \infty, t) = T_\infty \quad 3.29(c, d)$$

where  $T_\infty$ ,  $U(x, t)$  and  $q(x)$  are the free stream temperature, free stream velocity and the wall heat flux, respectively. It is assumed that wall heat flux is a prescribed function of the axial distance  $x$ . The reference velocity  $v_o$  represents the velocity at the sensor surface for permeable surfaces. This velocity is proportional to the normal velocity at the disturbed boundary and it increases as the size of the surface pores increases or when the surface is placed close to the disturbed boundary. Equations (3.27) and (3.28) can be transformed as similarity equations when the following variables and conditions are implemented

$$U = ax \quad \eta = y \sqrt{\frac{a}{\nu}} \quad a = \frac{1}{s + bt} \quad 3.30(a, b, c)$$

$$f(\eta) = \frac{\psi}{\sqrt{a\nu x}} \quad \theta(\eta) = \frac{T - T_\infty}{\frac{q_o}{k} \sqrt{\frac{\nu}{a} x}} \quad q(x) = q_o x \quad 3.30(d, e, f)$$

$$B_m = B_{mo} \sqrt{a} \quad v_o = v_i \sqrt{a} \quad 3.30(g, h)$$

where  $b$  and  $s$  are arbitrary constants. The parameters  $q_0$  and  $k$  are the reference wall heat flux and the thermal conductivity of the fluid, respectively. Conditions 3.30(a) and 3.30(c) reveal that the height belong to a certain time dependence relation:  $h(t)=h_0/(s+bt)^{(1/b)}$  for  $b>0$  and  $h(t)=h_0e^{-st}$  for  $b=0$  where  $h_0$  is a constant. The parameters  $B_{m0}$  and  $v_i$  are a reference magnetic field and a reference suction velocity, respectively.

The result of the transformation is the following similar equations:

$$f''' + \left(f + \frac{b\eta}{2}\right)f'' - (f' - b + N)f' + (1 - b + N) = 0 \quad (3.31)$$

$$\frac{1}{Pr}\theta'' + \left(f + \frac{b\eta}{2}\right)\theta' - \left(f' + \frac{b}{2}\right)\theta = 0 \quad (3.32)$$

where  $Pr$  is the Prandtl number ( $Pr=\nu/\alpha$ ). The prime is the derivative with respect to  $\eta$ .

The corresponding transformed boundary conditions are

$$f'(0) = 0 \quad f(0) = -f_0 \quad f'(\infty) = 1 \quad 3.33(a, b, c)$$

$$\theta(0) = -1 \quad \theta(\infty) = 0 \quad 3.33(d, e)$$

The parameters  $N$  and  $K$  are dimensionless parameters defined as

$$N = \frac{\sigma_m B_{m0}^2}{\rho} \quad f_0 = \frac{v_i}{\sqrt{\nu}} \quad 3.34(a, b)$$

The parameters:  $N$  and  $f_0$  represent the dimensionless magnetic and permeable velocity parameters, respectively. These parameters are functions of time. In the absence of magnetic field and wall permeable conditions, Equations (3.31) and (3.32) become self similar equations. The dimensionless local wall shear stress  $\tau^*$  and the local Nusselt number  $Nu$  can be calculated from the following:

$$\tau^* = \frac{\tau_w}{\mu a \text{Re}^{1/2}} = f''(0) \quad \text{Re} = \frac{ax^2}{\nu} \quad \text{Nu} = \frac{h_c x}{k} = \frac{x}{\theta(0)} \sqrt{\frac{a}{\nu}} \quad 3.35(a, b, c)$$

where  $\mu$ ,  $\tau_w$  and  $h_c$  are the dynamic viscosity of the fluid, wall shear stress and convective heat transfer coefficient, respectively.

### 3.6.2 Results and Discussions

Figure 3.3 shows the effect of the dimensionless magnetic parameter  $N$  on both velocity and temperature profiles over a horizontal surface inside squeezed free stream. It is noticed that the flow boundary layer thickness decreases as  $N$  increases causing the flow to be more attached to the horizontal surface. This causes an increase in the convective heat transfer coefficient. Thus, the surface temperature decreases as  $N$  increases which can be seen from Figure 3.3.

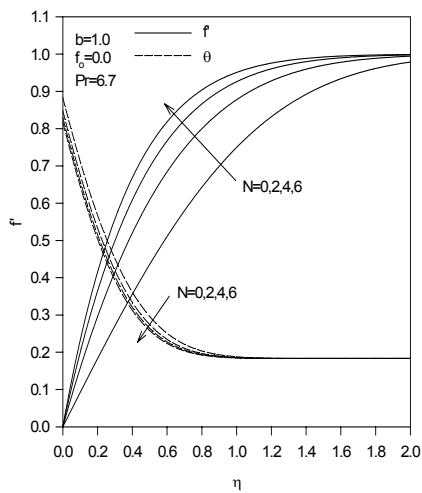


Figure 3.3: Effects of  $N$  on  $f'$  and  $\theta$

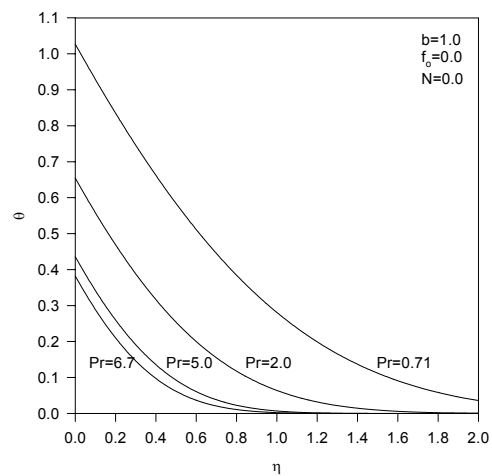


Figure 3.4: Effects of  $Pr$  on  $\theta$

Based on heat and mass transfer analogy with respect to chemical and biological applications, it is expected that the difference between analyte concentration at the microcantilever and the free stream concentration will decrease as  $N$  increases. Thus not only magnetic field can reduce flow instabilities inside thin film fluidic cells but it also increases mass transfer to the surface of the microcantilever. On the other hand, the increase in the velocity of the analyte molecules near the sensor due to magnetic may decrease the binding rate at the sensor surface (Pritchard et. al., 1995) since they will be in contact with the sensor surface for less time. Finally, cooling enhancements for the microantilever become prominent as the  $Pr$  increases as shown in Figure 3.4.

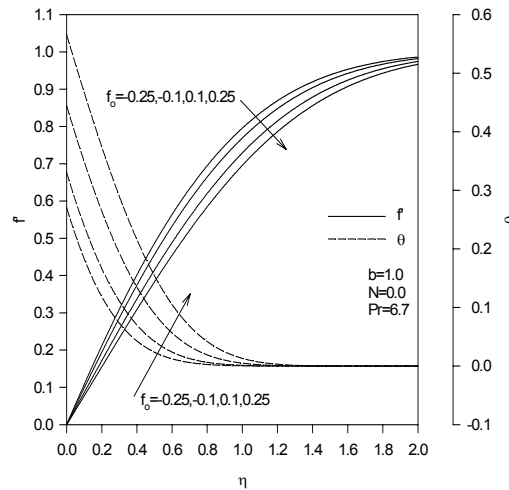


Figure 3.5. Effects of  $f_0$  on  $f'$  and  $\theta$

Figure 3.5 illustrates the effects of the wall dimensionless permeable velocity  $f_0$  on both  $f'$  and  $\theta$ . Suction conditions at the surface for negative  $f_0$  values causes the flow to be more attached to the surface when compared with blowing conditions as shown in

Figure 3.5 Thus, surface cooling is enhanced under suction conditions as shown in Figure 3.5 By heat and mass transfer analogy, it is expected that analyte concentration approaches free stream analyte concentration for suction conditions causing an enhancement in the sensor signal. It is worth noting that suction conditions is achieved if the active surface of the sensor is opposing the disturbed boundary

### 3.6.3 Correlations

The correlations shown in Table (1) relate the local wall shear stress and the local Nusselt number to the controlling parameters:  $b$ ,  $N$ ,  $K$  and  $Pr$ . it can be seen from these correlations that an increase in “ $b$ ” cause reductions in both the local wall shear stress and the local Nusselt number.

Correlation	Range and Maximum error
$\tau_w = 0.4565e^{-0.00717N} (1.0026 + 0.4684b - 0.0322b^2) \mu a Re^{1/2}$ $Nu = 1.174e^{0.00749N} \frac{Pr^{0.4566}}{b^{0.1919}} \left( \frac{x}{\sqrt{u(t+s/b)}} \right)$	$0.5 < b < 3.0, f_0 = 0, 1 < N < 10,$ Maximum error < 11%
$\tau_w = 1.1973e^{(-0.7f_0 - 0.176b - 0.103b^2)} \mu a Re^{1/2}$ $Nu = 1.102e^{1.105f_0} Pr^{0.456} (0.689 + 0.294b) \left( \frac{x}{\sqrt{u(s+bt)}} \right)$	$0.5 < b < 2.0, -0.2 < f_0 < 0.2,$ $N = 0,$ Maximum error < 12%

Table 3.1: Correlations for Local wall Shear Stress and Local Nusselt Number

## CHAPTER 4

### NUMERICAL METHODS

#### 4.1 Introduction

The energy and vorticity-stream function equations derived in chapter two represent non-linear partial differential equations that need to be solved numerically subject to boundary conditions in  $\xi$  and  $\eta$  directions and initial conditions with respect to  $\tau^*$ . No closed-form solution for the governing equations appears to be possible because of the presence of convective terms as well as the inertia terms. Also, approximate solutions are also difficult to be obtained because of the presence of the transient terms. Due to all of the above, the governing equations will be solved by both simple implicit finite-difference numerical method and using Alternating Direction Implicit ADI finite-difference methods. Successive over relaxation method will be used to solve for stream function formulation.

#### 4.2 The Simple Implicit Method

For flat thin film, the energy equation in the last chapter has the following form:

$$a \frac{\partial \theta}{\partial \tau^*} + b \frac{\partial \theta}{\partial \xi} + c \frac{\partial \theta}{\partial \eta} = d \frac{\partial^2 \theta}{\partial \xi^2} + e \frac{\partial^2 \theta}{\partial \eta^2} + f \quad (4.1)$$

By applying three points central differencing with respect to  $\xi$  and  $\eta$  for the first and second derivatives with respect to  $\xi$  and  $\eta$  and two points backward in time will result in the following difference equation:

$$\begin{aligned} & \left( \frac{b_{i,j}^{n+1}}{\Delta\xi} - \frac{d_{i,j}^{n+1}}{\Delta\xi^2} \right) \theta_{i+1,j}^{n+1} - \left( \frac{b_{i,j}^{n+1}}{\Delta\xi} + \frac{d_{i,j}^{n+1}}{\Delta\xi^2} \right) \theta_{i-1,j}^{n+1} + \left( \frac{c_{i,j}^{n+1}}{\Delta\eta} - \frac{e_{i,j}^{n+1}}{\Delta\eta^2} \right) \theta_{i,j+1}^{n+1} \\ & - \left( \frac{c_{i,j}^{n+1}}{\Delta\eta} + \frac{e_{i,j}^{n+1}}{\Delta\eta^2} \right) \theta_{i,j-1}^{n+1} + \left( \frac{a_{i,j}^{n+1}}{\Delta\tau^*} - \frac{2d_{i,j}^{n+1}}{\Delta\xi^2} - \frac{2e_{i,j}^{n+1}}{\Delta\eta^2} \right) \theta_{i,j}^{n+1} = \frac{a_{i,j}^{n+1}}{\Delta\tau^*} \theta_{i,j}^n + f_{i,j}^{n+1} \end{aligned} \quad (4.2)$$

where  $i, j$  is a specified point along  $\xi$  and  $\eta$  directions respectively. All dimensionless temperatures and their coefficients are evaluated at time step  $n+1$  except for one presenting in the first derivative with respect to time. The system presented by Equation (4.1) is unconditionally stable for any values of  $\Delta\xi$ ,  $\Delta\eta$  and  $\Delta\tau^*$  where they are the step size along the  $\xi$ -direction,  $\eta$ -direction and the time step size, respectively. The resulting errors are of order  $(\Delta\xi^2, \Delta\eta^2, \Delta\tau^*)$ . The only disadvantage is that the CPU time increases rapidly as the mesh becomes finer. To overcome this disadvantage, the Alternating Direction Implicit ADI technique is suggested.

### 4.3 The Alternating Direction Implicit Method (ADI)

In applying the ADI method for inclined thin films, the energy equation is transformed from its physical domain  $X, Y$  and  $\tau$  into the computational domain  $\xi, \eta, \tau^*$  as shown in Figure 4.1. The resulting equation has the following form:

$$aa \frac{\partial\Phi}{\partial\tau^*} + bb \frac{\partial\Phi}{\partial\xi} + cc \frac{\partial\Phi}{\partial\eta} = dd \frac{\partial^2\Phi}{\partial\xi^2} + dd_1 \frac{\partial^2\Phi}{\partial\xi\partial\eta} + ee \frac{\partial^2\Phi}{\partial\eta^2} + f \quad (4.3)$$

where  $\Phi$  can be the dimensionless temperature  $\theta$  or the dimensionless vorticity  $\Omega^*$ . Equation (4.3) is nonlinear because the coefficients are functions of the dependent

variables like  $U$  and  $V$ . To overcome this non-linearity, the coefficients are evaluated initially at the previous half time step. Further, the time step is taken to be relatively small in order to reduce errors associated with the latter approximation.

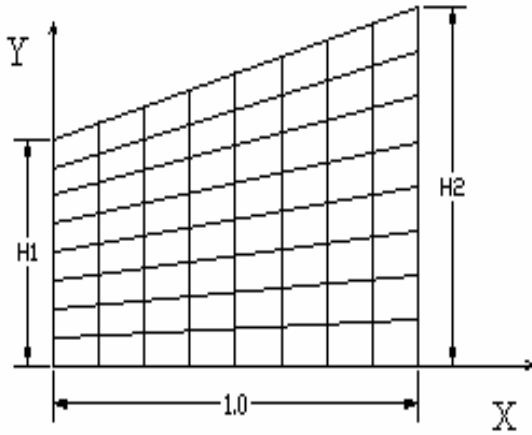


Figure 4.1(a): Physical Domain

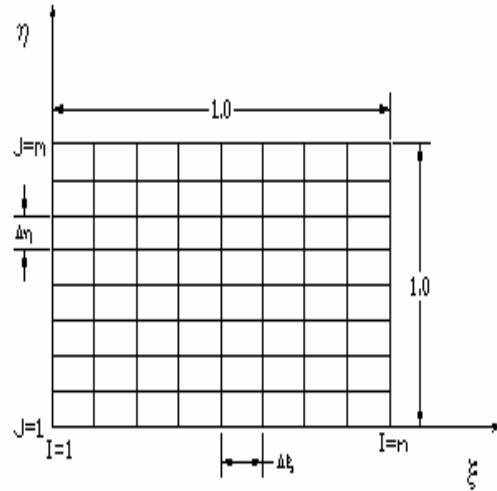


Figure 4.1(b): Computational Domain

The process of ADI technique assumes that each time step  $\Delta\tau^*$  is divided into two equal halves. For the first half, Equation (4.3) is discretized in certain way so that the resulting numerical system can be solved by sweeping the grid points in  $\xi$ -direction. The solution from the previous step is utilized for the second half where Equation (4.3) is now discretized to allow sweeping of the grid points in the  $\eta$ -direction. The resulting numerical system along each line,  $\xi=\text{constant}$  or  $\eta=\text{constant}$ , represents a tri-diagonal system of algebraic linear equations when three points finite differencing are used. This system can be solved using Thomas algorithm as discussed by Blottner (1970).

### 4.3.1 Finite Differencing in $\xi$ -Sweep

The following approximations are suggested for the derivatives in Equation (4.3)

$$\frac{\partial \Phi}{\partial \tau^*} \cong \frac{\Phi_{i,j}^{n+1/2} - \Phi_{i,j}^n}{\Delta \tau^* / 2} \quad (4.4)$$

$$\frac{\partial \Phi}{\partial \xi} \cong \frac{\Phi_{i+1,j}^{n+1/2} - \Phi_{i-1,j}^{n+1/2}}{2\Delta \xi} \quad (4.5)$$

$$\frac{\partial^2 \Phi}{\partial \xi^2} \cong \frac{\Phi_{i+1,j}^{n+1/2} - 2\Phi_{i,j}^{n+1/2} + \Phi_{i-1,j}^{n+1/2}}{\Delta \xi^2} \quad (4.6)$$

$$\frac{\partial \Phi}{\partial \eta} \cong \frac{\Phi_{i,j+1}^n - \Phi_{i,j-1}^n}{2\Delta \eta} \quad (4.7)$$

$$\frac{\partial^2 \Phi}{\partial \eta^2} \cong \frac{\Phi_{i,j+1}^n - 2\Phi_{i,j}^n + \Phi_{i,j-1}^n}{\Delta \eta^2} \quad (4.8)$$

$$\frac{\partial^2 \Phi}{\partial \xi \partial \eta} \cong \frac{\Phi_{i+1,j}^{n+1/2} - \Phi_{i+1,j-1}^{n+1/2} - \Phi_{i-1,j}^{n+1/2} + \Phi_{i-1,j-1}^{n+1/2}}{2\Delta \xi \Delta \eta} \quad (4.9)$$

The above differencing terms are of order  $\Delta \xi^2$  and  $\Delta \eta^2$  except for the finite difference term (4.9) which is of order  $\Delta \xi^2$  and  $\Delta \eta$ . The central differencing term (4.5) is expected to create a stability problem in highly convective flows. Therefore, a backward differencing will be used instead to avoid this problem (see Etefaqh et. al., 1991). Applying terms (4.4-4.9) to Equation (4.3) yields to the following finite difference equation:

$$\begin{aligned} \text{aax}_{i,j}^{n+1/2} \Phi_{i-1,j}^{n+1/2} + \text{bbx}_{i,j}^{n+1/2} \Phi_{i,j}^{n+1/2} + \text{ccx}_{i,j}^{n+1/2} \Phi_{i,j}^{n+1/2} = & \text{ddx}_{i,j}^{n+1/2} \Phi_{i,j-1}^n + \text{eex}_{i,j}^{n+1/2} \Phi_{i,j}^n \\ & + \text{ffx}_{i,j}^{n+1/2} \Phi_{i,j+1}^n + \text{ggx}_{i,j}^{n+1/2} \Phi_{i+1,j-1}^{n+1/2} + \text{hhx}_{i,j}^{n+1/2} \Phi_{i-1,j-1}^{n+1/2} + \text{llx}_{i,j}^{n+1/2} \end{aligned} \quad (4.10)$$

### 4.3.2 Finite Differencing in $\eta$ -Sweep

The following approximations are suggested for the derivatives in Equation (4.3)

$$\frac{\partial \Phi}{\partial \tau^*} \cong \frac{\Phi_{i,j}^{n+1} - \Phi_{i,j}^{n+1/2}}{\Delta \tau^* / 2} \quad (4.11)$$

$$\frac{\partial \Phi}{\partial \xi} \cong \frac{\Phi_{i+1,j}^{n+1/2} - \Phi_{i-1,j}^{n+1/2}}{2\Delta \xi} \quad (4.12)$$

$$\frac{\partial^2 \Phi}{\partial \xi^2} \cong \frac{\Phi_{i+1,j}^{n+1/2} - 2\Phi_{i,j}^{n+1/2} + \Phi_{i-1,j}^{n+1/2}}{\Delta \xi^2} \quad (4.13)$$

$$\frac{\partial \Phi}{\partial \eta} \cong \frac{\Phi_{i,j+1}^{n+1} - \Phi_{i,j-1}^{n+1}}{2\Delta \eta} \quad (4.14)$$

$$\frac{\partial^2 \Phi}{\partial \eta^2} \cong \frac{\Phi_{i,j+1}^{n+1} - 2\Phi_{i,j}^{n+1} + \Phi_{i,j-1}^{n+1}}{\Delta \eta^2} \quad (4.15)$$

$$\frac{\partial^2 \Phi}{\partial \xi \partial \eta} \cong \frac{\Phi_{i,j+1}^{n+1} - \Phi_{i-1,j+1}^{n+1} - \Phi_{i,j-1}^{n+1} + \Phi_{i-1,j-1}^{n+1}}{2\Delta \xi \Delta \eta} \quad (4.16)$$

The above differencing terms are of order  $\Delta \xi^2$  and  $\Delta \eta^2$  except for the finite difference term (4.16) which is of order  $\Delta \xi$  and  $\Delta \eta^2$ . The term (4.12) will be changed to a backward difference term for highly convective cases as discussed before. Applying terms (4.11-4.16) to Equation (4.3) yields to the following finite difference equation:

$$\begin{aligned} aay_{i,j}^{n+1} \Phi_{i,j-1}^{n+1} + bby_{i,j}^{n+1} \Phi_{i,j}^{n+1} + ccy_{i,j}^{n+1} \Phi_{i,j+1}^{n+1} = ddy_{i,j}^{n+1} \Phi_{i-1,j}^{n+1/2} + eey_{i,j}^{n+1} \Phi_{i,j}^{n+1/2} \\ + ffy_{i,j}^{n+1} \Phi_{i+1,j}^{n+1/2} + ggy_{i,j}^{n+1} \Phi_{i-1,j-1}^{n+1} + hhy_{i,j}^{n+1} \Phi_{i-1,j+1}^{n+1} + lly_{i,j}^{n+1} \end{aligned} \quad (4.17)$$

The ADI technique is found to be unconditionally stable for small values of the time step. The resulting linear tri-diagonal systems represented by the finite difference

equations (4.10) and (4.17) can be solved with a lower CPU time compared to simple implicit method discussed earlier. This will allow us to consider fine meshes and small time increments. Accordingly, errors due the finite differencing and linearizations are reduced.

#### 4.4 Solution to the Stream Function Formulation

The transformed stream function formulation is:

$$\varepsilon^2 \frac{\partial^2 \Psi^*}{\partial \xi^2} - \frac{2\eta\kappa\varepsilon^2}{H} \frac{\partial^2 \Psi^*}{\partial \xi \partial \eta} + \frac{2\eta\kappa^2\varepsilon^2}{H^2} \frac{\partial \Psi^*}{\partial \eta} + \left( \frac{1 + \eta^2\kappa^2\varepsilon^2}{H^2} \right) \frac{\partial^2 \Psi^*}{\partial \eta^2} = -\Omega^* \quad (4.18)$$

This equation is a linear partial differential equation and the most appropriate method that can be used to solve this equation is Successive-Over-Relaxation (SOR) method. This method is given by

$$\Psi_{i,j}^{*m+1} = \zeta(-\Omega_{i,j}^* + c_1 \Psi_{i-1,j-1}^{*m+1} + c_2 \Psi_{i+1,j-1}^{*m+1} + c_3 \Psi_{i-1,j}^{*m+1} + c_4 \Psi_{i+1,j}^{*m} + c_5 \Psi_{i,j-1}^{*m+1} + c_6 \Psi_{i,j+1}^{*m}) + (1 - \zeta) \Psi_{i,j}^{*m} \quad (4.19)$$

where  $\zeta$  is the over-relaxation parameter and  $1 \leq \zeta \leq 2$ . The notation  $m$  represents the iteration number. Equation (4.19) was derived using approximations (4.6), (4.7), (4.8) and (4.9) so that the grid points are swept in the increasing order in  $j$  and  $i$ . The solution is obtained by solving in a periodic manner, equations (4.10) and (4.19) and then equations (4.17) and (4.19). In each time step, iterations are required to correct for velocities and boundary conditions. The summary of the procedure of the solution is illustrated in Hoffmann and Chiang (1998).

Boundary conditions are discretized according to either first or second order backward or forward schemes. For example, the vorticity at the lower and upper plates are discretized according to a second order forward and backward differencing schemes

with respect to the normal dimension, respectively. While first order backward differencing were taken to discretize the exit thermal conditions for both CWT and UHF conditions. For UHF conditions, the time derivative in the exit thermal condition was discretized according to the first order backward scheme.

#### **4.5 Validations of Numerical Results**

Figure 4.2 shows a comparison between the solution of the Equation (4.2), simple implicit method, and the solution of the energy equation using ADI method for a special case of non-isothermal flat squeezed thin film with plates having different temperatures. The dimensionless time step used for ADI method was selected after many numerical experiments to be 0.001. However, this cannot be implemented for the simple implicit method because large CPU time will be needed. Accordingly, the dimensionless time step selected when simple implicit method is used is 0.05. An excellent agreement is noticed between the two approaches as shown in Figure 4.2.

Figure 4.3 shows a comparison between an analytical solution of a special case of squeezed thin film represented by Equation (3.10) shown in the last chapter and the corresponding numerical solution using simple implicit method. Excellent agreement exists between these two results as seen in Figure 4.3. Accordingly, a parametric study is established in the proceeding chapters in order to find out the influence of squeezing motions on the thermal behavior of incompressible thin films with various effects.

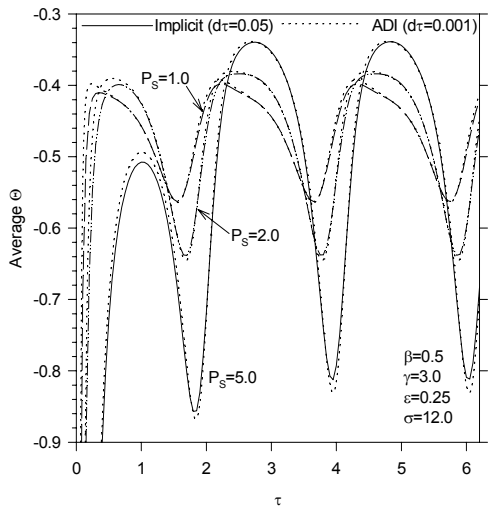


Figure 4.2: Implicit versus ADI

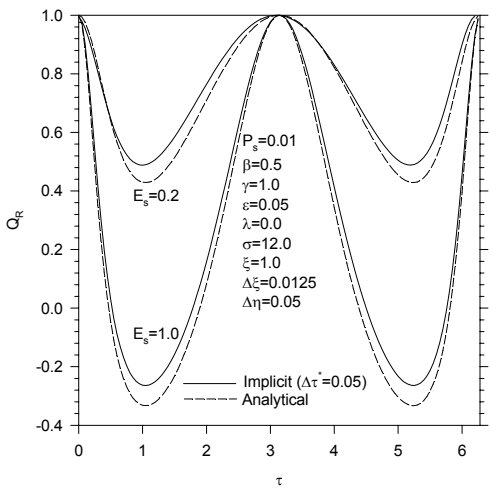


Figure 4.3: Analytical versus Implicit

## CHAPTER 5

### HEAT TRANSFER INSIDE THIN FILMS SUBJECT TO PURE OSCILLATORY SQUEEZING FLOW

In the parametric study performed in this chapter, the following are assumed: 1- the flow inside the thin film is only induced by the effect of oscillatory squeezing, thus  $\sigma=12$ , 2-the thermal boundary conditions are obtained from Equations 2.14(a) ( $C_2^* = 0$ ) and 3- cases where the squeezing Reynolds number is negligible are considered. Further, the effects of thermal squeezing number, dimensionless amplitude, perturbation parameter, viscous dissipation and the presence of ultrafine particles suspensions on heat transfer to the working fluid inside thin films are discussed in this chapter. The results of this chapter include figures for the average value of both the dimensionless heat transfer parameter and the dimensionless heat ratio against the dimensionless time for the various effects. These parameters were averaged between  $\xi=0.00625-1.0$ .

#### **5.1 Effects of the Thermal Squeezing Parameter and the Dimensionless Motion Amplitude**

Figure 5.1 and 5.2 represent the effects of thermal squeezing parameter  $P_S$  on the average dimensionless heat transfer parameter  $\Theta$  for a thin film with oscillating squeezing having a constant thermal conductivity. It is noticed that the frequency of the average  $\Theta$  is similar to the frequency of the upper plate motion. The increase in  $P_S$  values

results in enhancing the convection inside the thin film as predicted from Equation (2.25) in chapter 2 and this causes increases in the absolute values of average  $\Theta$  as shown in Figures 5.1 and 5.2. Further, it is noticed from Equation (2.39) in chapter 2 that axial convections play the significant role in the behavior of the average  $\Theta$  values.

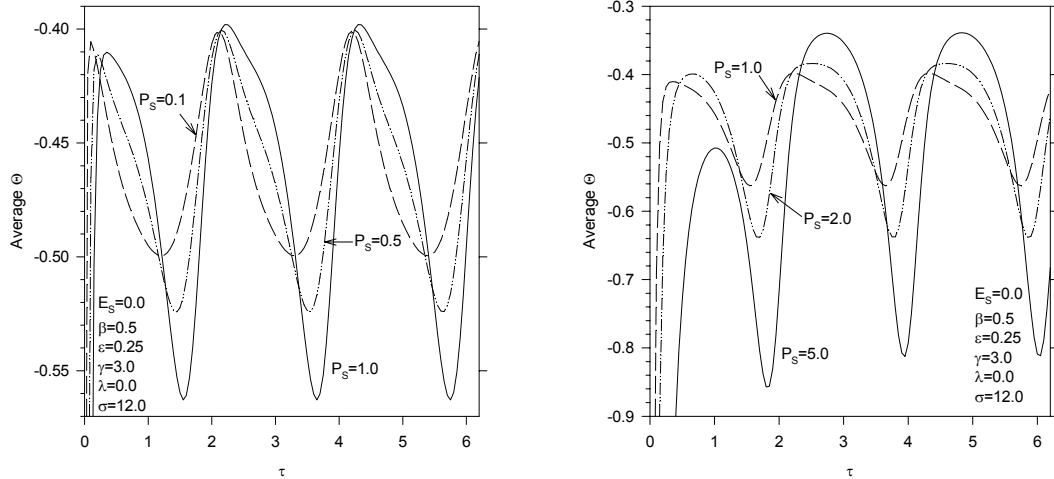


Figure 5.1: Effects of  $P_s$  on Average  $\Theta$  (1)    Figure 5.2: Effects of  $P_s$  on Average  $\Theta$  (2)

The absolute values of average  $\Theta$  are maximized during squeezing stages as shown in Figures 5.1 and 5.2. This can be interpreted to the fact that induced velocities during squeezing stages are directed outward from the thin film end that has the minimum temperature. Thus, the heat transfer from the upper plate is expected to increase due to enhancements in the convective heat transfer. On the other hand, absolute values of average  $\Theta$  are minimized when induced velocities are directed toward that end since they result in increasing the average fluid temperatures. Accordingly, the heat transfer from the upper plate is reduced. In addition, the peaks of average  $\Theta$  values are

observed to occur at periods where the thickness has almost its average value for larger values of  $P_S$  because dimensionless velocities  $U$  and  $V$  are maximum at these points thus convection is maximized as can be seen from Equations (2.18) and (2.19) in chapter 2. This is not the case for lower values of  $P_S$  since the conduction is dominant in these applications.

Figures 5.3 and 5.4 show the effects of the dimensionless motion amplitude  $\beta$  of the upper plate on the average dimensionless heat transfer parameter  $\Theta$  for two different values of  $P_S$  with a constant thermal conductivity. It is observed that increases in the values of  $\beta$  result in increases in the absolute values of the average  $\Theta$  in squeezing stages due to increased induced velocities as  $\beta$  increases. However, the increased induced velocities in relief stages due increases in  $\beta$  values results in increases in average fluid temperatures which cause average absolute  $\Theta$  values to decrease. Further, it is noticed that the trend of the absolute average  $\Theta$  values becomes more flat during relief stages and gets sharper as  $\beta$  increases as shown from Figure 5.4. This is because convective terms shown in Equation (2.39) in chapter 2 increase as  $\beta$  increases. However, the effects of these convective terms become smaller at the end of squeezing stages due to sharp decrease in the heat diffusion. Accordingly and due to the presence of large heat transfer enhancements during squeezing stages, the trend of average  $\Theta$  values gets sharper during squeezing stages as  $\beta$  increases as shown in Figure 5.4.

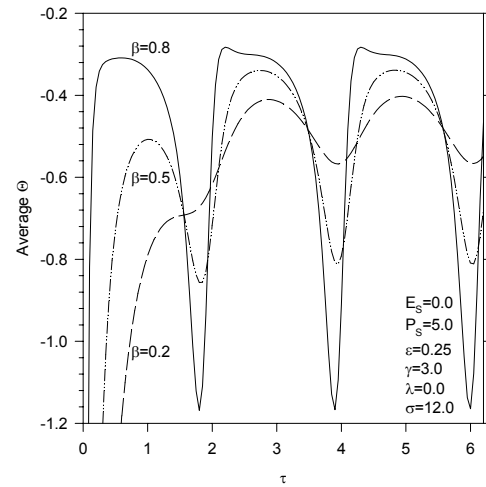
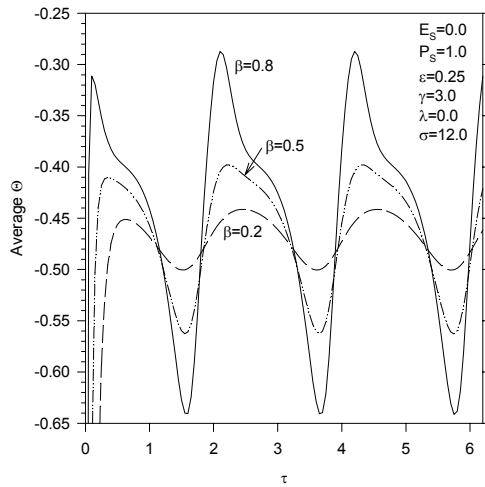


Figure 5.3: Effects of  $\beta$  on Average  $\Theta$  (1)      Figure 5.4: Effects of  $\beta$  on Average  $\Theta$  (2)

Figure 5.5 shows the effect of the perturbation parameter  $\varepsilon$  on the average  $\Theta$  values. It is shown that as  $\varepsilon$  increases, the absolute values of the average  $\Theta$  increase. As  $\varepsilon$  increases, axial conduction increases resulting in increases in average  $\Theta$  values. It is worth noting that as  $\varepsilon$  increases, two-dimensional effects on velocity profiles increases and solutions for the complete momentum equations are needed which will be discussed later. Finally, enhancements of heat transfer inside thin films are achieved by the following: increasing the amplitude of the motion of the oscillating plate, considering thin films with large thermal squeezing parameter and pumping fluid with minimum temperature to the thin film during relief stages.

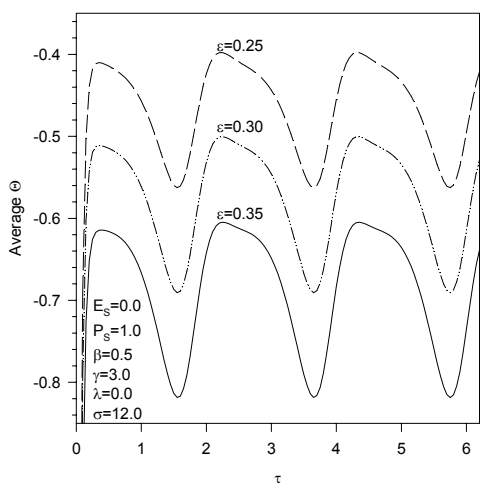


Figure 5.5: Effects of Perturbation Parameter  $\varepsilon$  on Average  $\Theta$

## 5.2 Effects of Viscous Dissipation and the Presence of Suspended Ultrafine Particles

Figure 5.6 represents the effects of the viscous dissipation on the average heat ratio  $Q_R$  for a thin film having an oscillating squeezing and constant thermal conductivity.

The average heat ratio  $Q_R$  is defined as

$$Q_R(\xi, \tau^*) = \left(1 + \lambda\varepsilon|\delta\beta\sin(\delta\tau^*)\right) \frac{\partial\theta(\xi, \eta, \tau^*)}{\partial\eta} \Big|_{\eta=1} / \frac{\partial\theta(\xi, \eta, \tau^*)}{\partial\eta} \Big|_{\eta=0} \quad (5.1)$$

It is noticed that the frequency of the average  $Q_R$  is also similar to the frequency of the upper plate motion. Further, it is noticed from this figure that the average  $Q_R$  decreases as  $E_S$  increases. Viscous dissipation effects on the average dimensionless heat parameter  $\Theta$  are shown in Figures 5.7 and 5.8 for two different values of  $P_S$ . The increase in  $P_S$  results in enhancing the convection inside the thin film at constant  $E_S$  number. Accordingly, this

results in a decrease in the average values of  $\Theta$  as shown in Figures 5.7 and 5.8. In addition, the following can be noticed from Figures 5.6, 5.7 and 5.8:

- the maximum average  $Q_R$  and the minimum average  $\Theta$  are found to occur in the early squeezing stages.
- the minimum average  $Q_R$  and maximum average  $\Theta$  are found to occur at times that makes the induced horizontal velocities reach almost their maximum and minimum values due to increases in viscous dissipation.

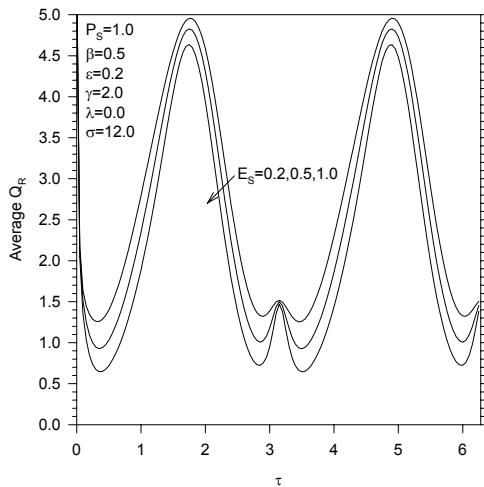


Figure 5.6: Effects of  $E_S$  on  $Q_R$

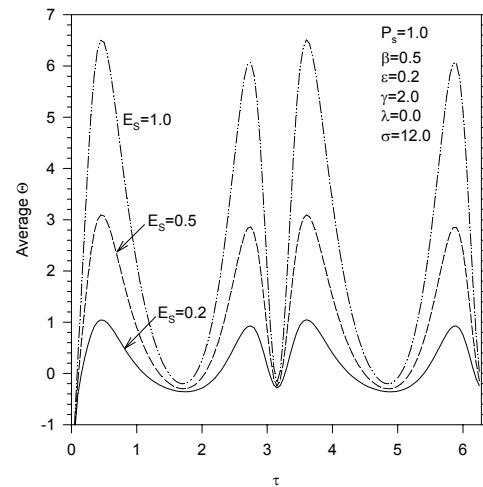


Figure 5.7: Effects of  $E_S$  on Average  $\Theta$  (1)

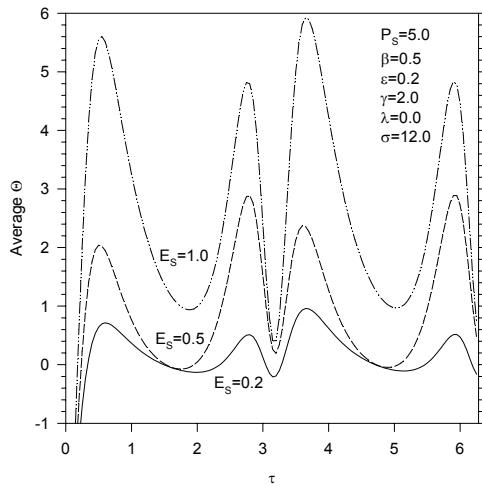


Figure 5.8: Effects of  $E_s$  on Average  $\Theta$  (2)

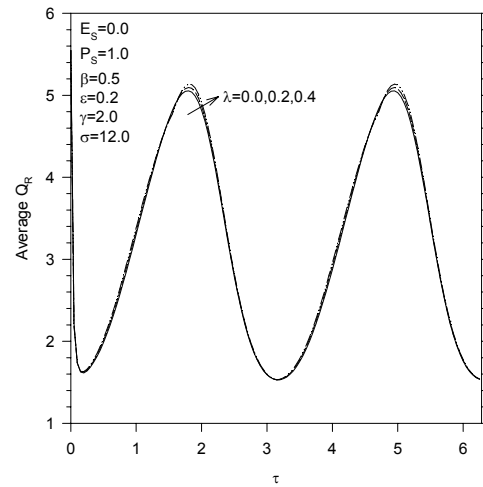


Figure 5.9: Effects of  $\lambda$  on  $Q_R$

Figure 5.9 shows the effects of thermal dispersion coefficient  $\lambda$  on the average heat ratio  $Q_R$  in the absence of viscous dissipation. It is noticed that the average  $Q_R$  increases as  $\lambda$  increases and these increases are significant early during the squeezing stage. The effects of thermal dispersion coefficient  $\lambda$  on the average  $\Theta$  are seen in Figures 5.10 and 5.11 for two different values of thermal squeezing parameters. The following are observed from Figures 5.10 and 5.11:

- the average  $\Theta$  decreases (absolute value of average  $\Theta$  increases) as  $\lambda$  increases. This is expected due to enhancements in the fluid thermal conductivity.
- the significant enhancements in the average value of  $\Theta$  occur during the squeezing stage. This is because induced velocities are directed outward from the

thin film's end that has the minimum temperature. During the relief stage, the induced velocities tend to increase the average fluid temperatures and this causes enhancements during the relief stage to be lower than those during squeezing stage.

- the performance of the thin film is improved during the relief stage due to enhancements in the thermal conductivity.

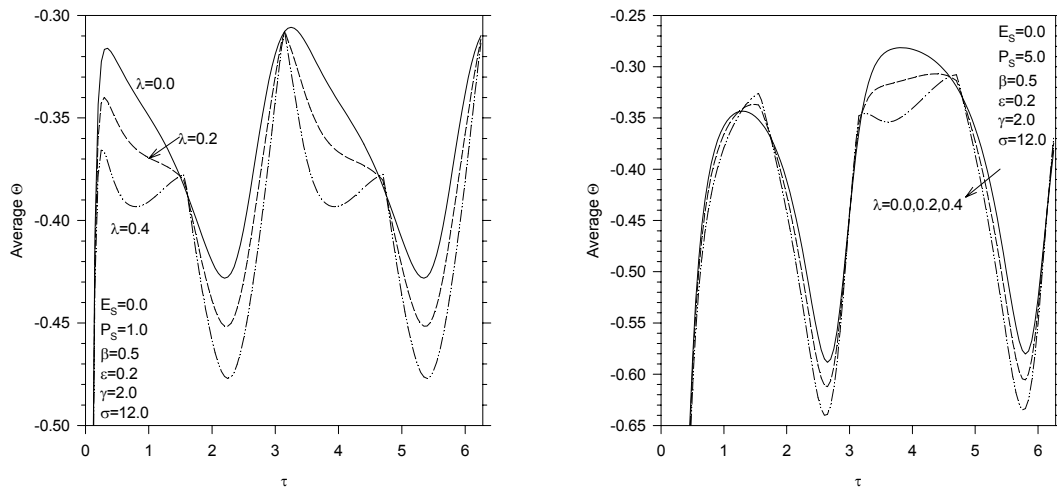


Figure 5.10: Effects of  $\lambda$  on Average  $\Theta$  (1)    Figure 5.11: Effects of  $\lambda$  on Average  $\Theta$  (2)

Figure 5.12 represents the influence of the motion amplitude  $\beta$  on the average dimensionless heat parameter  $\Theta$  in the presence of viscous dissipation effects. Induced velocities increase by an order of  $\beta$  as  $\beta$  increases. Meanwhile, viscous dissipation increases by an order of  $\beta^2$  as  $\beta$  increases. Accordingly, as seen in Figure 5.12, the values of the average  $\Theta$  are expected to increase as  $\beta$  increases.

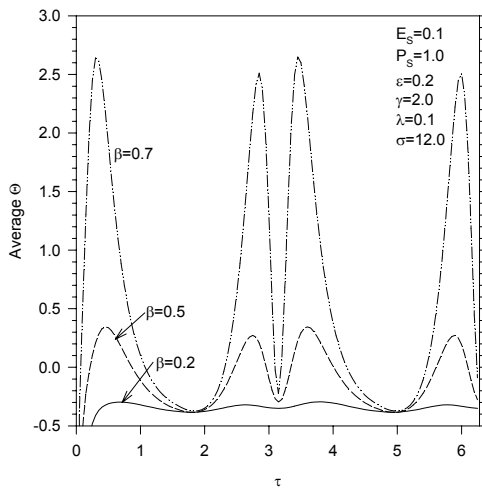


Figure 5.12: Effects of  $\beta$  on Average  $\Theta$  ( $E_s$  and  $\lambda$  are none zeros)

Finally, enhancements of heat transfer inside thin films with oscillating squeezing can be achieved by the following: introducing suspensions of metallic ultrafine particles in the working fluid such as suspensions of copper ultrafine particles, selecting the working fluid that will result in a minimum Eckert number, considering a thin film with large thermal squeezing parameter and increasing the motion amplitude if Eckert number is negligible.

### 5.3 Comments

From previous figures, it is noticed that the mean value of the average  $\Theta$  is unaffected by any changes in the values of  $P_s$  or  $\beta$  (in absence of viscous dissipation). However, it is clearly noticed that the mean value of the average  $\Theta$  is a function of the parameters  $\varepsilon$ ,  $E_s$  and  $\lambda$ . Therefore, external disturbances to an existing thin film can

change its mean thermal behavior which in turn can result in excessive cooling in cases where suspended ultrafine particles are present in the fluid and more heating when the fluid is viscous. The percentage fluctuation in the average  $\Theta$  increases as  $P_s$ ,  $\beta$  and  $\lambda$  increase and decreases as both  $\varepsilon$  and  $E_s$  increase. The fluctuation in thermal characteristics of thin films is an important aspect to be considered in the design of thin films especially for fluidic cells of many sensors. This is because many sensors are bimaterial such as the microcantilever. The presence of squeezing effects inside these thin films due to external disturbances can move the position for the thermally developed flow conditions forward and backward. As such, these sensors need to be placed in the fully developed regions where fluctuations in the temperature are minimized.

## CHAPTER 6

### ANALYSIS OF HEAT TRANSFER CHARACTERISTICS INSIDE OSCILLATORY SQUEEZED THIN FILMS SUBJECT TO A VARYING CLEARANCE

In this chapter, a parametric study is performed on inclined thin films in order to find out the influence of the geometry changes on the thermal characteristics of oscillatory squeezed thin films. In addition, the effects of the squeezing number and the thermal squeezing parameter are studied. Moreover, the effects of the presence ultrafine particles suspensions in the working are studied. The squeezing number is considered to be different than 12 in this chapter. The previous effects are considered for both constant wall temperature conditions and for the condition where the lower plate is under uniform wall heat flux condition while the upper plate is insulated. The values of  $\Delta\xi$ ,  $\Delta\eta$  and  $\Delta\tau$  are chosen to be 0.0055, 0.03 and 0.0015 for constant wall conditions and 0.01, 0.03 and 0.0025 for uniform wall heat flux conditions. These result in time and grid independent solutions.

#### 6.1 Controlling Parameters

The parameters studied in this chapter are the squeezing number  $\sigma$ , thermal squeezing parameter  $P_S$ , Eckert number  $E_S$ , dimensionless slope  $\kappa$ , dispersion coefficient  $\lambda$  and the dimensionless amplitude  $\beta$ . The values of  $P_S$  are varied from 1.0 to 8.0. This

corresponds to actual disturbance frequency varying from 1.5 to 13 s<sup>-1</sup> for a thin film having a thickness equal to 0.5 mm with water as the working fluid. The Eckert number is varied from 0 to 1 and the dispersion coefficient is allowed to vary from 0 to 2. These ranges are found to cause obvious variations in heat transfer, Nusselt number and fluid temperatures. The values of  $\sigma$  is varied from 5 where inlet average velocity is very large compared to squeezing velocities, for  $\beta=0.2$ , to 11 where inlet average velocity is relatively small. The values of  $\beta$  are considered to change from 0.1 for a stiff thin film to 0.4 for soft thin film. Finally, the generated results in this chapter except for section 6.8 are based on constant inlet average velocity.

## **6.2 Effects of the Squeezing and the Thermal Squeezing Numbers**

Figure 6.1 shows the behavior of the average dimensionless heat transfer parameter  $\Theta$  as functions of the dimensionless time  $\tau^*$  and the squeezing number  $\sigma$  for constant wall temperature conditions CWT. It is noticed that the average  $\Theta$  has an oscillatory trend and it decreases as  $\sigma$  increases. This is because the average axial velocities increase as  $\sigma$  decreases thus heat transfer by convection increases. The maximum and minimum values of average  $\Theta$  were found to occur at times where the upper plate has almost its maximum speed in squeezing and relaxation stages, respectively. The behavior of average lower plate temperature  $\theta_w$  as a function of  $\sigma$  is shown in Figure 6.2 for UHF conditions. Decreases in the values of  $\sigma$  results in increases in average axial velocities thus more cooling is encountered for the lower plate and its average temperature is reduced as  $\sigma$  decreases.

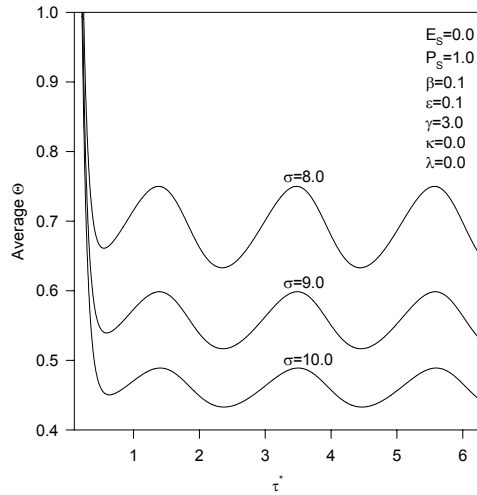


Figure 6.1: Effects of  $\sigma$  on Average  $\Theta$

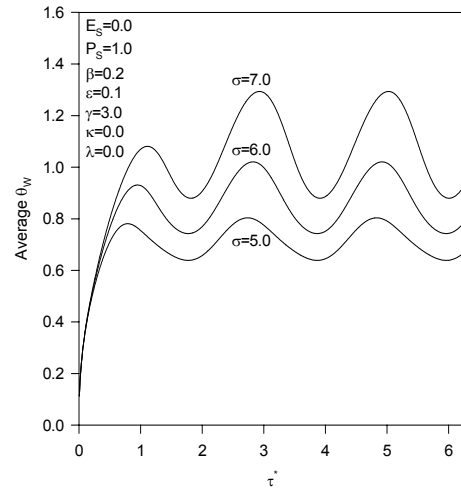


Figure 6.2: Effects of  $\sigma$  on Average  $\theta_w$

The effects of  $\sigma$  on the Nusselt number at the lower plate  $Nu_L$  is shown in Figure 6.3 for the uniform heat flux UHF condition. It is noticed that  $\sigma$  does not have a great effect on  $Nu_L$  and that  $Nu_L$  has an oscillatory behavior. The maximum values of  $Nu_L$  occur when the film thickness reaches almost its minimum values while the minimum values of  $Nu_L$  occur when the film thickness is almost maximum. Figure 6.4 represents the effect of thermal squeezing parameter  $P_S$  on the  $Nu_L$  for the UHF condition. It is found that  $Nu_L$  increases as  $P_S$  increases. However, increasing  $P_S$  by a factor of 8 resulted in a maximum increase in  $Nu_L$  by factor of 1.09 as can be shown from Figure 6.4. This indicates that  $Nu_L$  is not sensitive to either  $\sigma$  and  $P_S$  as long as the mean flow inside the thin film produces thermally developed conditions at the exit. Also, it is noticed that the

plot of  $Nu_L$  moves slightly to the right as  $P_S$  increases as a result of increases in transient effects.

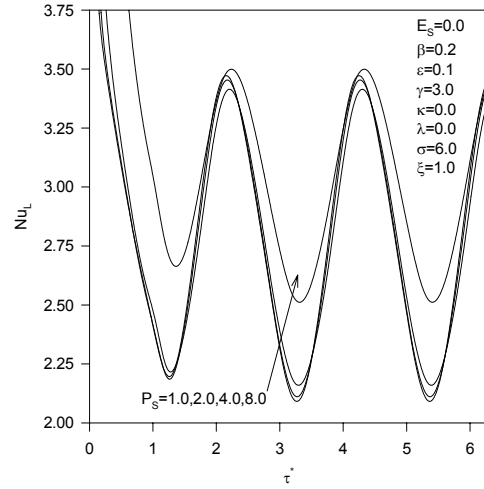
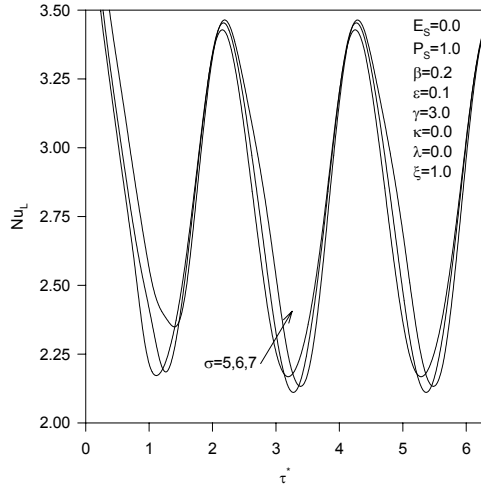


Figure 6.3: Effects of  $\sigma$  on  $Nu_L$  (UHF)      Figure 6.4: Effects of  $P_S$  on  $Nu_L$  (UHF)

### 6.3 Effects of the Dimensionless Slope of the Thin Film

Figures 6.5 and 6.6 illustrate the effect of the dimensionless slope of the upper plate of the thin film  $\kappa$  on the Nusselt number for CWT and UHF conditions, respectively. It is noticed that the trend of  $Nu_L$  and  $Nu_U$  for CWT conditions and the trend of  $Nu_L$  for UHF condition have an oscillatory behavior. Further, the values of both  $Nu_L$  and  $Nu_U$  for CWT conditions and  $Nu_L$  for UHF conditions decrease as  $\kappa$  increases due decreases in both the average axial velocities and the local velocities near the plates as  $\kappa$  increases. An interesting feature for inclined thin films is that variations in the Nusselt number due to the squeezing effects decreases as  $\kappa$  increases. Moreover, it is noticed

from Figure 6.5 that the values of  $Nu_U$  is always greater than that for  $Nu_L$  for convergent thin films while the opposite is true for divergent thin films.

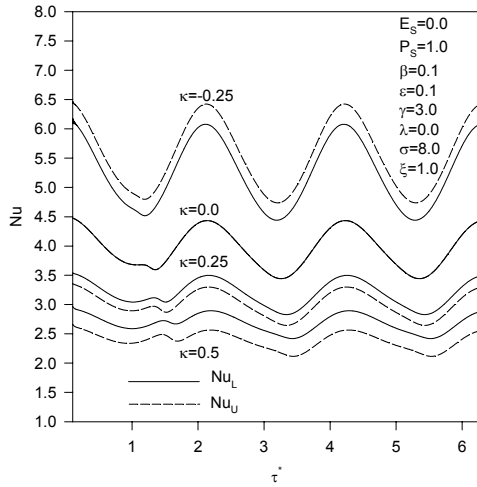


Figure 6.5: Effects of  $\kappa$  on  $Nu$  (CWT)

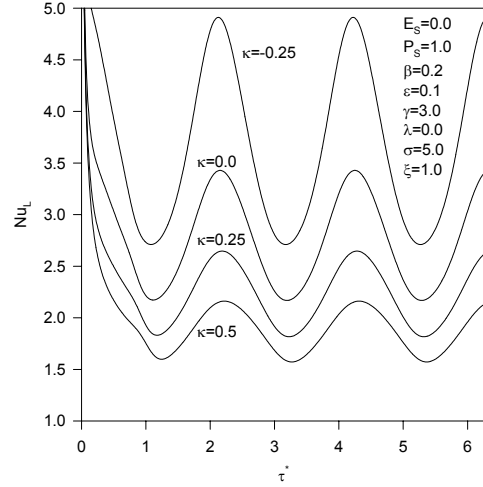


Figure 6.6: Effects of  $\kappa$  on  $Nu_L$  (UHF)

As initial thermal effects diminish, kinks are noticed to appear for Nusselt numbers as in Figures 6.5 and 6.6 due to the transition with the steady periodic solution. These are clear for divergent thin films and at larger  $\sigma$  values. This is because the increased fluid volume in divergent cells and the decreased inlet velocities for larger  $\sigma$  values increase the transient effects and accordingly we see these kinks occur at further times. These kinks can be seen in many vibrated dynamical systems.

The axial distribution of  $Nu_L$  is shown in Figure 6.7 and 6.8 for CWT conditions and UHF conditions, respectively. The trend of  $Nu_L$  is almost constant for  $\kappa=0.0$  except near the inlet where the flow there is not thermally developed. However for the cases

where  $\kappa$  is different than zero, The values of  $Nu_L$  increase almost linearly as  $\xi$  increases far from the inlet for negative values of  $\kappa$  and they decrease almost linearly for positive values of  $\kappa$  as  $\xi$  increases. These facts are observed from Figures 6.7 and 6.8.

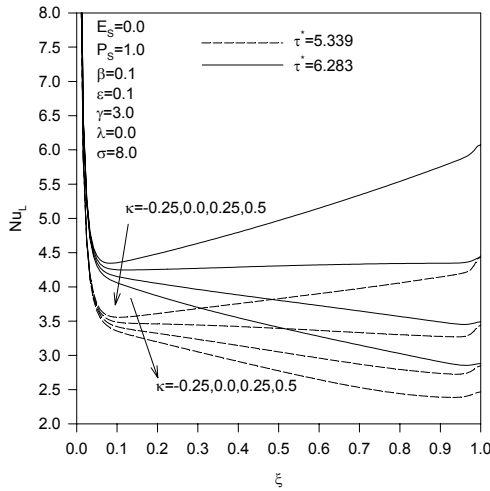


Figure 6.7:  $Nu_L$  Distribution (CWT)

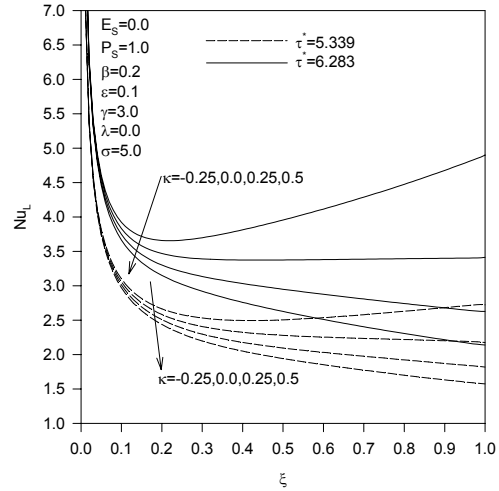


Figure 6.8:  $Nu_L$  Distribution (UHF)

The influence of  $\kappa$  on  $\theta_m$  is shown in Figure 6.9 for CWT conditions. The values of  $\theta_m$  increase as  $\kappa$  decreases. As  $\kappa$  decreases, the Nusselt numbers increase resulting in more heat transferred to the fluid for CWT conditions. This additional heat will result in increasing the fluid temperatures. For UHF conditions, average lower plate temperature  $\theta_w$  is found to increase as  $\kappa$  increases due to decreases in convective heat transfer coefficients. This can be seen from Figure 6.10. Further, it is noticed that the average  $\theta_w$  has an oscillatory behavior almost similar to the upper plate motion with an approximate phase shift equal to  $\pi/6$ . That is the maximum average  $\theta_w$  occurs at times that results in

maximum upper plate velocity in relaxation stages and the minimum are at times that makes the velocity of that plate maximum in squeezing stages.

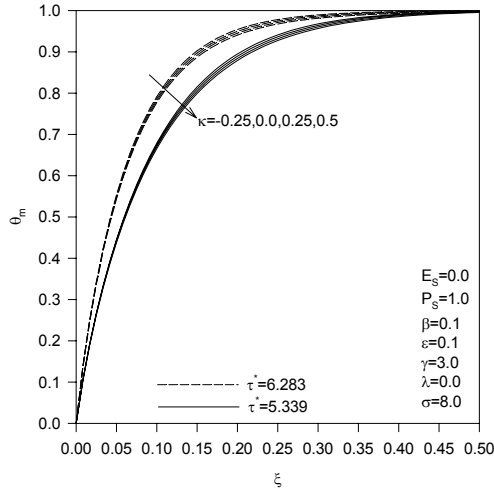


Figure 6.9: Effects of  $\kappa$  on  $\theta_m$  (CWT)

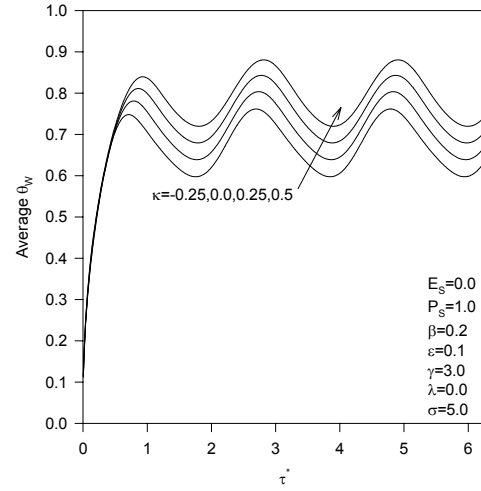


Figure 6.10: Effects of  $\kappa$  on  $\theta_w$  (UHF)

#### 6.4 Effects of Viscous Dissipation and Thermal Dispersion Effects

External vibrations have a significant influence on heat transfer inside thin films especially if the working fluid possesses a high viscosity. The induced motions results in increasing viscous dissipation especially at large values of  $\sigma$  as shown in the previous chapter. This results in reducing the cooling capacity of the thin film as shown in Figure 6.11 which describes the relation between the average dimensionless heat parameter and the squeezing Eckert number for CWT conditions. On the other hand, the cooling capacity of the thin film can be increased in the presence of metallic ultrafine suspensions inside the thin film due to thermal dispersion effects as shown in Fig. 6.12 for UHF

conditions. This figure shows the effects of the dimensionless thermal dispersion parameter  $\lambda$  on the average lower plate temperature.

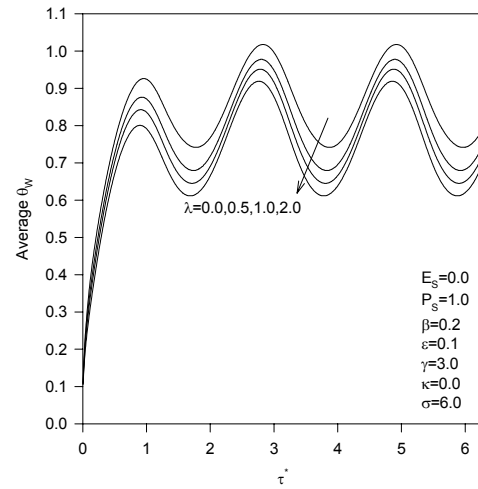
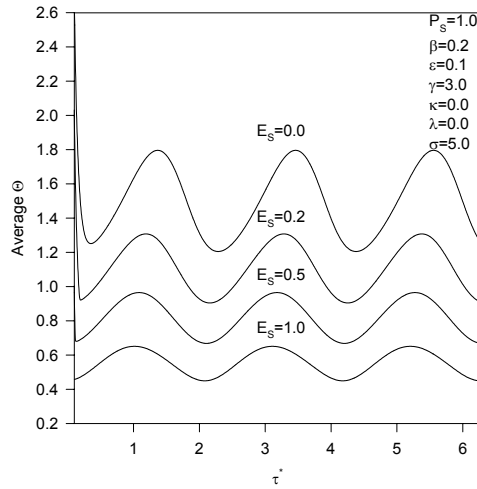


Figure 6.11: Effects of  $E_s$  on Average  $\Theta$  (CWT)    Figure 6.12: Effects of  $\lambda$  on  $\theta_w$  (UHF)

### 6.5 Effects of Dimensionless Amplitude of the Upper Plate Motion

Figure 6.13 display the effect of the dimensionless amplitude of the upper plate of the thin film  $\beta$  on the Nusselt number for CWT conditions. It is seen that the amplitude of  $Nu_L$  ( $Nu_U=Nu_L$ ) increases as  $\beta$  increases. Further, it is also noticed that mean value of the Nusselt number at the steady periodic behavior is independent of  $\beta$ . The increase in the noise level at the upper plate motion is expected to increase the fluctuation in the lower plate temperature for UHF conditions as shown in Figure 6.14.

Figure 6.14 shows that average lower plate temperature is increased by 40% over the mean plate temperature for  $P_s=1.0$  and  $\beta=0.4$ . This increase will reduce the viscosity

especially in lubrications where the viscosity of the lubricant is a strong function of temperature. Accordingly, the thin film will not be able to carry the load at all times and the possibility of wear increases. As  $P_s$  and  $\beta$  increase, the working temperatures at certain times for the electronic component increases when the thin film is used to cool these devices. Therefore, a correction factor has to be included in designs of microchannels or heat pipes to account for external vibrations.

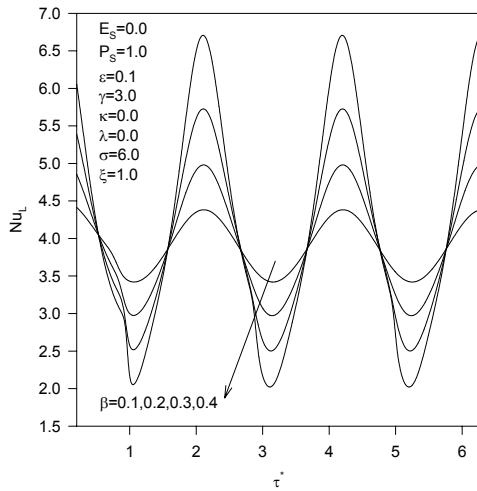


Figure 6.13: Effects of  $\beta$  on  $Nu_L$  (CWT)

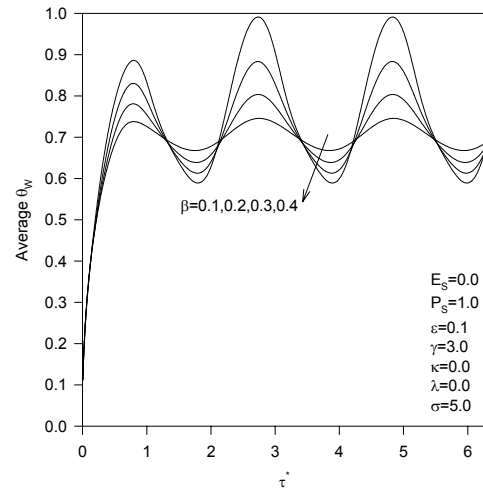


Figure 6.14: Effects of  $\beta$  on  $\theta_w$  (UHF)

## 6.6 Correlations

The following equation represents the behavior of Nusselt numbers for both CWT and UHF conditions as a function of the dimensionless time  $\tau^*$  in the absence of transient effects and viscous dissipation.

$$\text{Nu}_L(X, \tau) = \frac{\text{Nu}_{Lm}(X, \tau) \sqrt{(1 + \kappa X)^2 - \beta^2}}{(1 - \beta \cos(\gamma\tau) + \kappa X)} \quad (6.1)$$

where the square root term represents the reciprocal of the average of the term  $1/H$ . The values of  $\text{Nu}_{Lm}$  are obtained from Table 6.1. These values can be taken for different values of  $P_S$  and  $\sigma$  as long as the mean flow produce thermally developed conditions at the exit as shown before. Equation (6.3) can be applied also for evaluating the Nusselt number at the upper plate for CWT conditions. The mean value of the Nusselt number  $\text{Nu}_{Lm}$  or  $\text{Nu}_{Lm}$  and the percentage fluctuation in the Nusselt number are evaluated from the following relations

$$\text{Nu}_{Lm}(X) = \frac{\gamma}{2\pi} \int_{2\pi\left(1-\frac{1}{\gamma}\right)}^{2\pi} \text{Nu}_L(X, \tau^*) d\tau^* \quad (6.2)$$

$$\frac{\Delta \text{Nu}_L}{\text{Nu}_{Lm}} = \frac{(\text{Nu}_{L\max} - \text{Nu}_{L\min})}{2(\text{Nu}_{Lm})} \quad (6.3)$$

Equations (6.1)-(6.3) are also valid for the Nusselt number and its corresponding variation at the upper plate. It is noticed that some of correlations in Table 6.1 are functions of the dimensionless distance  $X$  and they are valid for  $X$  far from the inlet. This generalization is obtained by noticing that the Nusselt numbers at  $X=X_0$  can be evaluated at  $X=1.0$  for a different case with a dimensionless slope and perturbation parameter equal to  $\kappa X_0$  and  $h_0/(X_0 B)$  instead of  $\kappa$  and  $h_0/B$ . The squeezing number will be reduced but as shown before Nusselt numbers are less influenced by  $\sigma$  and axial conductions are small compared to axial convections far from the inlet. The maximum error between these

correlations and the numerical results are 6% for the Nusselt numbers and about 15% for the values of  $\Delta Nu_L / Nu_{Lm}$  and  $\Delta Nu_U / Nu_{Um}$ .

Condition	Correlation	Ranges
CWT	$Nu_{Lm} = 3.853e^{-0.004\kappa X} \left[ (1 + \kappa X)^2 - \beta^2 \right]^{-0.497}$ $\frac{\Delta Nu_L}{Nu_{Lm}} = 1.674e^{-0.678\kappa X} (0.0478 + \beta)^{1.361}$	$-0.25 \leq \kappa \leq 0.5$  $\lambda=0$
CWT	$Nu_{Um} = 3.846e^{-0.194\kappa X} \left[ (1 + \kappa X)^2 - \beta^2 \right]^{-0.496}$ $\frac{\Delta Nu_U}{Nu_{Um}} = 1.675e^{-0.610\kappa X} (0.0468 + \beta)^{1.356}$	$-0.25 \leq \kappa \leq 0.5$  $\lambda=0$
CWT	$Nu_{Lm} = (1.132\lambda + 3.978)(1 - \beta^2)^{-0.278}$ $\frac{\Delta Nu_L}{Nu_{Lm}} = (-0.0716\lambda^2 + 0.242\lambda + 1.470)\beta^{1.138}$	$0 \leq \lambda \leq 2.0$  $\kappa=0$
UHF	$Nu_{Lm} = 2.719e^{0.117\kappa X} \left[ (1 + \kappa X)^2 - \beta^2 \right]^{-0.519}$ $\frac{\Delta Nu_L}{Nu_{Lm}} = 1.187e^{-1.163\kappa X} \beta^{1.026}$	$-0.25 \leq \kappa \leq 0.5$  $\lambda=0$
UHF	$Nu_{Lm} = (0.888\lambda + 2.763)(1 - \beta^2)^{-0.451}$ $\frac{\Delta Nu_L}{Nu_{Lm}} = (0.380\lambda + 1.211)\beta^{1.054}$	$0 \leq \lambda \leq 2.0$  $\kappa=0$

Table 6.1: Correlations for mean Nusselt numbers and Fluctuations in Nusselt numbers

( $E_S=0$ ,  $P_S=1.0$ ,  $0.1 \leq \beta \leq 0.4$ ,  $\sigma=5.0$ )

## 6.7 An Approximate Correlation for the Exit Thermal Boundary Condition

Figure 6.15 shows the axial development of the temperature inside the thin film for UHF conditions at two different times and flow conditions.

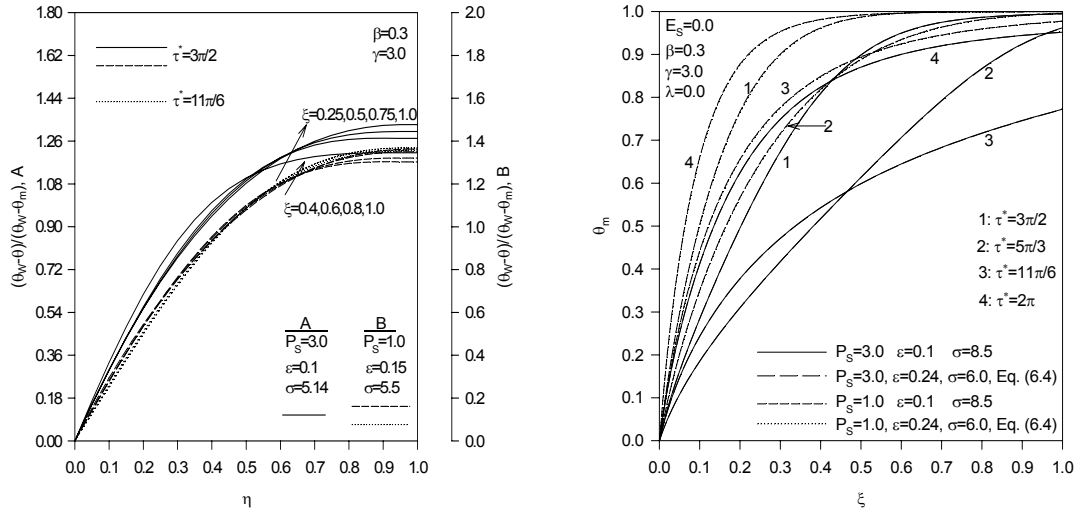


Figure 6.15: Temperature Development(UHF) Figure 6.16: Validation for Eq. (6.4)(CWT)

According to Figure 6.15, the following exit condition is suggested as the exit thermal boundary condition for UHF conditions:

$$\frac{\partial}{\partial \xi} \left( \frac{\theta_w(\xi, \tau) - \theta(\xi, \eta, \tau)}{\theta_w(\xi, \tau) - \theta_m(\xi, \tau)} \right) \cong 0 \quad (6.4)$$

Equation (6.4) will be used in subsequent chapters when backflows occur at the exit, negative velocities appear, for UHF conditions since singularity is introduced by the original boundary condition when axial velocity reaches zero at the exit and axial conduction can not be neglected for these conditions. Figure 6.16 represents a comparison between a solution to a squeezed thin film having CWT conditions,  $\sigma=6.0$

and  $\varepsilon=0.244$  with exit thermal condition represented by equation (6.4) and a portion of a long squeezed thin film having  $\sigma=8.5$  and  $\varepsilon=0.1$  satisfying at its exit approximately the zero values for the axial gradient of the temperature at two different  $P_S$  values. The plotted portion of the last thin film which ranges from  $X=0.0$  and extending to  $X=0.41$  represents a thin film having  $\sigma=6.0$  and  $\varepsilon=0.244$ . The solution for  $\theta_m$  of the chopped thin film with equation (6.4) as an exit thermal condition is found to be in excellent agreement with the resulting solution of the extended thin film as shown in Figure 6.16. Therefore, Equation (6.4) is also suggested for cases where the gradient of  $\theta_m$  is not zero for CWT conditions.

### **6.8 Effects of Inlet Axial Velocity Conditions on Nusselt Numbers**

Figure 6.17 show the Nusselt number at the lower plate of the thin film at two different inlet flow conditions for CWT and UHF thermal wall conditions. The two different inlet flow conditions are the constant inlet flow rate CIF condition and the constant inlet average velocity CIV condition. It is noticed from these figures that the fully developed values for the Nusselt number are almost unaffected by changes that occur in the inlet flow conditions except for CWT conditions near the maximum relief at large  $\beta$  values. Therefore, the previously generated correlations for CIV conditions can also be applied also for CIF conditions.

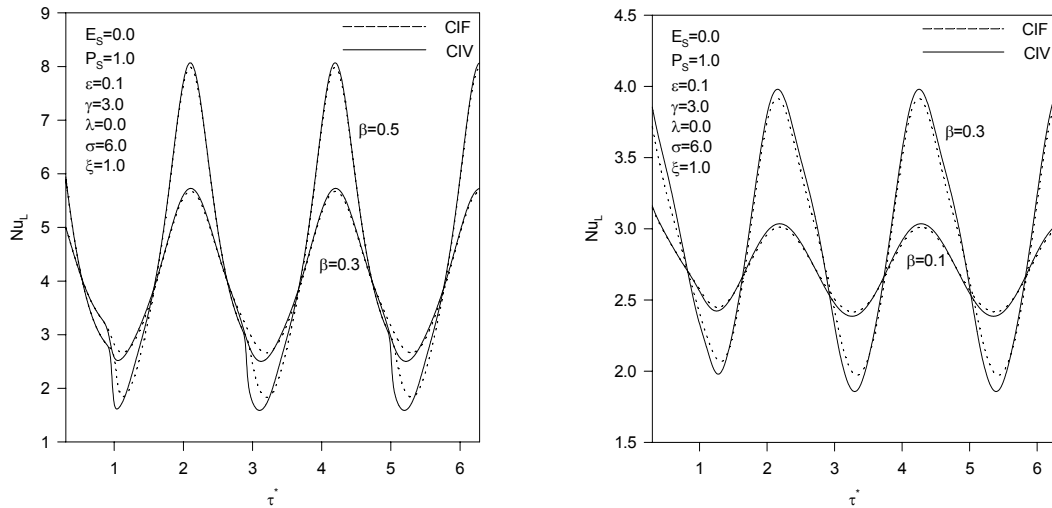


Figure 6.17: Inlet Flow Conditions versus Nusselt: (a) CWT and (b) UHF

## 6.9 Comments

Two main factors affect the function of a fluidic cell. Flow factors and thermal factors. With regards to flow factors, the bioprobes are calibrated for certain flow rates. Accordingly, external disturbances will cause inaccurate readings due to the resulting fluctuations in the flow rate. The fluctuations in the flow rate increases as the distance between the probe and the inlet of the cell increases. Therefore, one idea is to place the probe as close as possible to the inlet.

As for thermal factors, many bioprobes are bimaterial such as the microcantilever. Decreasing the squeezing number  $\sigma$  will move the fluctuations in the temperature further down stream. Also, increasing the thermal squeezing number  $P_s$  and the dimensionless amplitude  $\beta$  will increase the fluctuations in the fluid temperature and the possibility of

inaccurate measurements due to bimaterial effects increases. To eliminate bimaterial effects, both  $P_S$  and  $\beta$  have to be reduced. They can be reduced by the following:

- Increasing fluid thermal conductivity by using high conductive solvent or by using thermal conductivity enhancers such as suspended ultrafine particles.
- Decreasing thermal capacitance by removing any scales from the biofluid that have high thermal capacitance.
- Decreasing the thickness of the cell in order to minimize bimaterial effects.
- Eliminate any sources of disturbances from the surroundings.
- Using stiff sealing between the plates of the cell.
- Using rigid upper plate
- Operating the fluidic cell at low flow rates.
- Using convergent cells as they tend to reduce the thermal entrance length.

Although these factors can reduce bimaterial effects, they can produce counter actions. For example, a stiff seal will increase the leakage problem thus decreasing the accuracy of the measurements. Finally, decreasing the thickness of the thin film results in increasing the values of  $\beta$ . In the previous analysis, the inertia of the fluid is neglected as for fluidic cells designed for a single microcantilever. However, this might not be the case for cells containing array of sensors, operating at large flow rates or when the frequency of the disturbance is large. Therefore, inertia effects on flow and heat transfer inside oscillatory squeezed thin films will be discussed in the next chapter.

## CHAPTER 7

### ANALYSIS OF FLOW AND HEAT TRANSFER INSIDE OSCILLATORY SQUEEZED THIN FILMS WITH LARGE INERTIA EFFECTS

In this chapter, inertia effects are considered in the analysis of flow and heat transfer inside oscillatory squeezed thin films. The effects of changing the squeezing Reynolds number on the velocity profiles as well as thermal characteristics of squeezed thin films are discussed. Further, influences of increasing the disturbance frequency, dimensionless slope of the upper plate and the squeezing number of the thin film are analyzed taking in the presence of inertia effects. The values of  $\Delta\xi$ ,  $\Delta\eta$  and  $\Delta\tau$  are chosen to be 0.0125, 0.04 and 0.001 for both constant wall temperature and uniform wall heat flux conditions below which grid independent solutions are obtained. The maximum error between the subsequent values for the dimensionless stream function and the dimensionless velocity at each time step were selected to be  $10^{-6}$  and  $10^{-5}$ , respectively.

#### 7.1 Controlling Parameters

The parameters studied in this chapter are the Prandtl number  $Pr$ , squeezing Reynolds number  $R_s$ , squeezing number  $\sigma$ , squeezing frequency, dimensionless amplitude of the motion  $\beta$ , and the dimensionless slope  $\kappa$ . The  $Pr$  values are taken to be 0.03 and 3.0. The first value represents a typical value for liquid metals (mercury) while the second value represents a moderate value for  $Pr$ . The values of  $R_s$  are varied from

from 0.5 to 80. This corresponds to thin films filled with water and having intermediate film thicknesses ranges from 0.4mm to 6mm. Also, this corresponds to thin films filled with liquid metals (e.g. mercury) having intermediate film thicknesses, 0.2mm to 2mm. the previous thin films are designed to produce a mean wall shear stress of 2 dyn/cm<sup>2</sup> when the squeezing number  $\sigma$  is equal to 5.14.

The values of  $\sigma$  are varied from 5 where inlet average velocity is very large compared to squeezing velocities to 9 where inlet average velocity is relatively small.  $\beta$  values are considered to change from 0.1 for stiff thin film to 0.3 for soft thin film. The dimensionless slope is taken to be -0.2 for convergent thin film and 0.4 for divergent thin film. It should be mentioned that all the results are generated for constant inlet average velocity conditions CIV unless stated where comparisons is performed between CIV and constant inlet flow rate CIF conditions.

## **7.2 Effects of Varying the Squeezing Reynolds Number**

Figures 7.1(a) and 7.1(b) show the effects of the squeezing Reynolds number  $R_S$  on the axial velocity profiles at  $\tau^* = 3\pi/2$  when the upper plate reaches its maximum speed in a relaxation stage. It is noticed that inlet effects convect to large distances from the inlet as  $R_S$  increases. This is shown in Figure 7.1(b) where the core of the velocity profile becomes more flat at  $\xi=0.25$  as  $R_S$  increases. Further, it is observed at this time that the vorticity at both boundaries decreases as  $R_S$  increases while they are expected to increase during squeezing stages as  $R_S$  increases. Flow instabilities start to appear at larger  $R_S$  values during relief stages as shown in Figure 7.1(b). It is worth noting the values of  $R_S$  can be increased either by increasing the film thickness or by decreasing the fluid

viscosity and that the frequency of disturbance is kept constant since the squeezing number  $\sigma$  is kept constant.

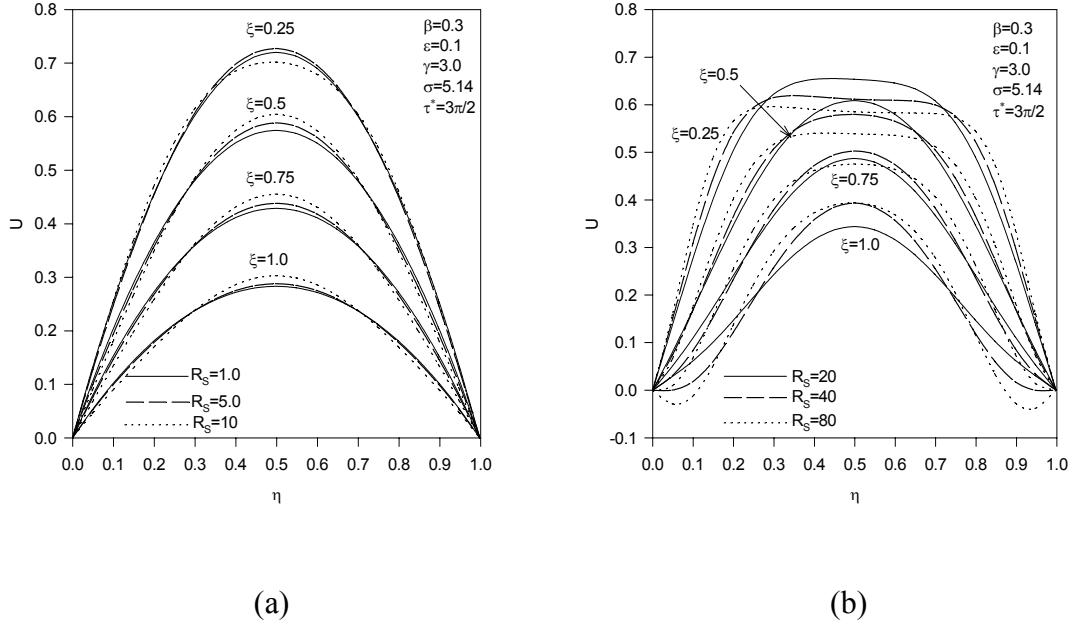


Figure 7.1: Effects of  $R_S$  on  $U$ : (a) Low  $R_S$  and (b) High  $R_S$

Although the average velocity at all times for the previous case is always positive, negative velocities appear near the lower plate for  $R_S$  greater than 40 as shown in Figure 7.1(b). This instability or flow separation is due to reductions in the flow kinetic energy and increases in fluid pressure as a result of upper plate relaxation. The critical  $R_S$  value that causes flow separations from both the lower and upper plates is found to decrease as the dimensionless slope  $\kappa$  increases as shown in Figure 7.2 for both CIV and CIF conditions, respectively. Figure 7.2 shows that constant inlet flow rate condition enlarge

exit flow instabilities during relief stages because flow kinetic energy is reduced due to reductions in inlet velocities and flow induced by vibration.

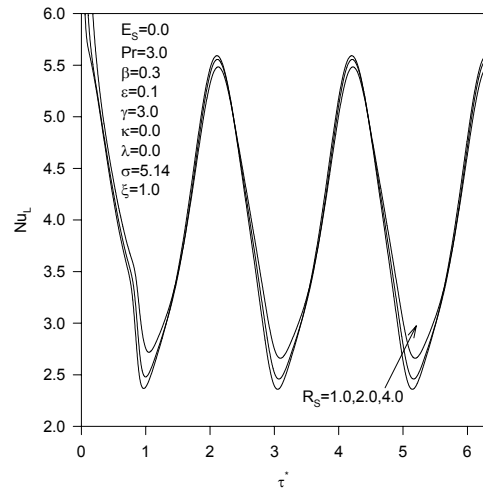
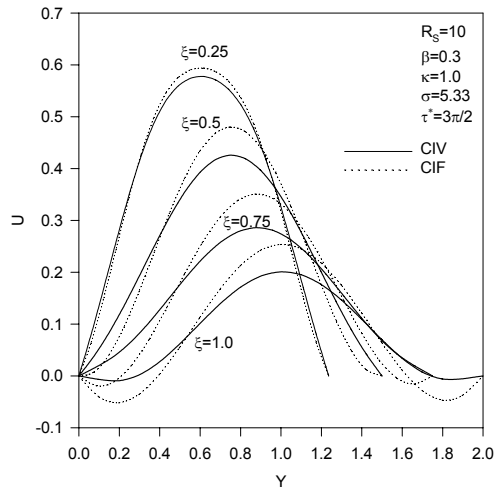


Figure 7.2: U for Divergent Film (High  $R_S$ )      Figure 7.3: Effects of  $R_S$  on  $Nu_L$  (CWT, 1)

Figures 7.3 and 7.4 represent the effects of  $R_S$  on the history of the local Nusselt numbers  $Nu_L$  at the exit of the thin film for CWT conditions. Variations in Nusselt numbers are significant in relaxation stages where fluid inertia, thermal transient effects and thermal convections are maximized due to increases in flow rates as the volume inside the thin film increases in these stages. This can be seen from Figures 7.3 and 7.4 for CWT conditions and from Figure 7.5 for UHF conditions. It is noticed from Figure 7.6 that there is no significant difference between the Nusselt number history for CIV and CIF conditions.

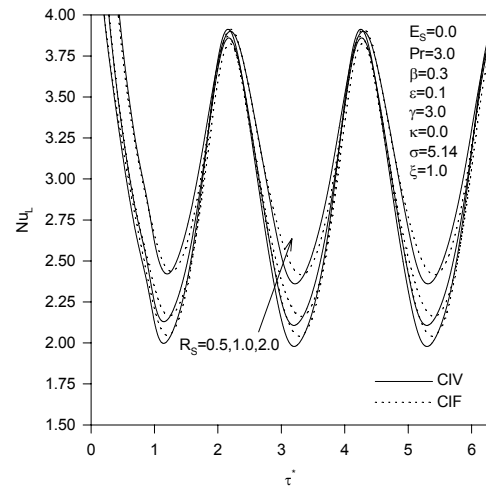
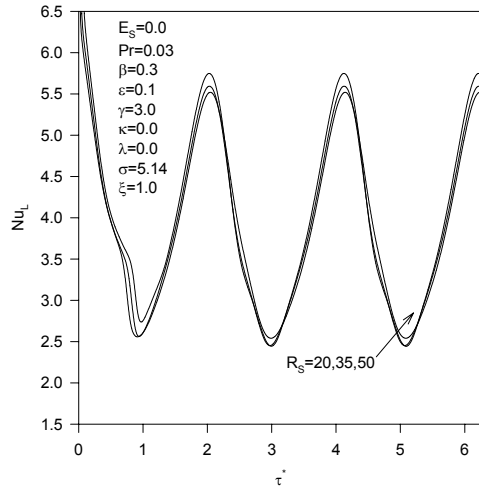


Figure 7.4: Effects of  $R_S$  on  $Nu$  (CWT, 2)      Figure 7.5: Effects of  $R_S$  on  $Nu_L$  (UHF)

The effects of  $R_S$  on mean bulk temperature  $\theta_m$  at dimensionless times  $\tau^* = 3\pi/2$ ,  $5\pi/3$ ,  $11\pi/6$  and  $2\pi$  is illustrated in Figure 7.6 for CWT conditions at constant frequency of disturbance and the Prandtl number. These values of dimensionless times represent the values when the upper plate has maximum speed in a relaxation stage, zero speed in a relaxation stage, maximum speed in a squeezing stage and zero speed in a squeezing stage, respectively. Increasing  $R_S$  can be achieved in this case by increasing the film thickness. As the film thickness increases, the flow rate increases. Accordingly, inlet conditions are furthermore convected toward the down stream as observed from Figure 7.6. It is also noticed that fluctuations in  $\theta_m$  at the exit is increased when  $R_S$  is increased as depicted from Figure 7.6.

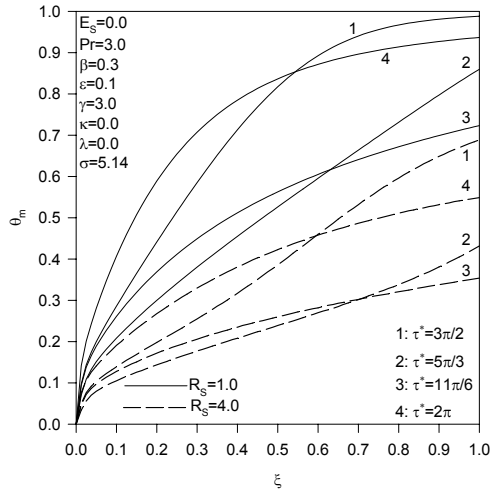


Figure 7.6: Effects of  $R_s$  on  $\theta_m$  (CWT)

Also, Figure 7.6 shows that maximum and minimum cooling effects near the inlet occur at  $\tau^* = 5\pi/3$  and  $\tau^* = 2\pi$ , respectively. This is because the flow at these times are maximum and minimum at  $\tau^* = 5\pi/3$  and  $\tau^* = 2\pi$ , respectively, while squeezing effects are minimum near the inlet. Far from the inlet, the maximum and minimum cooling effects occur at  $\tau^* = 11\pi/6$  and  $\tau^* = 3\pi/2$  as long as  $\sigma$  is large enough to cause increases in squeezing effects.

### 7.3 Effects of Varying the Squeezing Frequency

Figures 7.7 and 7.8 illustrate the effects of varying the squeezing frequency on the average dimensionless heat transfer  $\Theta$  and average  $\theta_w$  for CWT and UHF conditions, respectively, at relatively low frequencies. It is observed from Figure 7.7 that increasing the squeezing frequency resulted in an increase in both the delay phase shift between the plots and  $\tau^*$  and the variations in the average  $\Theta$ . Regarding UHF conditions, Figure 7.8 predicts

that fluctuations in average  $\theta_w$  decrease as the squeezing frequency increases for two different inlet flow conditions. For large squeezing frequencies, both fluctuations in average  $\Theta$  and  $\theta_w$  decrease as the squeezing frequency increases as shown in Figures 7.9 and 7.10. This is because changes that happen to the flow at large squeezing frequencies occur at fast rate as the frequency increases causing inefficient heat diffusion.

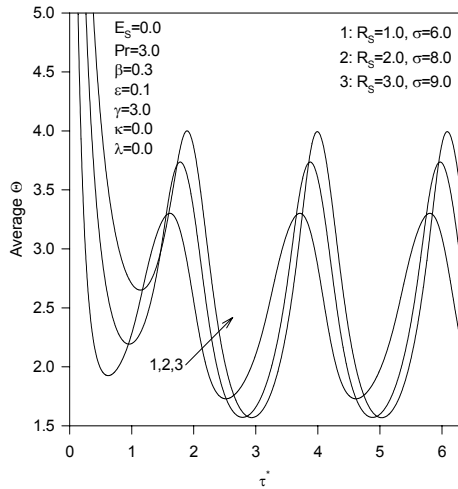


Figure 7.7: Effects of  $\omega$  on Average  $\Theta$

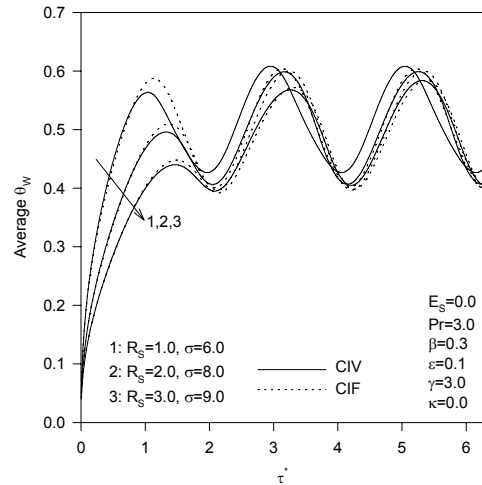


Figure 7.8: Effects of  $\omega$  on Average  $\theta_w$

Figures 7.9 and 7.10 shows that mean cooling effects for both conditions increase until reaching asymptotic values as squeezing frequency increases for large frequencies. These asymptotic values represent the average values of  $\Theta$  and  $\theta_w$  at zero amplitude of vibrations as shown in Figures 7.9 and 7.10. Also, these figures suggest that thermal disturbance effects due to external squeezing are more pronounced at relatively low squeezing frequencies which necessitate isolations of thin films against vibrations having lower frequencies.

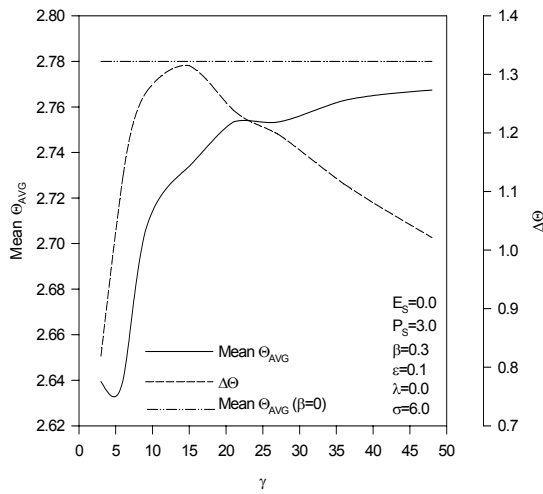


Figure 7.9: Effects of  $\omega$  on  $\Delta\Theta$  (CWT)

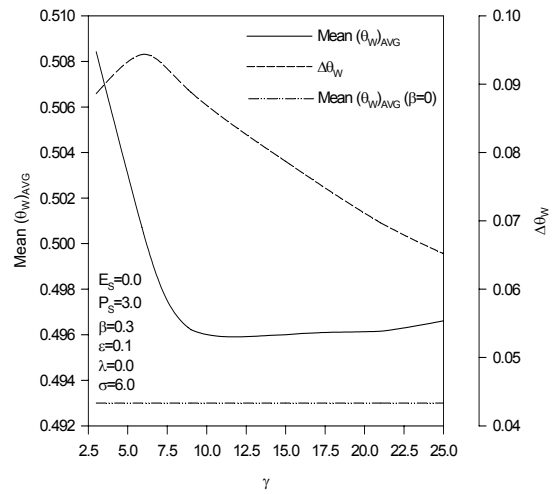
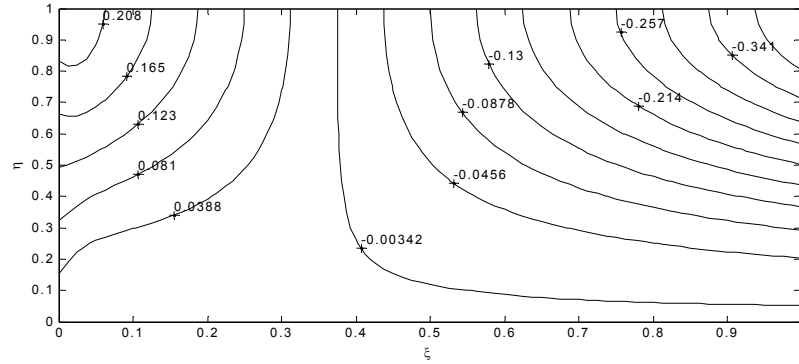


Figure 7.10: Effects of  $\gamma$  on  $\Delta\theta_W$  (UHF)

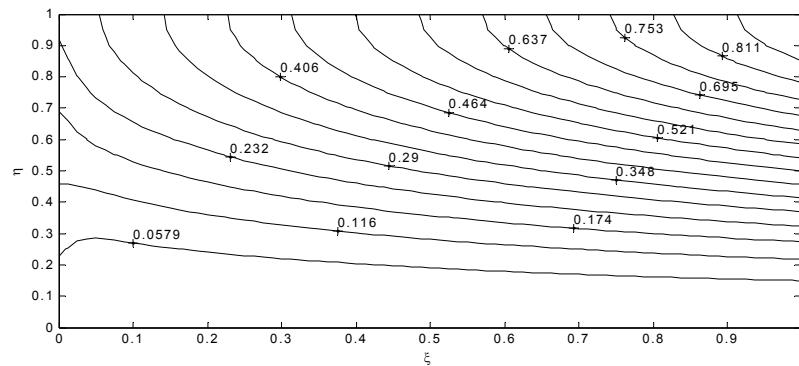
#### 7.4 Effects of Varying the Inlet Velocity

Figures 7.11(a) and 7.11(b) represent the contour plots for the stream lines at two different times,  $\tau^*=3\pi/2$  and  $11\pi/6$ , for  $\sigma=9$ . This case represents a case where the inlet velocity is small such that backflow is resulted during the relaxation stage as shown in Figure 7.11(a). It is noticed from Figure 7.11(a) and 7.11(b) that stream lines are directed toward the exit of the thin film and they are sloped towards the lower plate during squeezing stages. In relaxation stages, the stream lines are directed to the exit and they are sloped towards the upper plate before occurrence of the backflow. After the backflow, the stream lines are directed toward the inlet and they are tilted upwards. These can be shown in Figure 7.11(a). Figures 7.11(a) and 7.11(b) suggest that the least affected region

by the disturbance at the upper plate is the lower region and near the inlet of the thin film since variations in the slops stream lines is small in this region.



(a)



(b)

Figure 7.11: Stream lines: (a)  $\tau^* = 3\pi/2$  and (b)  $\tau^* = 11\pi/6$   
 (Pr=3.0,  $R_S=1.0$ ,  $\beta=0.3$ ,  $\varepsilon=0.1$ ,  $\gamma=3.0$ ,  $\kappa=0.0$ ,  $\sigma=9.0$ )

Figure 7.12(a) describes the axial behavior of  $\theta_m$  for two different inlet velocities for CWT conditions. The inlet velocity for the dashed lines is one third that for the solid lines. It is observed from this figure that both thermal entrance length and fluctuations in  $\theta_m$  are increased as the inlet velocity increases. Decreasing inlet flow rates result in more

heating to the fluid. Therefore, the values of  $\theta_m$  are increased as  $\sigma$  increases as shown in Figure 7.12(a). Flow fluctuations are expected to increase for CIV conditions and therefore fluctuations in the mean bulk temperature increases for CIV conditions compared to CIF conditions as shown in Figure 7.12(b).

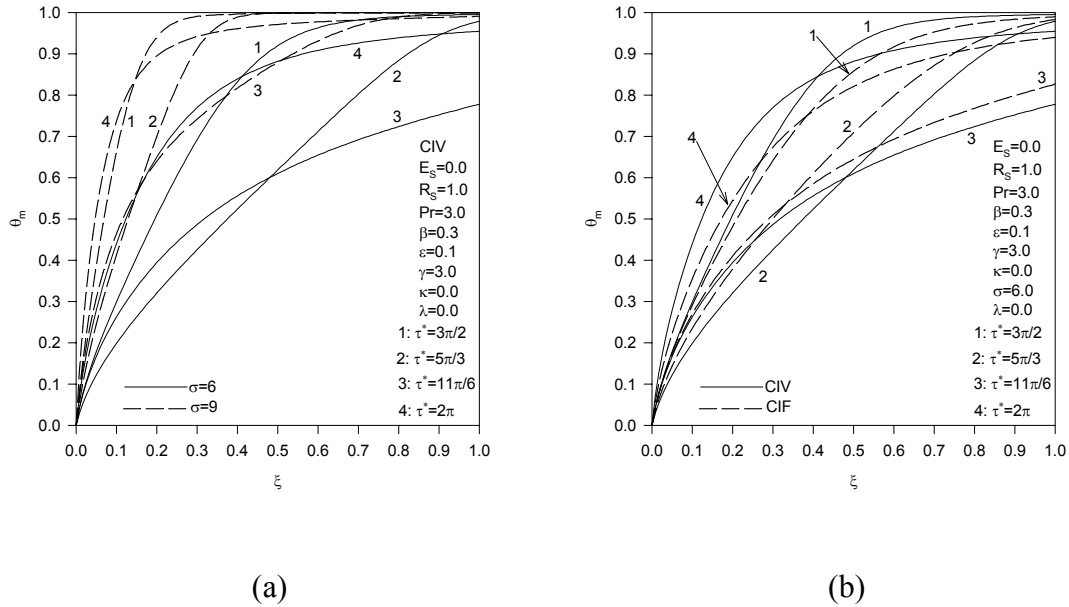
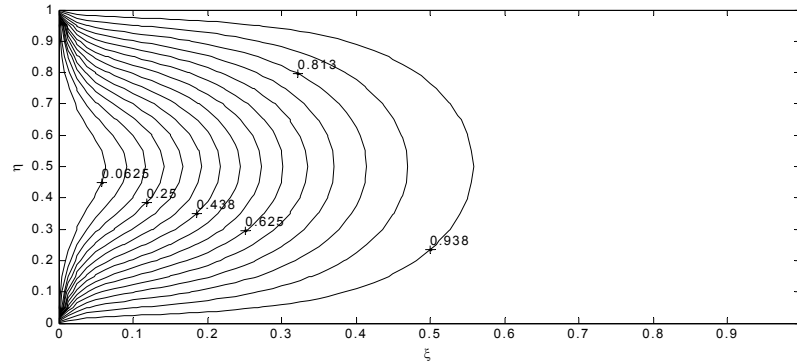
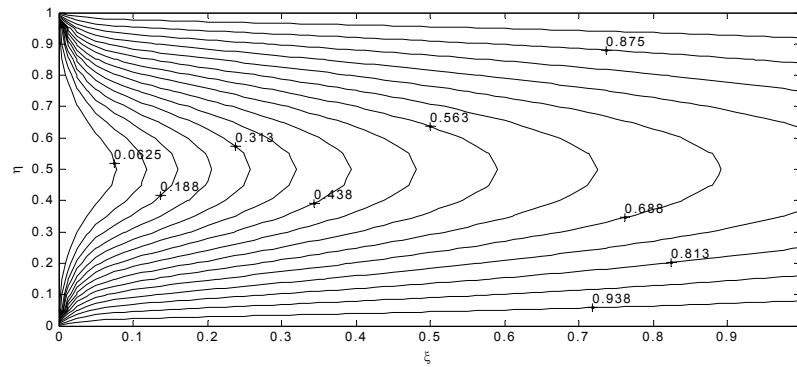


Figure 7.12: Effects of (a)  $V_0$  and (b) Inlet Flow Conditions on  $\theta_m$  (CWT)

Figures 7.13(a) and 7.13(b) show the contour plots for the isotherms at two different times,  $\tau^* = 3\pi/2$  and  $11\pi/6$  for  $\sigma=9$ , for CWT conditions. It is noticed from both figures that isotherms are almost symmetric. Further, more energy is being convected down streams in squeezing stages than in relaxation stages. Figures 7.13(a) and 7.13(b) suggest that the least affected region by the disturbance from thermal point of view is the exit region near either the lower or the upper plates. This is because the dimensionless temperature is almost unity.



(a)



(b)

Figure 7.13: Isotherms: (a)  $\tau^* = 3\pi/2$  and (b)  $\tau^* = 11\pi/6$

(Pr=3.0,  $R_S=1.0$ ,  $\beta=0.3$ ,  $\varepsilon=0.1$ ,  $\gamma=3.0$ ,  $\kappa=0.0$ ,  $\sigma=9.0$ , CWT)

### 7.5 Effects of Varying the Dimensionless Slope

Figures 7.14 and 7.15 explain the influences of dimensionless slope of the upper plate  $\kappa$  on the axial and normal velocity profiles at the exit of the thin film, respectively. Axial velocities and the corresponding shear rates increase as  $\kappa$  decreases as illustrated in Figure 7.14. For undisturbed thin films, the minimum normal velocities are for flat thin

films but convergent thin films have higher normal velocities than divergent ones because these velocities are proportional to the gradient of the axial velocities which is proportional to  $\kappa/(\kappa+1)^2$ . Yet the variation in normal velocities near the fixed plate of squeezed thin films can be minimized significantly for divergent thin films. This can be seen from Figure 7.15. Also, Equation 2.19(c) suggests that divergent cells having  $\kappa$  near unity have a minimized normal velocities near the lower plate for small values of  $\beta$  and at large values of  $\sigma$ .

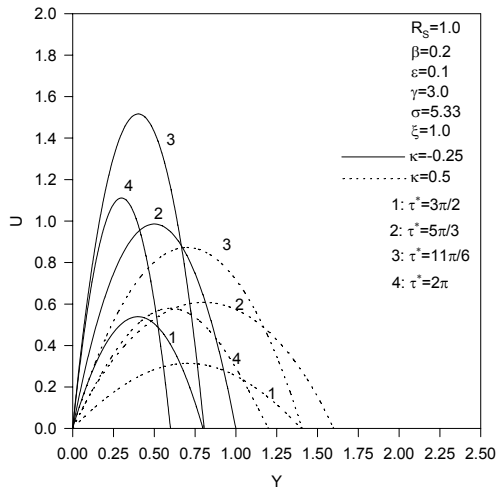


Figure 7.14: Effects of  $\kappa$  on U Profiles

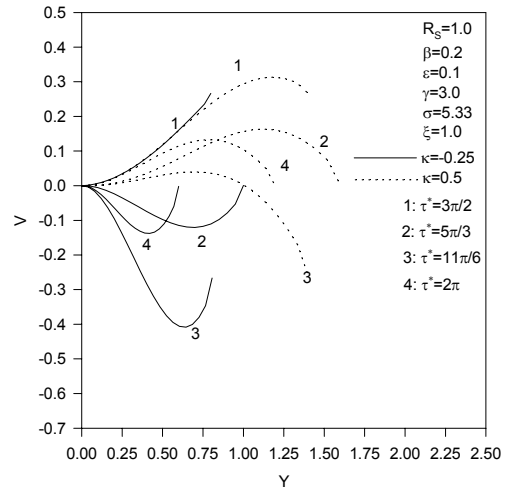


Figure 7.15: Effects of  $\kappa$  on V Profiles

The effects of  $\kappa$  on mean bulk temperature  $\theta_m$  and  $\theta_w$  at dimensionless times  $\tau^* = 3\pi/2, 5\pi/3, 11\pi/6$  and  $2\pi$  is exemplified in Figures 7.16 and 7.17 for CWT and UHF conditions, respectively. The values of  $\theta_m$  for the studied convergent thin film,  $\kappa = -0.2$ , are found to be greater than those for the studied divergent thin film,  $\kappa = 0.4$ . The

increased axial velocities in convergent thin films results in increasing the convective heat transfer coefficient. This in turn increases the heat transfer to the fluid for CWT conditions. Accordingly,  $\theta_m$  increases as  $\kappa$  increases. Further, increases in convective heat transfer coefficient causes  $\theta_w$  to decrease as shown in Figure 7.17. It is further noticed from Figures 7.16 that fluctuations in  $\theta_m$  at the exit of the thin film increase as  $\kappa$  increases.

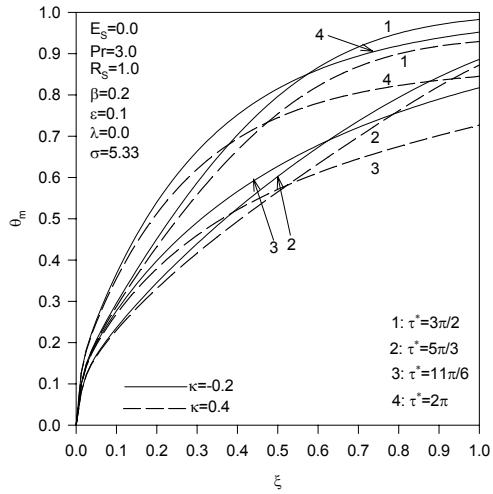


Figure 7.16: Effects of  $\kappa$  on  $\theta_m$  (CWT)

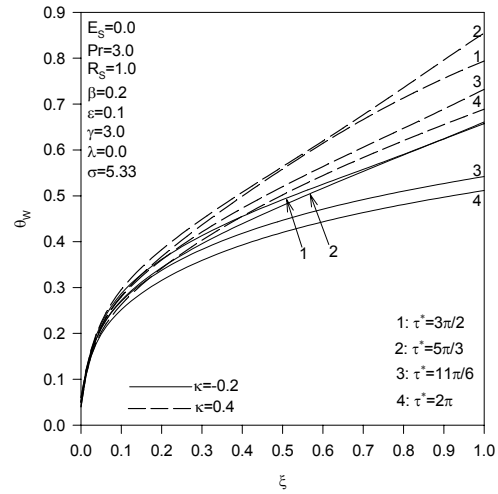
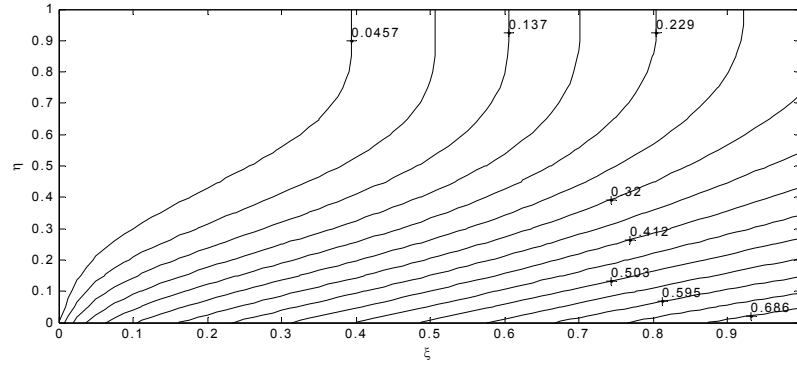
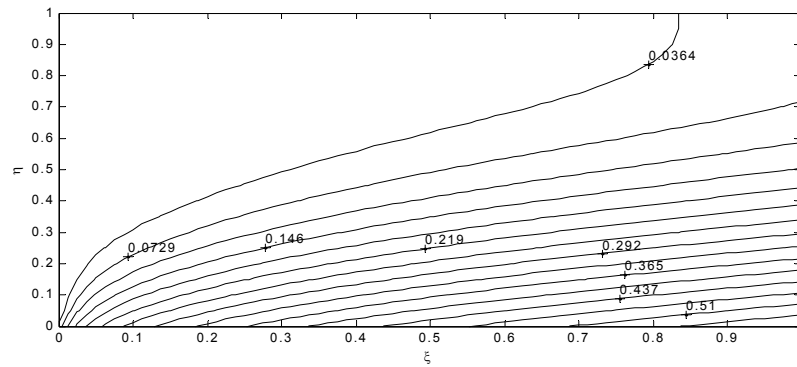


Figure 7.17: Effects of  $\kappa$  on  $\theta_w$  (UHF)

Figures 7.18(a) and 7.18(b) present the contour plots for the isotherms at two different times,  $\tau^* = 3\pi/2$  and  $11\pi/6$  for  $\sigma = 5.14$ , for a flat thin film at UHF conditions. It is noticed that more energy is being convected down streams during squeezing stages than during relaxation stages. The plots show that the least affected region by the disturbance from thermal point of view is the region close to the upper plate where heat transfer is minimized there.



(a)



(b)

Figure 7.18: Isotherms: (a)  $\tau^* = 3\pi/2$  and (b)  $\tau^* = 11\pi/6$

(Pr=3.0,  $R_S=1.0$ ,  $\beta=0.3$ ,  $\varepsilon=0.1$ ,  $\gamma=3.0$ ,  $\kappa=0.0$ ,  $\sigma=5.14$ , UHF)

It is clear from Figure 7.18 that axial gradients of the fluid temperature at the exit are not uniform. This arises from the fact that the assumption of the uniformity of the exit gradients of the temperature is not valid. Although this is true at certain times, the suggested thermal condition at the exit, Equation 2.48(d), produces small errors if it is applied near the inlet because it satisfies the integral energy balance as long as the perturbation parameter is small which ensures negligible conductions. Further, the

suggested boundary condition presented in Equation 6.4 can be applied resulting in reducing the errors associated with Equation 2.48(d).

Finally, it is noticed from Figure 7.19 that the effects of increasing  $R_S$  on the Nusselt number are dominant for divergent thin films and during relief stages. This figure is developed based on equal  $P_S$  values for each case to ensure a similar average thermal convection for each plot. The Nusselt number is found to decrease as  $R_S$  increases for divergent thin films because it is expected that velocities near the wall will decrease at larger rates during relief stages as  $R_S$  increases as can be seen from Figure 7.1.

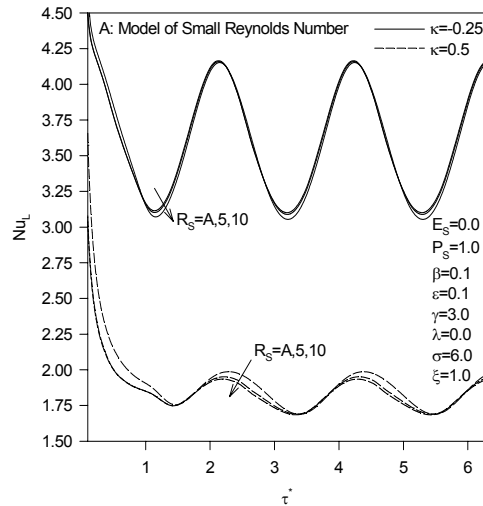


Figure 7.19: Inertia effects on  $Nu_L$  ( $P_S=const.$ , UHF)

## 7.6 Comments

It was found earlier that backflows and the disturbance level due to external squeezing can be reduced by using relatively short thin films. However, flow separations and flow instabilities start to appear at relatively large squeezing Reynolds numbers and especially for divergent thin films. One way to eliminate these instabilities in fluidic cells is to use convergent fluidic cells. However, variations in normal velocities inside disturbed convergent cells are higher than those for divergent cells. Also, the wall shear stress in convergent cells is relatively higher than that for divergent cells leading to a fact that the efficiency of the detection of the bioprobes may be reduced for convergent cells for certain applications as target molecules will be in contact with the receptor for short periods of times. Therefore, divergent cells are recommended to eliminate flow disturbances in the absence of flow instabilities while convergent cells are preferred when flow instabilities are encountered.

Most chemical and biological sensors are sensitive to the temperature such as bimaterial microcantilevers. The use of convergent cells as fluidic cells is found to reduce variations in fluid temperatures due to external disturbances as well decrease the thermal entrance length. Further, reducing inlet flow rates results in reducing the variations in fluid temperatures. Variations in fluid temperatures are found to be great only at relatively low squeezing frequency. This requires a design of fluidic cells that are highly isolated against external vibrations having small band of vibrating frequencies. If such a cell is designed, then convergent cells represent a good candidate for fluidic cells that can reduce bimaterial effects.

One of the bad influences of flow separations and instabilities is that they cause the Nusselt number to decrease especially during relief stages. This may affect the cooling capacity of microchannels or heat pipes in electronic cooling applications in the presence of disturbed conditions. Therefore, an additional factor of safety is needed in their designs to account for these disturbances. Finally, the presence of flow instabilities inside thin film channels when inertia of the fluid is not negligible can be eliminated by introducing hydromagnetic effects on the working fluid inside squeezed thin films. This will be discussed in the next chapter. As such, the performance of divergent fluidic cells can be improved.

## CHAPTER 8

### HYDROMAGNETIC CONTROL OF FLOW AND THERMAL EXIT CONDITIONS INSIDE OSCILLATORY SQUEEZED THIN FILMS

#### 8.1 Mathematical Model for the Magnetic Field Effects

In the presence of a uniform transverse magnetic field normal to the flow direction inside a flat thin film, the dimensional momentum equations for a flat squeezed thin film having its upper plate moving according to Equation (2.1) will be

$$\frac{\partial u}{\partial t} + u \frac{\partial u}{\partial x} + v \frac{\partial u}{\partial y} = -\frac{1}{\rho} \frac{\partial p}{\partial x} + \nu \left( \frac{\partial^2 u}{\partial x^2} + \frac{\partial^2 u}{\partial y^2} \right) - \frac{\sigma_m B_m^2}{\rho} u \quad (8.1)$$

$$\frac{\partial v}{\partial t} + u \frac{\partial v}{\partial x} + v \frac{\partial v}{\partial y} = -\frac{1}{\rho} \frac{\partial p}{\partial y} + \nu \left( \frac{\partial^2 v}{\partial x^2} + \frac{\partial^2 v}{\partial y^2} \right) \quad (8.2)$$

where  $\sigma_m$  and  $B_m$  are the electric conductivity of the fluid and the applied magnetic strength, respectively. The vorticity-stream function formulation resulted from Equation (8.1) and (8.2) are approximated by the following

$$\frac{\partial \Omega}{\partial t} + u \frac{\partial \Omega}{\partial x} + v \frac{\partial \Omega}{\partial y} = \nu \left( \frac{\partial^2 \Omega}{\partial x^2} + \frac{\partial^2 \Omega}{\partial y^2} \right) + \frac{\sigma_m B_m^2}{\rho} \frac{\partial u}{\partial y} \quad (8.3)$$

$$\frac{\partial^2 \Psi}{\partial x^2} + \frac{\partial^2 \Psi}{\partial y^2} = -\Omega \quad (8.4)$$

The last term in Equation (9.3),  $\frac{\partial u}{\partial y}$ , is of order  $\frac{V_o + \omega B}{h_o}$  which is much greater than

$\frac{\partial v}{\partial x}$  that is of order  $\frac{\varepsilon(V_o + \omega B)}{B}$ . Therefore it can be approximated by the vorticity  $\Omega$ . That

is Equation (8.3) can be approximated by the following for thin films filled with electrically conducting fluids in the presence of magnetic field normal to the flow:

$$\frac{\partial \Omega}{\partial t} + u \frac{\partial \Omega}{\partial x} + v \frac{\partial \Omega}{\partial y} = \nu \left( \frac{\partial^2 \Omega}{\partial x^2} + \frac{\partial^2 \Omega}{\partial y^2} \right) - \frac{\sigma_m B_m^2}{\rho} \Omega \quad (8.5)$$

Utilizing dimensionless variables listed in Equations (2.31) in Equations (8.5) results in

$$R_s \left( \frac{\partial \Omega^*}{\partial \tau} + \left( 1 + \frac{R_L}{R_s} \right) \left( \frac{\partial \Psi^*}{\partial Y} \frac{\partial \Omega^*}{\partial X} - \frac{\partial \Psi^*}{\partial X} \frac{\partial \Omega^*}{\partial Y} \right) \right) = \left( \varepsilon^2 \frac{\partial^2 \Omega^*}{\partial X^2} + \frac{\partial^2 \Omega^*}{\partial Y^2} \right) - H_a^2 \Omega^* \quad (8.6)$$

where  $Ha$  is the Hartmann number. It is equal to

$$Ha = \sqrt{\frac{\sigma_m}{\mu}} B_m h_o \quad (8.7)$$

The boundary conditions for the vorticity-stream function formulation are similar to those of Equations (2.36) and (2.37) where constant inlet average velocity is considered at the inlet.

### 8.1.1 Effects of the Magnetic Field on the Flow inside Squeezed Thin Films

Figures 8.1 and 8.2 show the influence of the square of Hartmann number  $Ha^2$  on dimensionless axial and normal velocity profiles at the exit, respectively. Imposition of a magnetic field normal to axial flow produces a resistive force. This force is called the Lorentz force which has a tendency to suppress the movement of the fluid. This suppression is noticed in Figure 8.1 where the core of the velocity profiles decreases as

Ha increases. However the uniformity of the velocity profiles increases as Ha increases. With regards to normal velocities, increases in the values of Ha is noticed to increase the variations in the dimensionless velocity profiles near the lower plate, yet these variations are small compared to the variations in the values of Ha. This can be noticed from Figure 8.2.

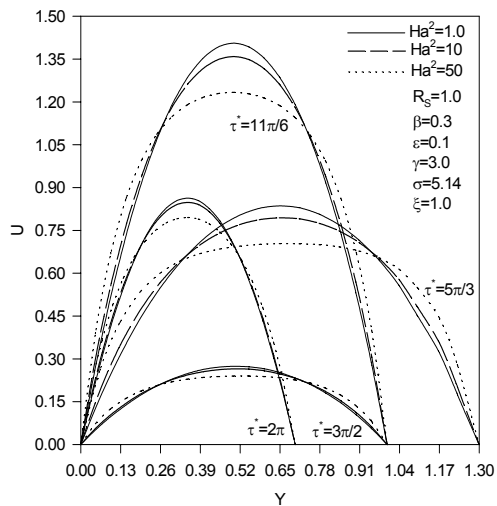


Figure 8.1: Effects of Ha on U

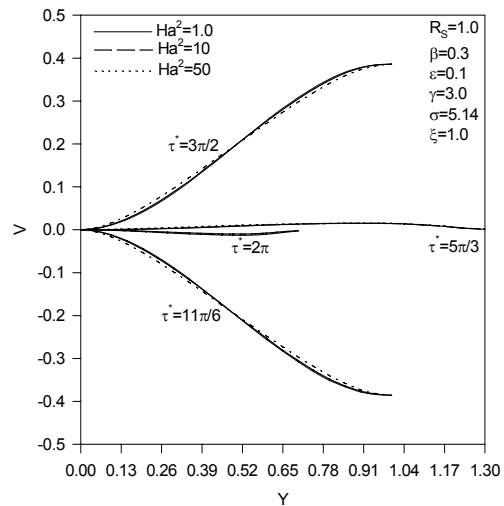


Figure 8.2: Effects of Ha on V

Figure 8.3 shows the effects of Ha on axial dimensionless velocity profiles for relatively large value of squeezing Reynolds number  $R_s$  at  $\tau^* = 3\pi/2$ . The increased uniformity in the velocity profile that resulted from the imposition of the normal magnetic field caused the fluid near the plates to have enough kinetic energy to overcome the instabilities due to increases in the pressure during relief stages.

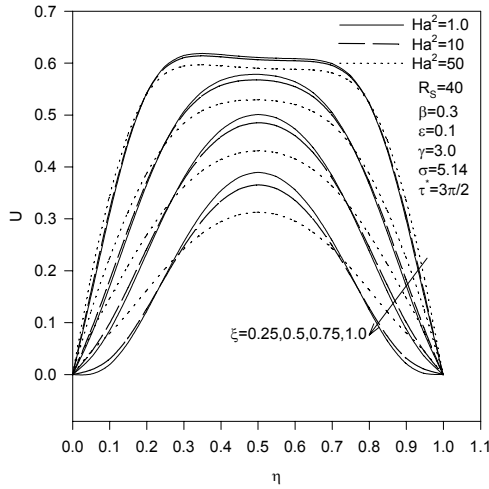


Figure 8.3: Effects of Ha on U (high  $R_S$ )

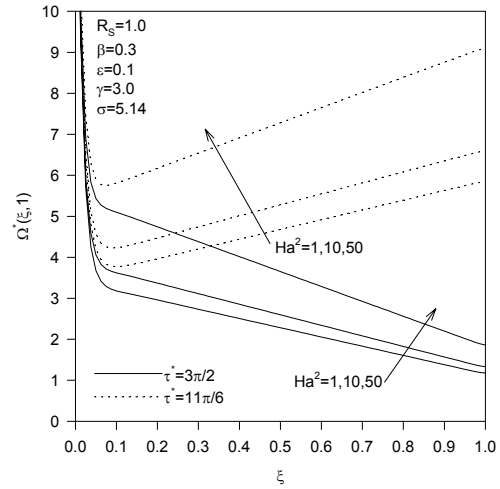


Figure 8.4: Effects of Ha on  $\Omega^*(\xi, 1)$

Figure 8.4 describes the effects of Ha on the axial distribution of the vorticity evaluated at the top surface  $\Omega^*(\xi, 1)$  of the thin film at two different times. It is noticed that  $\Omega^*(\xi, 1)$  increases as Ha increases due to increases in the Lorentz resistive force. This implies that surface stresses increases as Ha increases since wall shear stress is proportional to  $\Omega^*(\xi, 1)$ . Note that wall shear stresses increase as dimensionless axial distance  $\xi$  increases during squeezing periods while they decrease during relief stages as seen in Figure 8.4. While magnetic field resulted in a reduction in flow instabilities inside the thin film at large  $R_S$  values, it introduced larger flow resistances. As such, larger pumping power is required to maintain a constant average velocity.

### 8.1.2 Effects of the Magnetic Field on the Heat Transfer inside Squeezed Thin films

Figure 8.5 illustrates the effects of Ha on the Nusselt numbers for constant wall temperature CWT conditions. Increasing the magnetic strength when Ha increases results

in increasing the flow near the plates of the thin film resulting in increasing heat transfer at the thin film plates by convections thus Nusselt numbers increases as Ha increases for thin films having similar average flow rates. These increases in convective heat transfer are also noticeable for uniform wall heat flux UHF conditions as seen from Figure 9.6. Furthermore, Figures 8.5 and 8.6 show that fluctuations in the Nusselt numbers decrease as Ha increases.

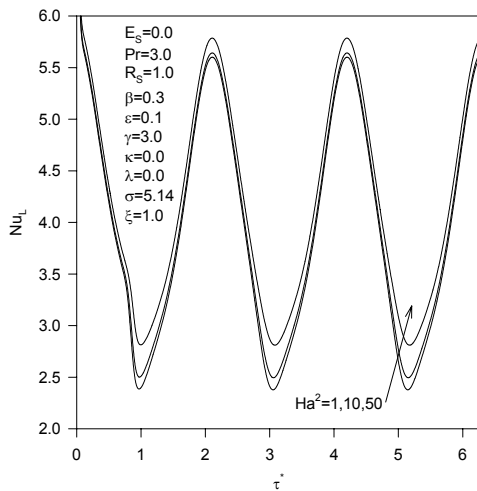


Figure 8.5: Effects of Ha on  $Nu_L$  (CWT)

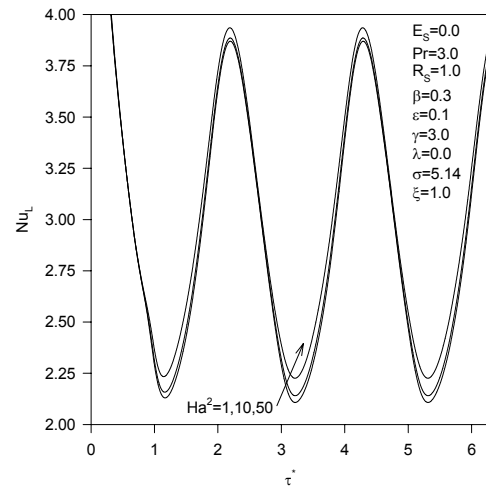


Figure 8.6: Effects of Ha on  $Nu_L$  (UHF)

Figure 8.7 displays the effects of Ha on the dimensionless temperature profiles at maximum squeezing velocity for CWT conditions. The plotted dimensionless temperature is the ratio of the difference between the wall temperature and the temperature at specific point to the difference between the wall temperature and the mean bulk temperature. This plotted temperature is found to increase slightly as Ha increases. This is because increases in heat transfer as a result of increases in Ha causes the mean

bulk temperature  $\theta_m$  to increase thus the difference between the wall temperature and  $\theta_m$  to decrease.

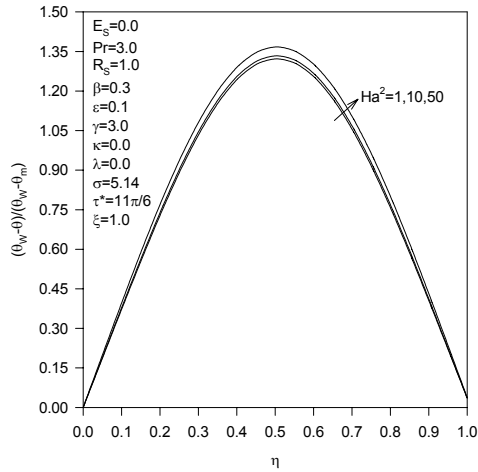


Figure 8.7: Effects of Ha on  $\theta$  (CWT)

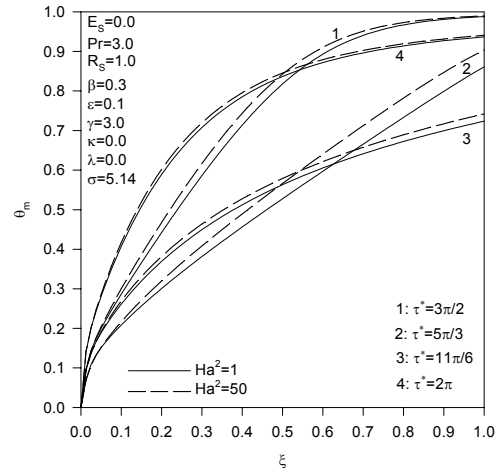


Figure 8.8: Effects of Ha on  $\theta_m$  (CWT)

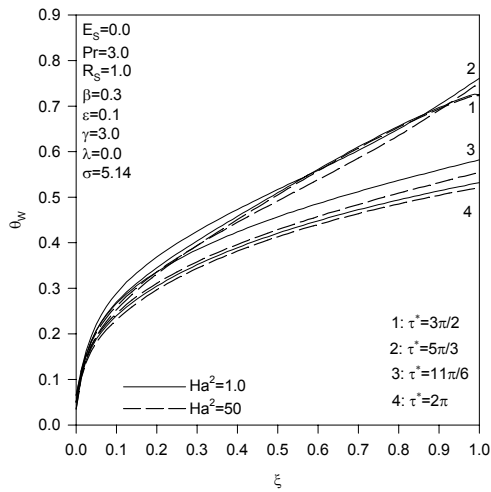


Figure 8.9: Effects of Ha on  $\theta_w$  (UHF)

Figure 8.8 demonstrates that the values of  $\theta_m$  increase as  $Ha$  increases for CWT conditions. For UHF conditions, increases in  $Ha$  cause increases in convective heat transfer coefficient which lower the temperature of the heated plate compared to the effects of having small values of  $Ha$  as seen from Figure 8.9.

### **8.3 Comments**

In the previous analysis, it is found that imposition of the magnetic field normal to the flow has mainly two influences on flow and heat transfer inside squeezed thin films: 1- Reducing the possibility of flow separations and flow instabilities near the plates of the thin film, and 2- Increasing heat transfer convections inside the thin films having similar inlet flow rates. By the analogy between heat and mass transfer, mass transfer to biosensors can be increased by hydromagnetic effects. Also, flow instabilities can be damped within fluidic cells in the presence of magnetic fields resulting in a reduction in the noise in the biosensor measurement. On the other hand, the variation in the normal velocity increases as the magnetic strength increases.

By imposing of a magnetic field normal to the flow direction, fluctuations in the temperature due to external squeezing will be reduced and the temperature will reach its far stream value at a shorter distance compared to cases where the magnetic field is not present. Thus, thermal noise in the measurement of many bimaterial sensors are expected to be reduced as the strength of the applied magnetic field is increased.

## CHAPTER 9

### EFFECTS OF INTERNAL PRESSURE PULSATIONS ON FLOW AND HEAT TRANSFER INSIDE OSCILLATORY SQUEEZED FLAT THIN FILMS

The plates of thin films are usually separated by seals as shown in Figure 9.1(a). These are elastic materials and can be deformed easily as a result of any external disturbances or changes that occur to the pressure inside the thin film. The effects of variations in external disturbances on flow and heat transfer inside thin films are studied in the previous chapters. In this chapter, the effects of pulsations in the inlet pressure on heat transfer characteristics will be analyzed inside thin films supported by soft seals. Also, the effects of the softness of the supporting seals are analyzed on flow and thermal characteristics inside thin films subject to oscillatory variations in both internal pressures and external disturbances. The supporting seals are considered soft because they can eliminate fluid leakage problems.

#### 9.1 Problem Formulation

The dimensionless pressure defined earlier in Equation 2.7(f) is reconsidered to be

$$\Pi = \frac{p - p_e}{\mu \left( \omega + \frac{V_o}{B} \right) \varepsilon^{-2}} \quad (9.1)$$

where  $p_e$  is constant representing the exit pressure. This will result in zero dimensionless pressure at the exit, i.e.  $\Pi_e = 0$ . Further, the inlet dimensionless pulsating pressure is considered to have the following relation:

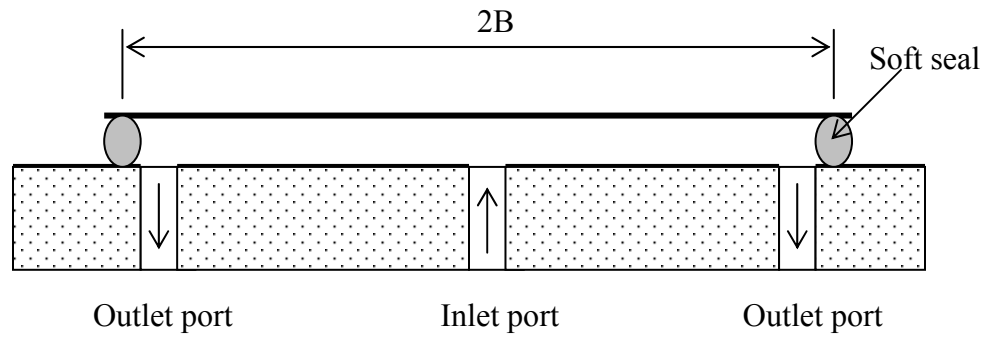
$$\Pi_i = \Pi_o(1 + \beta_p \sin(\gamma_p \omega t + \phi_p)) \quad (9.2)$$

where  $\beta_p$ ,  $\Pi_i$  and  $\Pi_o$  are the dimensionless amplitude in the pressure, inlet dimensionless pressure and the mean dimensionless pressure, respectively.  $\gamma_p$  and  $\phi_p$  are the dimensionless frequency of the pressure and a phase shift angle so that  $\Pi_i$  will have a more general form, respectively.

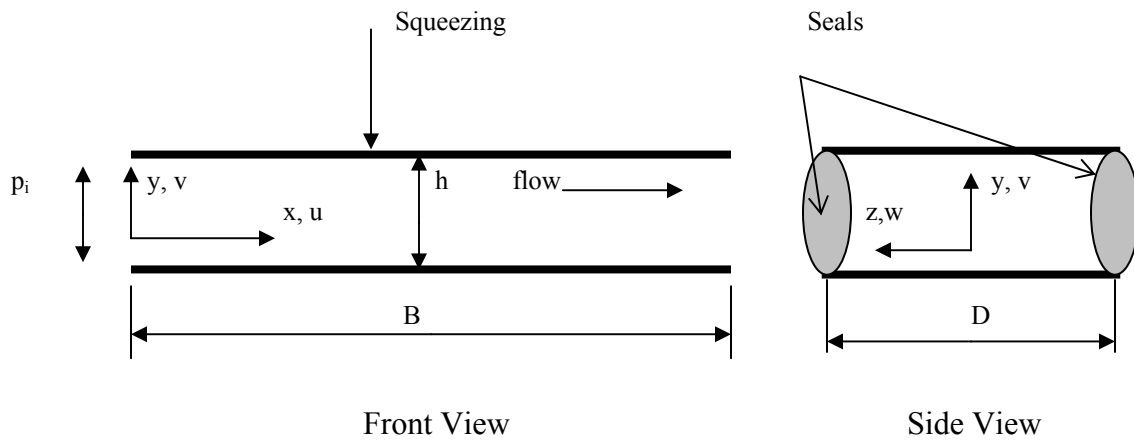
Due to both pulsations in internal pressure and external disturbances, the dimensionless film thickness, Equation (2.13), can be represented by the following:

$$H = 1 - \beta \cos(\gamma \omega t) + H_p \quad (9.3)$$

where  $H_p$  is dimensionless deformation of the seals that resulted from pulsations in the internal pressure. It is assumed that the lower plate is fixed and that the upper plate of the thin film is rigid such that the magnitude of the deformation in the seals is similar to displacement of the upper plate, Figure 9.1(a). The dimensionless deformation in the seals due variations in the external pressure is the second term of Equation 9.3 on the right. The dimensionless frequency  $\gamma$  is allowed to be different than  $\gamma_p$ .



(a)



(b)

Figure 9.1: (a) Schematic Diagram for a Thin Film and, (b) Coordinate system

Most flows inside thin films are laminar and could be creep flows especially in the applications of biological detection systems. Therefore, the model of low Reynolds numbers is adopted in this chapter. The dimensionless pressure gradient inside the thin film as a result of the solution to the Reynolds equation, Equation 2.17, for thin films is

$$\frac{\partial \Pi}{\partial X} = \frac{\sigma}{H^3} \frac{dH}{d\tau} \left( X - \frac{1}{2} \right) - \Pi_o \left( 1 + \beta_p \sin(\gamma_p \tau + \varphi_p) \right) \quad (9.4)$$

The reference velocity  $V_o$  that is used to define the dimensionless pressure, axial dimensionless velocity and the squeezing number is taken to be related to the average velocity,  $u_m$ , inside the thin film at zero  $\beta$  and  $\beta_p$  and the dimensionless thickness of the thin film that results from the application of the corresponding inlet mean pressure,  $H_m$ , through the following relation:

$$V_o = \frac{u_m}{H_m^2} \quad (9.5)$$

The previous scaled reference velocity is only function of the mean pressure, viscosity and the reference dimensions of the thin film and it results in the following relation between the inlet mean dimensionless pressure to the squeezing number:

$$\Pi_o = 12 - \sigma \quad (9.6)$$

Accordingly, the dimensionless pressure gradient, the dimensionless pressure and the average dimensionless pressure  $\Pi_{AVG}$  inside the thin film are related to the squeezing number through the following equations:

$$\frac{\partial \Pi}{\partial X} = \frac{\sigma}{H^3} \frac{dH}{d\tau} \left( X - \frac{1}{2} \right) - (12 - \sigma) \left( 1 + \beta_p \sin(\gamma_p \tau + \varphi_p) \right) \quad (9.7)$$

$$\Pi(X) = \frac{\sigma}{2H^3} \frac{dH}{d\tau} (X^2 - X) - (12 - \sigma) \left( 1 + \beta_p \sin(\gamma_p \tau + \varphi_p) \right) (X - 1) \quad (9.8)$$

$$\Pi_{AVG} = -\frac{\sigma}{12H^3} \frac{dH}{d\tau} + \frac{(12 - \sigma)}{2} \left( 1 + \beta_p \sin(\gamma_p \tau + \varphi_p) \right) \quad (9.9)$$

The average dimensionless change in the film thickness is related to the average dimensionless pressure inside the thin film fluidic cell  $\Pi_{AVG}$  through the theory of linear

elasticity. It assumes that the pressure force on the upper plate is linearly proportional to the average change in the thin film thickness (Boresi et. al., 1978), by the following relation:

$$H_p = F_n \Pi_{AVG} \quad (9.10)$$

It is assumed that in Equation (9.10) that the displacement of the upper plate due to internal pressure pulsations is independent on the axial coordinate. This serves as a good approximation and can be clearly seen in symmetrical thin films where the fluid is being injected from the center at the axis of symmetry, Figure 9.1(a). The injection can be made by syringe or peristaltic pumps.

The parameter  $F_n$  is named, the fixation parameter. A larger  $F_n$  value indicates softer sealing. The fixation parameter  $F_n$  is equal to

$$F_n = \frac{\mu(V_o + \omega B)D}{2(B + 0.5D)E\varepsilon^2 h_s} \quad (9.11)$$

where  $E$  and  $h_s$  are the effective modulus of elasticity and the effective dimension of the seal ( $h_s=h_o$  for a square seal cross section), respectively. The parameter  $F_n$  can have different forms depending on the type of the fixation of the thin film plates and whether the seals are originally unloaded or compressed. The parameter  $F_n$  becomes apparent when the thin film thickness is very small. The fixation parameter  $F_n$  represents a ratio between shear stresses inside thin films to the elastic forces exerted by the seal. The values of  $F_n$  are of order 0.001-0.1 for long thin films supported by soft seals.

Equation (9.10) is based on the assumption that the inertia effect of the upper plate is negligible. This effect, relative to stiffness of the seal, is proportional to  $(m\omega^2)/(EB)$  where  $m$  is the mass of the upper plate. The previous parameter is negligible

at low pulsation frequencies as in our studied cases. In large frequency applications, the film thickness may encounter resonance leading to instability in the film thickness response. Also, the assumptions of creep flows will not be valid at large frequencies and the problem becomes more complex.

The first set of dimensionless boundary conditions that will be used is for constant wall temperatures CWT at both the lower and the upper plates while the second set is by assuming that the lower plate is at uniform wall heat flux conditions UHF and the upper plate is insulated. As such the dimensionless boundary conditions can be written as

$$\begin{aligned} \text{CWT} \quad & \theta(X, Y, 0) = 0, \quad \theta(0, Y, \tau) = 0, \quad \theta(X, 0, \tau) = 1 \\ & \theta(X, H, \tau) = 1, \quad \frac{\partial}{\partial X} \left( \frac{1 - \theta(1, Y, \tau)}{1 - \theta_m(1, \tau)} \right) = 0 \end{aligned} \quad (9.12)$$

$$\begin{aligned} \text{UHF} \quad & \theta(X, Y, 0) = 0, \quad \theta(0, Y, \tau) = 0, \quad \frac{\partial \theta(X, 0, \tau)}{\partial Y} = -1 \\ & \frac{\partial \theta(X, H, \tau)}{\partial Y} = 0, \quad \frac{\partial \theta(1, Y/H, \tau)}{\partial X} = \frac{\sigma}{12U_m} \left( \frac{1}{P_s H} - \frac{\partial \theta(1, Y/H, \tau)}{\partial \tau} \right) \end{aligned} \quad (9.13)$$

The last condition of Equation (9.12) is based on the assumption that the flow at the exit of the thin film is thermally fully developed. Moreover, the last thermal condition of Equation (9.13) is derived based on an integral energy balance at the exit of the thin film realizing that the axial conduction is negligible at the exit. The calculated thermal parameters that will be considered are the Nusselt numbers at the lower and upper plates, and the dimensionless heat transfer from the upper and lower plates,  $\Theta$ , for CWT conditions. They are defined according to the following equations:

$$\begin{aligned}
\text{CWT} \quad \text{Nu}_U(X, \tau) &\equiv \frac{h_c h_o}{k} = \frac{1}{1 - \theta_m(X, \tau)} \frac{\partial \theta(X, H, \tau)}{\partial Y} \\
\text{Nu}_L(X, \tau) &\equiv \frac{h_c h_o}{k} = \frac{-1}{1 - \theta_m(X, \tau)} \frac{\partial \theta(X, 0, \tau)}{\partial Y} \\
\Theta(X, \tau) &= \left( \frac{\partial \theta(X, H, \tau)}{\partial Y} - \frac{\partial \theta(X, 0, \tau)}{\partial Y} \right)
\end{aligned} \tag{9.14}$$

$$\text{UHF} \quad \text{Nu}_1(X, \tau) \equiv \frac{h_c h_o}{k} = \frac{1}{\theta(X, 0, \tau) - \theta_m(X, \tau)} \tag{9.15}$$

## 9.2 Numerical Methods

The dimensionless thickness of the thin film was determined by solving Equations (9.3), (9.9) and (9.10) simultaneously. Accordingly, the velocity field,  $U$  and  $V$ , was determined from low Reynolds number flow model. The reduced energy equation was then solved using the Alternative Direction Implicit techniques (ADI) by transferring the problem to one with constant boundaries using the following transformations:  $\tau^* = \tau$ ,  $\xi = X$  and  $\eta = \frac{Y}{H}$ . Iterative solution was employed for the  $\xi$ -sweep of the energy equation for CWT conditions so that both the energy equation and the exit thermal condition, Equation (9.12), are satisfied. The values of 0.008, 0.03, 0.002 were chosen for  $\Delta\xi$ ,  $\Delta\eta$  and  $\Delta\tau^*$ .

## 9.3 Effects of Pressure Pulsations on the Dimensionless Film Thickness

Figures 9.2 and 9.3 describe the importance of the fixation parameter  $F_n$  on the dimensionless film thickness  $H$  and the dimensionless normal velocity at the upper plate  $V(X, H, \tau)$ , respectively. It is noticed that as  $F_n$  increases,  $H$  and absolute values of  $V(X, H, \tau)$  increase. It is worth noting that Soft fixations have large  $F_n$  values. Increases in

the viscosity and flow velocities or a decrease in the thin film thickness, perturbation parameter and the seal's modulus of elasticity increase the value of  $F_n$ .

The effects of pressure pulsations on  $H$  are clearly seen for large values of  $F_n$  as shown in Figures 9.2 and 9.3. At these values, the frequency of the local maximum or minimum of  $H$  is similar to the frequency of the pressure pulsations as seen from Figure 9.2. Further, the degree of turbulence at the upper plate is increased when  $F_n$  increases as shown in Figure 9.3. The fluctuations and the number of local maximum and minimum in  $V(X,H,\tau)$  are meant by the degree of turbulence at the upper plate. This is also obvious when the values of  $\gamma_p$  increase as shown in Figure 9.4. The increase in turbulence level at the upper plate may produce back flows inside the thin film at large values of  $\gamma_p$ . This affects the function of the thin film.

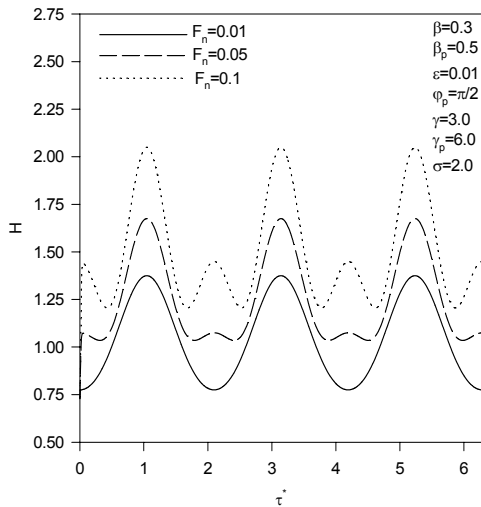


Figure 9.2: Effects of  $F_n$  on  $H$

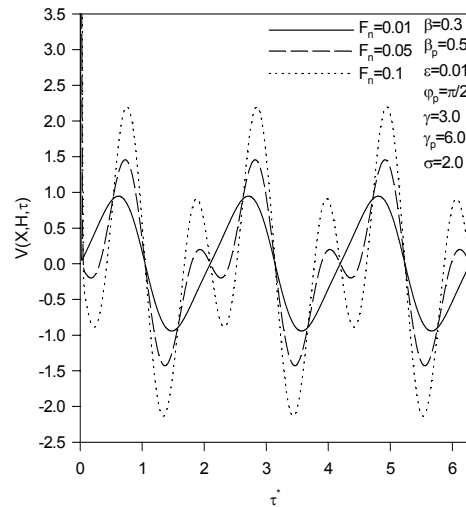


Figure 9.3: Effects of  $F_n$  on  $V(X,H,\tau)$

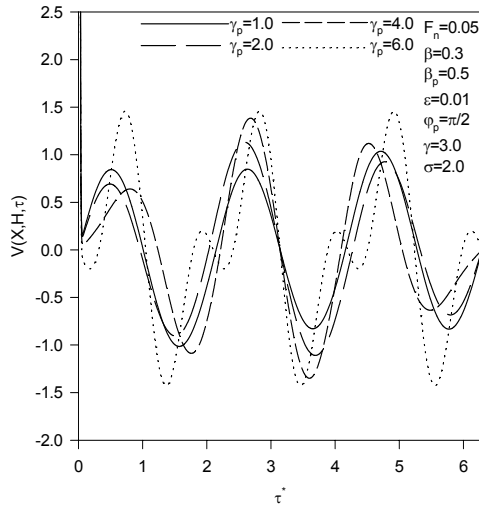


Figure 9.4: Effects of  $\gamma_p$  on  $V(X,H,\tau)$

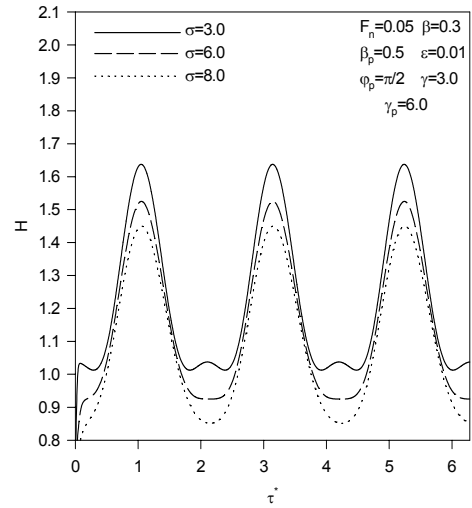


Figure 9.5: Effects of  $\sigma$  on  $H$

For  $\sigma=12$  where the time average of the average gage pressure inside the thin film is zero, the variation in  $H$  decreases as  $F_n$  increases. This effect can be seen from Equations (9.9) and (9.10) and will cause reductions in the flow and in the cooling process. However, the mean value of  $\Pi_{AVG}$  is always greater than zero for other values of  $\sigma$  which causes an increase in the mean value of  $H$  as  $F_n$  increases resulting in an increase in the mean value of the flow rate inside the thin film.

Figure 9.5 shows the effects of the squeezing number  $\sigma$  on  $H$ . Small values of  $\sigma$  indicates that the thin film is having relatively large inlet flow velocities thus it has large pressure gradients and large values of  $\Pi_0$ . Accordingly,  $H$  increases as  $\sigma$  decreases as seen in Figure 9.5. Further, it is noticed that the degree of turbulence at the upper plate increases as  $\sigma$  decreases. This is shown in Figure 9.6. The changes in the pressure phase

shift results in similar changes in the dimensionless thin film thickness phase shift as shown in Figure 9.7.

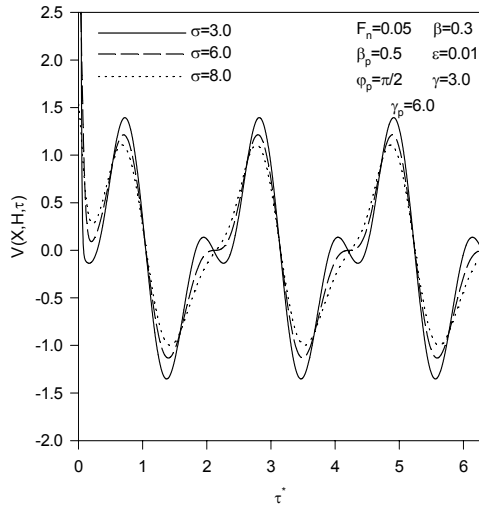


Figure 9.6: Effects of  $\sigma$  on  $V(X,H,\tau)$

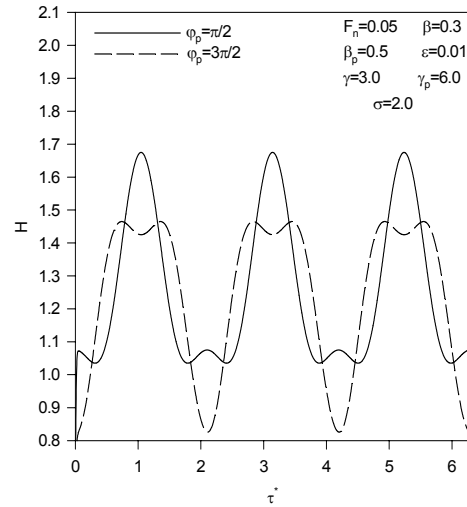


Figure 9.7: Effects of  $\phi_p$  on  $H$

#### 9.4 Effects of Pressure Pulsations on Heat Transfer Characteristics of Thin Films

Figures 9.8 and 9.9 illustrate the effects of  $F_n$  and  $P_s$  on the dimensionless mean bulk temperature  $\theta_m$  and the average lower plate temperature  $\theta_w$ , average of  $\theta(X,0,\tau)$ , for constant wall temperature CWT and uniform heat flux UHF conditions, respectively. As  $F_n$  increases when softer seals are used, the induced pressure forces inside the thin film due to internal pressure pulsations will increase the displacement of the upper plate as shown before. This enables the thin film to receive larger flow rates since all the cases presented in these figures have similar values for the dimensionless pressure at the inlet.

Thus, more cooling to the plates results as  $F_n$  increases resulting in a decrease in the  $\theta_m$  and average  $\theta_w$  values and their corresponding fluctuations for CWT and UHF conditions, respectively. The effect of the thermal squeezing parameter  $P_S$  on the cooling process is also shown in Figures 9.8 and 9.9. It is shown that the cooling at the plates is enhanced as  $P_S$  increases.

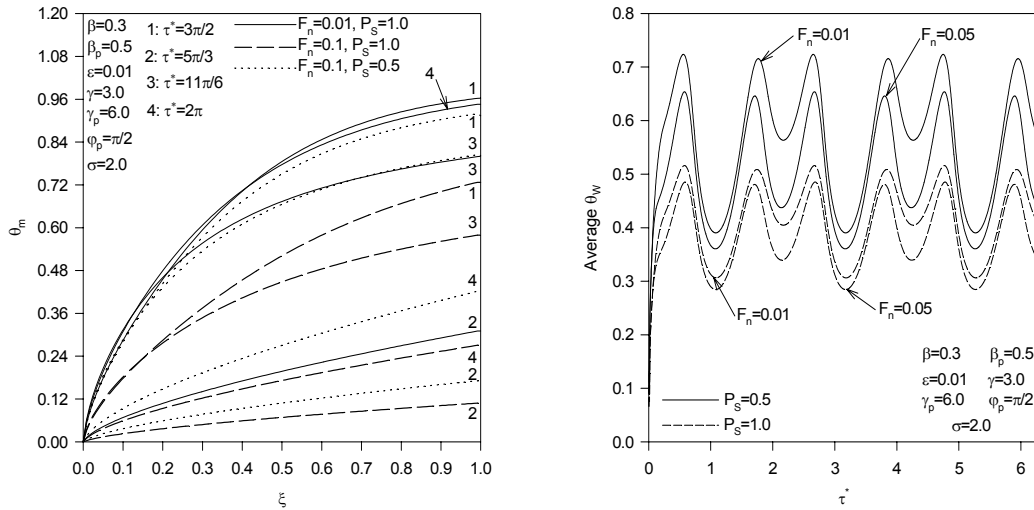


Figure 9.8: Effects of  $F_n$  and  $P_S$  on  $\theta_m$       Figure 9.9: Effects of  $F_n$  and  $P_S$  on  $\theta_w$  (UHF)

Figures 9.10 and 9.11 show the effects of  $F_n$  on the Nusselt number at the lower plate  $Nu_L$  for CWT and UHF conditions, respectively. It is noticed that the irregularity in  $Nu_L$  decrease as  $F_n$  decreases. This is because the upper plate will not be affected by the turbulence in the flow if the used seals have relatively large modulus of elasticity. In other word, the induced flow due to the upper plate motion is reduced as  $F_n$  decreases resulting in less disturbances to the flow inside the thin film. This can be seen in Figure 9.12 for UHF conditions where  $Nu_L$  reaches a constant value at low values of  $F_n$  after a

certain distance from the inlet. The values of  $Nu_L$  and the corresponding fluctuations are noticed to decrease as  $F_n$  increases.

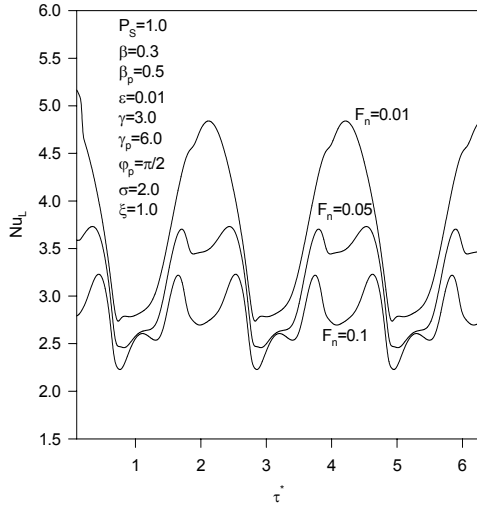


Figure 9.10: Effects of  $F_n$  on  $Nu_L$  (CWT)

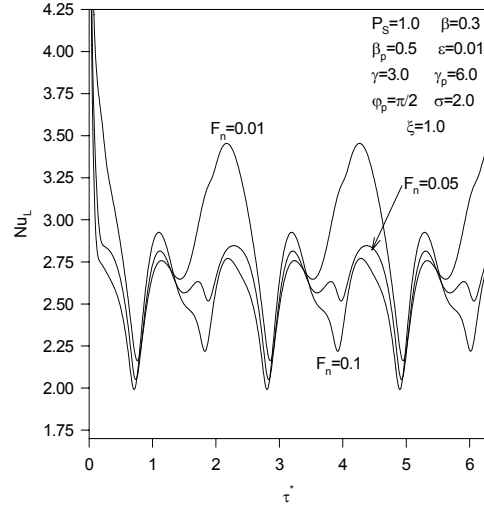


Figure 9.11: Effects of  $F_n$  on  $Nu_L$  (UHF)

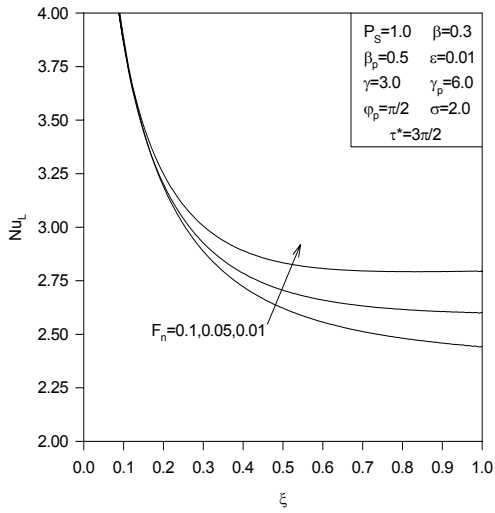


Figure 9.12:  $Nu_L$  versus  $\xi$  and  $F_n$  (UHF)

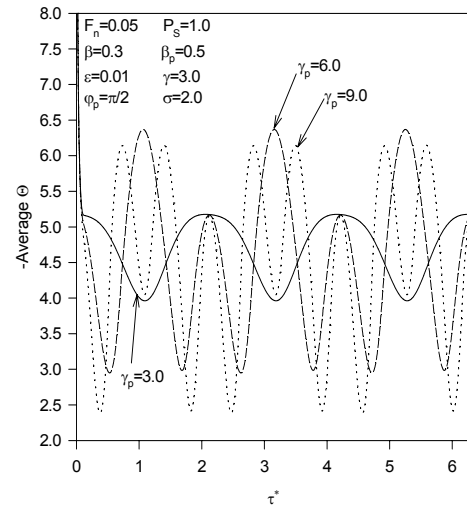


Figure 9.13: Effects of  $\gamma_p$  on Average  $\Theta$

Figures 9.13 and 9.14 illustrate the effects of dimensionless frequency of the inlet pressure pulsations  $\gamma_p$  on the average dimensionless heat transferred from the plates  $\Theta$  and the average  $\theta_w$  for CWT and UHF conditions, respectively. The figures show that the mean value of  $\Theta$  and  $\theta_w$  are unaffected by  $\gamma_p$  and that the frequency of the average values of  $\Theta$  and  $\theta_w$  increase as  $\gamma_p$  increases. Figure 9.15 describes the effects of  $\gamma_p$  on the fluctuation in the average  $\Theta$  and  $\theta_w$ , half the difference between the maximum and the minimum values of the average  $\Theta$  and  $\theta_w$ . The effects of  $\gamma_p$  on the fluctuation in the average  $\Theta$ ,  $\delta\Theta$ , and the fluctuation in the average  $\theta_w$ ,  $\delta\theta_w$ , are more pronounced at relatively lower values of  $\gamma_p$ .

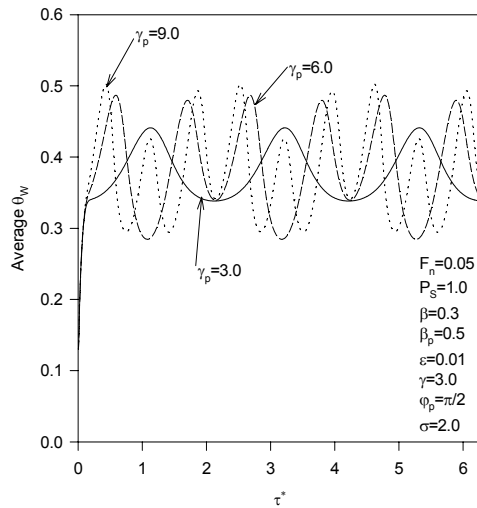


Figure 9.14: Effects of  $\gamma_p$  on Average  $\theta_w$

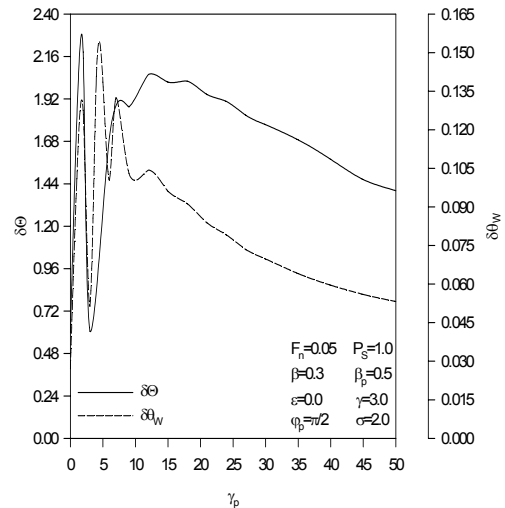


Figure 9.15: Effects of  $\gamma_p$  on  $\delta\Theta$  and  $\delta\theta_w$

## 9.5 Comments

So far, it was found that disturbances at the upper plate increase as both  $F_n$  and  $\gamma_p$  increase while they decrease as  $\sigma$  increases. The increase in the disturbance level at the upper plate result in an increase in fluctuations in both the axial and normal velocity components and may result in an increase in the fluctuation in the thermal behavior of the thin film especially at low frequency of inlet pressure pulsations. As such, the noise level in the measurements of many sensors inside fluidic cells will increase.

To eliminate these disturbances, it is recommended to decrease the value of  $F_n$ . That is to have stiff seals. However, leakage problems rise as the seals become stiffer. Another way to reduce the values of  $F_n$  is to consider working fluids with minimized viscosity. However, this will be the possibility for flow instabilities to occur as both the thickness of the thin film and frequency of vibration increase.

One of the methods that can be used to eliminate the disturbances at the upper plate is to try to reduce the frequency of the pressure pulsations or to eliminate them. This may be achieved by introducing the flow inside the thin film fluidic cell by gravitational effects because it will produce minimum pulsations.

## CHAPTER 10

### FLOW AND HEAT TRANSFER INDUCED BY NATURAL CONVECTIONS INSIDE AN OSCILLATORY SQUEEZED OPEN-END VERTICAL CHAMBER

#### 10.1 Mathematical Model

Figure 10.1 shows a schematic diagram for a vertical chamber which is open from the top. The laminar two-dimensional vorticity-stream function formulations that are applicable for this chamber and accounts for buoyancy forces are

$$\frac{\partial \Omega}{\partial t} + u \frac{\partial \Omega}{\partial x} + v \frac{\partial \Omega}{\partial y} = \nu \left( \frac{\partial^2 \Omega}{\partial x^2} + \frac{\partial^2 \Omega}{\partial y^2} \right) - g \beta_0 \frac{\partial T}{\partial y} \quad (10.1)$$

$$\frac{\partial^2 \Psi}{\partial x^2} + \frac{\partial^2 \Psi}{\partial y^2} = -\Omega \quad (10.2)$$

where  $\beta_0$  and  $g$  are the volumetric thermal expansion coefficient of the of the working fluid and the acceleration of the gravity, respectively. It is assumed that Boussinesq approximation is valid and that the x-axis is directed to the opposite direction of  $g$  as shown in Figure 10.1. Utilizing dimensionless variables listed in Equations (2.31) in Equations (10.1) and setting the reference velocity  $V_0$  to zero results in

$$\frac{\partial \Omega^*}{\partial \tau} + \frac{\partial \Psi^*}{\partial Y} \frac{\partial \Omega^*}{\partial X} - \frac{\partial \Psi^*}{\partial X} \frac{\partial \Omega^*}{\partial Y} = \frac{1}{R_s} \left( \varepsilon^2 \frac{\partial^2 \Omega^*}{\partial X^2} + \frac{\partial^2 \Omega^*}{\partial Y^2} \right) - \frac{Gr}{R_s^2} \varepsilon \frac{\partial \theta}{\partial Y} \quad (10.3)$$

where Gr is the Grashof number. It is equal to

$$Gr = \frac{g\beta_o(T_2 - T_1)h_o^3}{\nu^2} \quad (10.4)$$

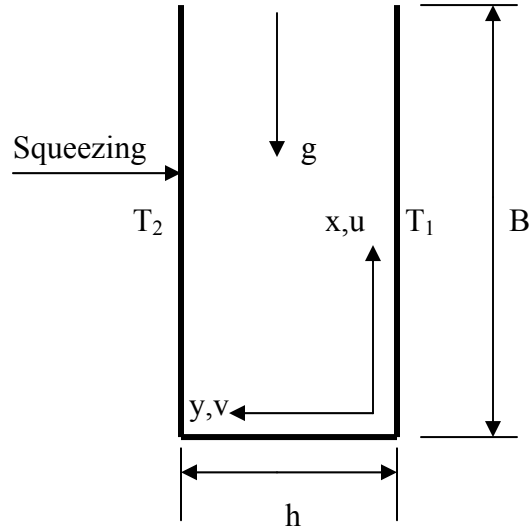


Figure 10.1: Schematic Diagram

The dimensionless stream function formulation and the dimensionless energy equation can be reduced to the following when  $V_o$  is set to zero:

$$\left( \varepsilon^2 \frac{\partial^2 \Psi^*}{\partial X^2} + \frac{\partial^2 \Psi^*}{\partial Y^2} \right) = -\Omega^* \quad (10.5)$$

$$\left( \frac{\partial \theta}{\partial \tau} + \frac{\partial \Psi^*}{\partial Y} \frac{\partial \theta}{\partial X} - \frac{\partial \Psi^*}{\partial X} \frac{\partial \theta}{\partial Y} \right) = \frac{1}{R_s Pr} \left( \varepsilon^2 \frac{\partial^2 \theta}{\partial X^2} + \frac{\partial^2 \theta}{\partial Y^2} \right) \quad (10.6)$$

Notice that as the perturbation parameter decreases, buoyancy effects decreases. The dimensionless boundary conditions that are suitable for the studied problem are:

$$\begin{aligned}
\Psi^*(0, Y, \tau) = 0, \quad \frac{\partial^2 \Psi^*(1, Y, \tau)}{\partial X^2} = 0 \\
\Psi^*(X, 0, \tau) = 0, \quad \Psi^*(X, H, \tau) = -X\beta\gamma \sin(\gamma\tau) \\
U(0, Y, \tau) = 0, \quad U(X, 0, \tau) = 0, \quad U(X, H, \tau) = 0 \\
V(X, 0, \tau) = 0, \quad V(X, H, \tau) = \gamma\beta \sin(\gamma\tau)
\end{aligned} \tag{10.7}$$

$$\begin{aligned}
\Omega^*(0, Y, \tau) = -\varepsilon^2 \frac{\partial^2 \Psi^*(0, Y, \tau)}{\partial X^2}, \quad \frac{\partial^2 \Omega^*(1, Y, \tau)}{\partial X^2} = 0 \\
\Omega^*(X, 0, \tau) = -\frac{\partial U(X, 0, \tau)}{\partial Y}, \quad \Omega^*(X, H, \tau) = -\frac{\partial U(X, H, \tau)}{\partial Y}
\end{aligned} \tag{10.8}$$

$$\begin{aligned}
\theta(X, 0, \tau) = 0, \quad \theta(X, H, \tau) = 1 \\
\theta(0, Y, \tau) = 0, \quad \frac{\partial \theta(1, Y, \tau)}{\partial X} = 0 \\
\theta(X, Y, 0) = 0
\end{aligned} \tag{10.9}$$

The isothermal cold wall conditions used in Equations (10.9) were found to enhance the convection (Sezai and Mohamad, 2000). The left wall was heated except near the lower left corner to avoid the discontinuity in the temperature. That is, the boundary condition  $\theta(X, H, \tau) = 1$  is valid when  $X > \Delta X / 2$  below which this wall is insulated ( $\Delta X$ : step size along  $X$ ). The Nusselt numbers at the left and right walls are defined as follows:

$$\begin{aligned}
Nu_L(X, \tau) = \frac{1}{1 - \theta_{AVG}(X, \tau)} \frac{\partial \theta(X, H, \tau)}{\partial Y} \\
Nu_R(X, \tau) = \frac{1}{\theta_{AVG}(X, \tau)} \frac{\partial \theta(X, 0, \tau)}{\partial Y}
\end{aligned} \tag{10.10}$$

where  $\theta_{AVG}$  is defined as follows:

$$\theta_{AVG}(X, \tau) = \frac{1}{H} \int_0^H \theta(X, Y, \tau) dY \tag{10.11}$$

## 10.2 Analytical Solution for a Special Case

Equations (10.3) and (10.6) can be reduced to the following for small values of the following parameters:  $R_s$ ,  $Pr$  and  $\varepsilon$  numbers

$$\frac{\partial^2 \Omega^*}{\partial Y^2} = \frac{Gr}{R_s} \varepsilon \frac{\partial \theta}{\partial Y} \quad (10.12)$$

$$\frac{\partial^2 \theta}{\partial Y^2} = 0 \quad (10.13)$$

Accordingly, the dimensionless analytical solutions for the velocities, temperature and thermal parameters are listed below for the first case:

$$U(X, Y, \tau) \equiv \frac{u}{\omega B} = -\frac{Gr}{R_s} \varepsilon H^2 \left[ \frac{1}{6} \left( \frac{Y}{H} \right)^3 - \frac{1}{4} \left( \frac{Y}{H} \right)^2 + \frac{1}{12} \left( \frac{Y}{H} \right) \right] + \frac{6X\beta\gamma \sin(\gamma\tau)}{H} \left[ \left( \frac{Y}{H} \right)^2 - \left( \frac{Y}{H} \right) \right] \quad (10.14)$$

$$V(X, Y, \tau) \equiv \frac{v}{h_o \omega} = \beta\gamma \sin(\gamma\tau) \left[ 3 \left( \frac{Y}{H} \right)^2 - 2 \left( \frac{Y}{H} \right)^3 \right] \quad (10.15)$$

$$\theta(X, Y, \tau) = \left( \frac{Y}{H} \right) \quad (10.16)$$

$$Nu_L = Nu_R = \frac{2.0}{H} \quad (10.17)$$

The numerical procedure is similar to that discussed in chapter 4. The values of  $\Delta X$ ,  $\Delta(Y/H)$ ,  $\Delta\tau$ , the maximum error for both the stream function and the iterations for the velocity field were chosen to be 0.0125, 0.04, 0.001 and  $10^{-6}$ , respectively. The numerical results of Equations (10.3-6) for the dimensionless axial velocities are in excellent agreement with the Equation (10.14) as shown in Figure 10.2. As such, a parametric study is performed to investigate the effects of external squeezing on natural convection inside vertical chambers.

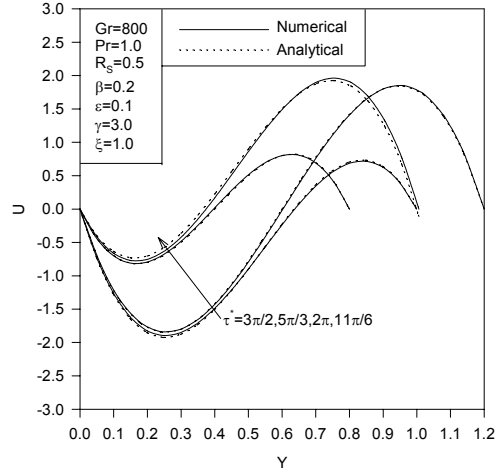


Figure 10.2: Validation for Numerical Results

### 10.3 Contours of Stream lines and Isotherms

Figure 10.3 shows the effects of the  $Gr$  on the stream lines for an oscillatory squeezed vertical chamber. It is noted that a cell originates at the lower right portion of the chamber at relatively low values of Grashof number during squeezing stages,  $5\pi/3 \leq \tau^* \leq 2\pi$ . As the  $Gr$  increases, suction velocities near the right wall increase such that they can exceed the induced squeezed velocities due to vibration or squeezing. As a result, this cell collapses and the flow achieves normal conditions for large  $Gr$  values. This could create a problem in controlling the outdoor vibrations since they can isolate the measuring device for certain times resulting in inaccurate measurements. Figure 10.4 illustrates the effects of  $R_s$  on the corresponding isotherms. It is noticed that as  $R_s$  increases, axial convection increases resulting in a maximum convections around  $\tau^* = 11\pi/6$ . Note that  $R_s$  can be increased by increasing the vibrational frequency.

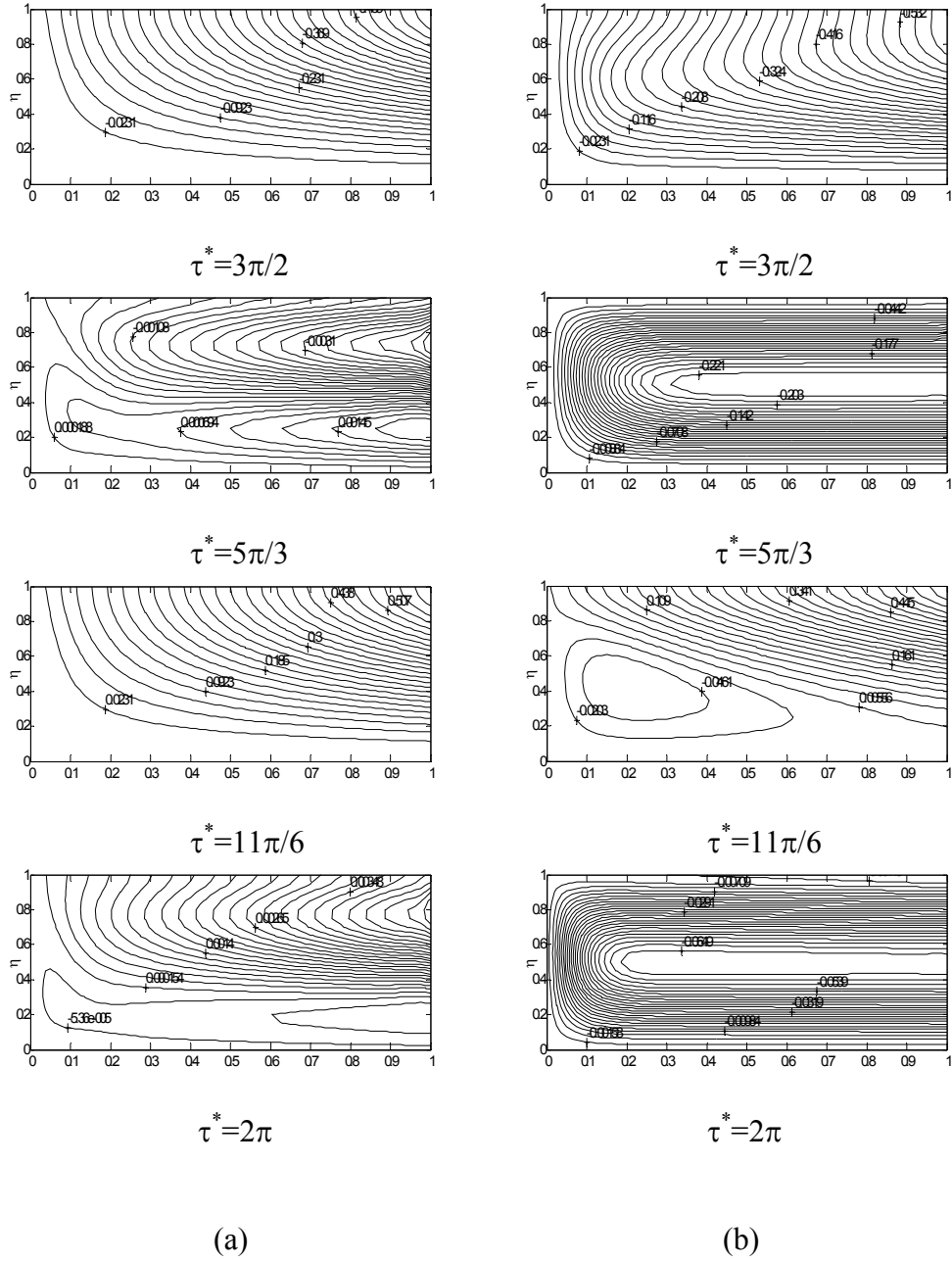


Figure 10.3: Dimensionless Stream Lines:  
 (a)  $\frac{Gr}{R_S} = 0.0$ , (b)  $\frac{Gr}{R_S} = 200$ , (c)  $\frac{Gr}{R_S} = 600$  and (d)  $\frac{Gr}{R_S} = 1200$   
 ( $Pr=1.0$ ,  $R_S=1.0$ ,  $\varepsilon=0.25$ ,  $\beta=0.2$ ,  $\gamma=3.0$ )

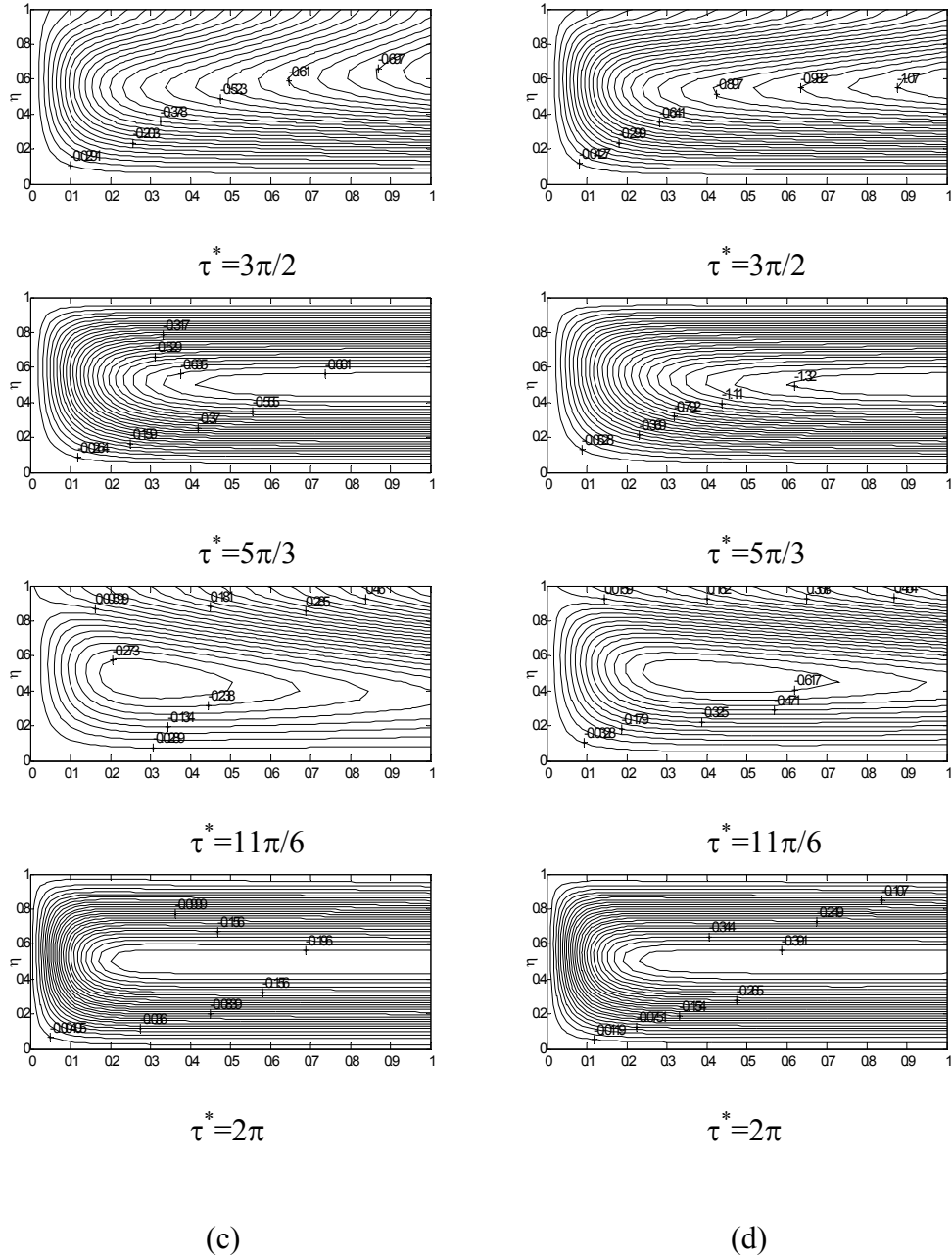


Figure 10.3: Dimensionless Stream Lines:  
(a)  $\frac{Gr}{R_S} = 0.0$ , (b)  $\frac{Gr}{R_S} = 200$ , (c)  $\frac{Gr}{R_S} = 600$  and (d)  $\frac{Gr}{R_S} = 1200$   
(Pr=1.0,  $R_S=1.0$ ,  $\varepsilon=0.25$ ,  $\beta=0.2$ ,  $\gamma=3.0$ ).....Continued

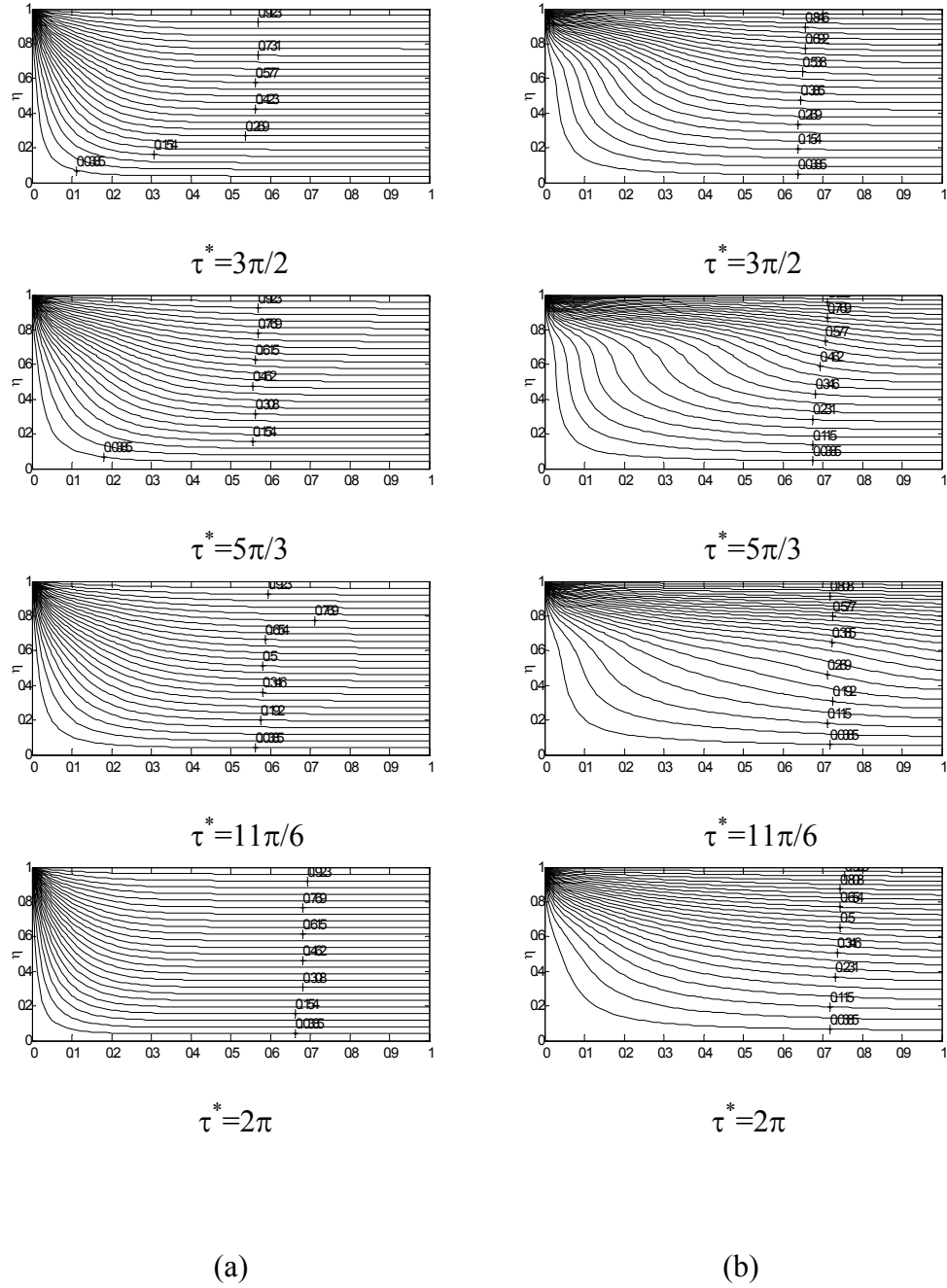


Figure 10.4: Dimensionless Isotherms (a)  $R_S=1.0$ , (b)  $R_S=10$   
 $(Pr=1.0, \frac{Gr}{R_S} = 600, \varepsilon=0.25, \beta=0.2, \gamma=3.0)$

#### 10.4 Effects of $R_S$ and $Gr$ on Average Nusselt Numbers

Equation 10.14 suggests that vibrations affect both buoyancy forces and the flow induced by the motion of the wall. This interaction between vibrations and the oscillatory buoyancy forces resulted from variations in the channel thickness cause the trend of the average Nusselt number to change according to Figure 10.5 as  $\frac{Gr}{R_S}$  increases. Figure 10.5

shows that amplitude of oscillations for Nusselt numbers decrease as  $\frac{Gr}{R_S}$  increases at the

vibrated wall because a substantial increase in the Nusselt number at maximum thickness is expected due to buoyancy effects. Fluid temperatures inside the channel are expected to decrease as the Grashof number increases due to enhancements in thermal convections.

Therefore, average Nusselt numbers at the vibrated wall increase as  $\frac{Gr}{R_S}$  increases while it

is decreased at the fixed wall with increases in  $\frac{Gr}{R_S}$  as clearly seen from Figure 10.5. The

suggested correlations that are presented at the end of this chapter show that mean Nusselt numbers are less affected by  $R_S$  at fixed values of  $Gr$ .

#### 10.5 Effects of $R_S$ and $Gr$ on Flow inside Vertical Chambers

Dimensionless axial velocity profiles are seen in Figure 10.6 at four different times. It can be seen that induced velocities increase as  $\frac{Gr}{R_S}$  increases. Also, it is noticed

that as  $R_S$  increases, the flow becomes more attached to the left wall, the source of disturbance. The effects of  $\frac{Gr}{R_S}$  on dimensionless vorticity at the right wall  $\Omega^*(\xi,0)$  are

shown in Figures 10.7 for two different  $R_S$  values. As  $\frac{Gr}{R_S}$  increases,  $\Omega^*(\xi, 0)$  increases.

Further, it should be noted that as  $R_S$  increases, instabilities in  $\Omega^*(\xi, 0)$  start to appear at larger values of  $\frac{Gr}{R_S}$ .

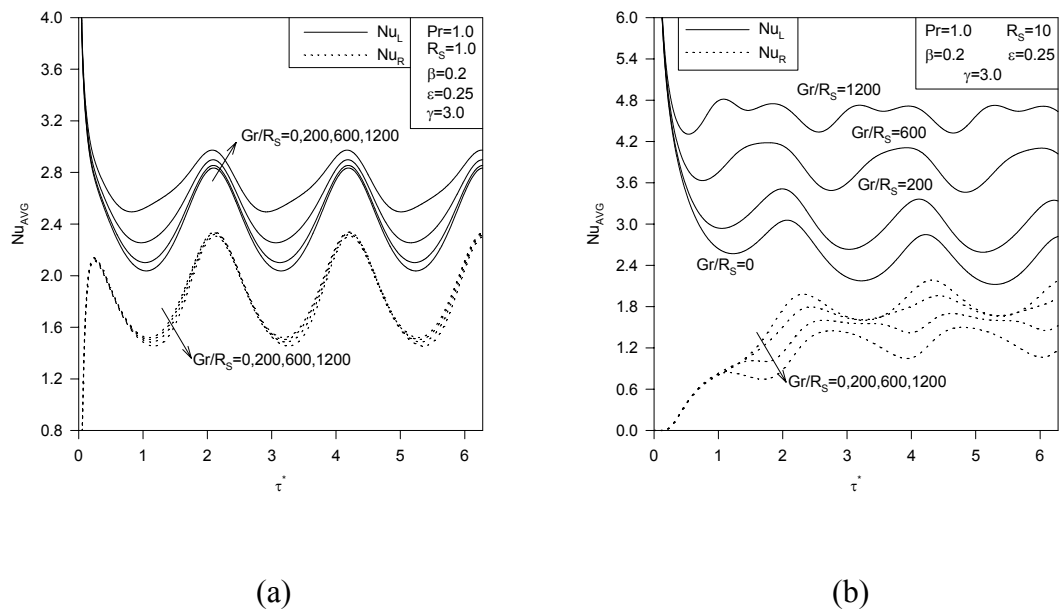


Figure 10.5: Effects of  $Gr$  on  $Nu_{AVG}$ : (a)  $R_S = 1.0$  and (b)  $R_S = 10$

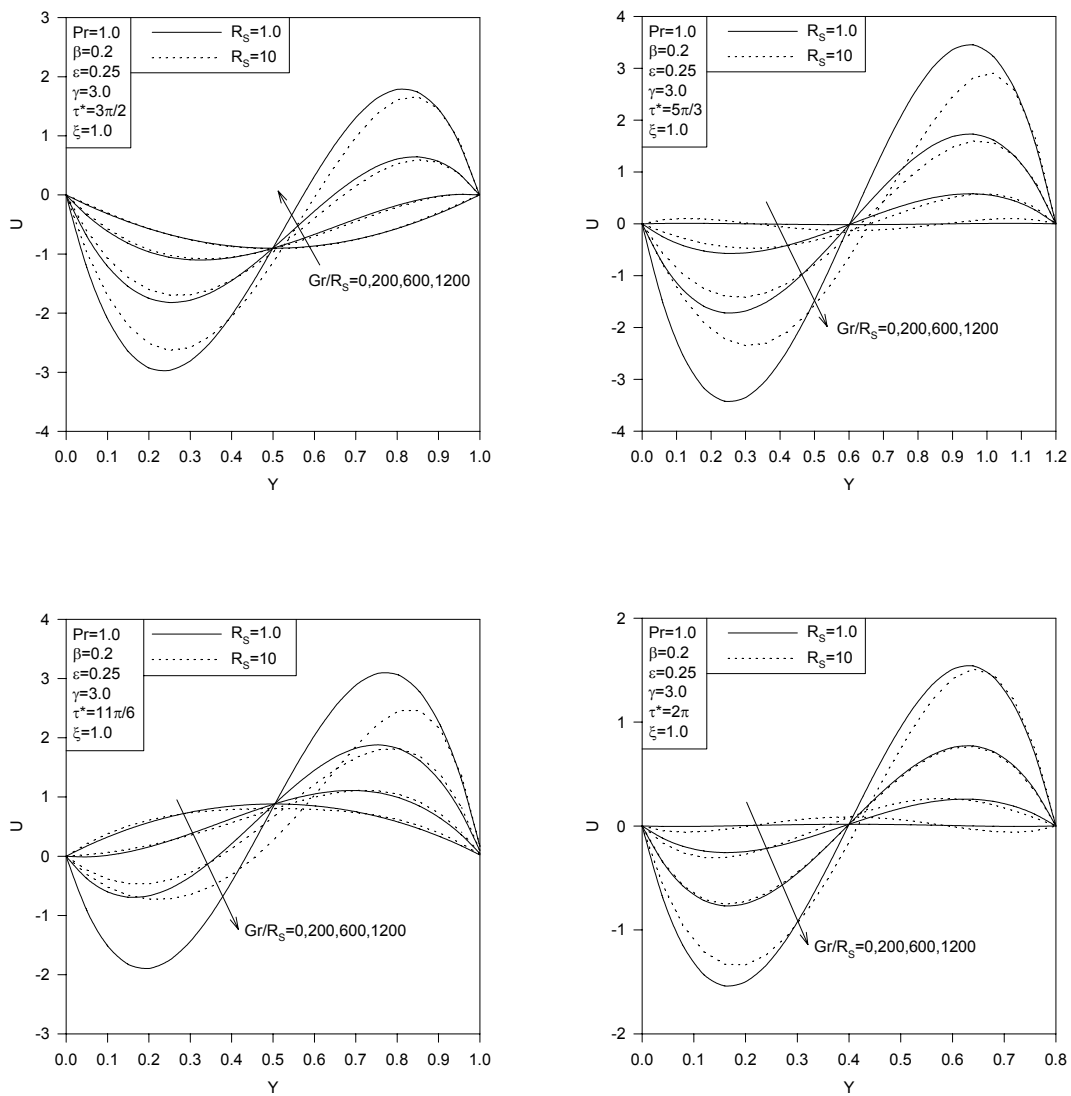


Figure 10.6: Effects of  $\frac{Gr}{R_s}$  on  $U$  at Different Times

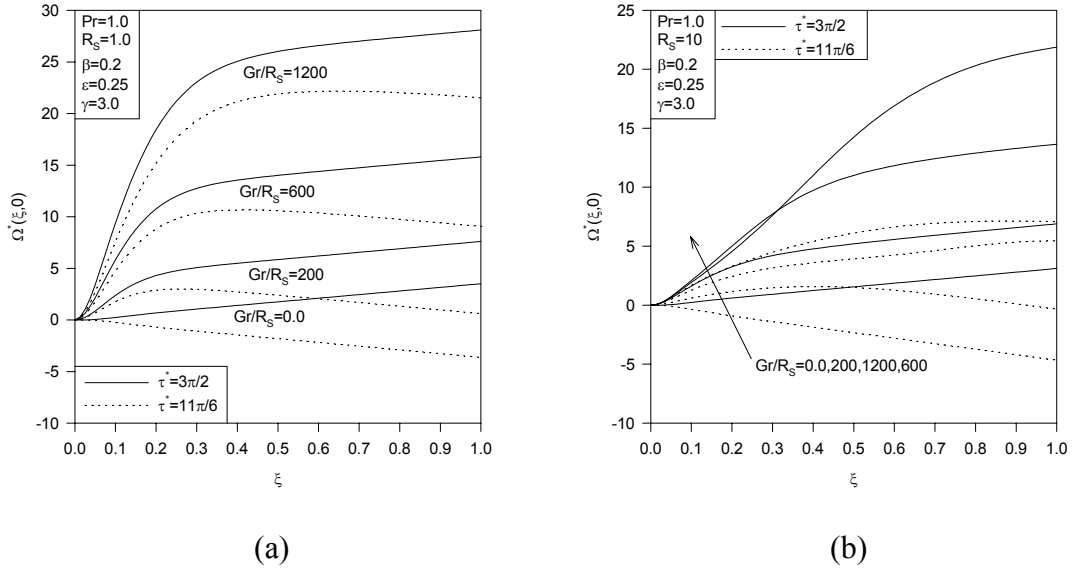


Figure 10.7: Effects of  $\frac{Gr}{R_s}$  on  $\Omega^*(\xi, 0)$ : (a)  $R_s=1.0$  and (b)  $R_s=10$

## 10.6 Correlations

The correlations listed in Table 10.1 are for the mean value of the average Nusselt numbers,  $(Nu_{L,Ravg})_{mean}$ , at the right and left walls and their corresponding fluctuation,

$\Delta Nu_{L,Ravg}$ . These are defined as follows:

$$(Nu_{L,Ravg})_{mean} \cong \frac{\gamma}{2\pi} \int_{2\pi\left(1-\frac{1}{\gamma}\right)}^{2\pi} Nu_{L,Ravg}(\tau^*) d\tau^* \quad (10.18)$$

$$\Delta Nu_{L,Ravg} = \frac{(\text{Nu}_{L,Ravg})_{\text{Max}} - (\text{Nu}_{L,Ravg})_{\text{Min}}}{2} \quad (10.19)$$

where  $(\text{Nu}_{L,Ravg})_{\text{Max}}$  and  $(\text{Nu}_{L,Ravg})_{\text{Min}}$  are the maximum and minimum average Nusselt numbers. In these correlations,  $\text{Nu}_{L,Ravg}$  stands for either  $\text{Nu}_{Lavg}$  or  $\text{Nu}_{Ravg}$  which are the average Nusselt numbers for the left or the right walls, respectively. The listed correlations are derived for a Prandtl number equal to unity and a perturbation parameter equal to one-fourth. The maximum value of  $R_s$  was selected to be 5. As such these correlations are valid for actual vibrational frequency less than 20 rpm for a vertical channel having a thickness equal to 10-20 mm.

Correlations	Maximum Error
$(\text{Nu}_{Lavg})_{\text{mean}} = \frac{2.298(1 + R_s)^{0.0134}}{(1 - \beta^2)^{0.4599}} + 4.725(10^{-4})(50 + \text{Gr})^{0.9214}$	1%
$\frac{\Delta \text{Nu}_{Lavg}}{(\text{Nu}_{Lavg})_{\text{mean}}} = \frac{2.147\beta^{1.067}}{(110 + \text{Gr})^{0.1733}(1 + R_s)^{0.01734}}$	14%
$(\text{Nu}_{Ravg})_{\text{mean}} = \frac{2.682}{(110 + \text{Gr})^{0.02355}} - 0.4564(1 + R_s)^{0.1548}(1 - \beta^2)^{2.237}$	5%
$\frac{\Delta \text{Nu}_{Ravg}}{(\text{Nu}_{Ravg})_{\text{mean}}} = 0.9326\beta^{1.042}(110 + \text{Gr})^{0.04196}$	1%, $R_s=1$

Table 10.1: Correlations for Nusselt Numbers and their Corresponding Fluctuations  
( $\text{Pr}=1.0$ ,  $\varepsilon=0.25$ ,  $\gamma=3.0$ ,  $0 \leq R_s \leq 5$ ,  $0 \leq \text{Gr}/R_s \leq 1000$ ,  $0 \leq \beta \leq 0.3$ )

In addition to the above correlations, the steady periodic behavior for the average Nusselt number at either left or right wall can be approximated by the following correlation for relatively low values of  $\frac{Gr}{R_s}$  ratio:

$$Nu_{L,Ravg}(t) = \frac{(Nu_{L,Ravg})_{mean} \sqrt{1-\beta^2}}{1-\beta \cos(\gamma\omega t)} \quad (10.18)$$

## CHAPTER 11

### **ANALYSIS OF OSCILLATORY FLOW DISTURBANCES AND THERMAL CHARACTERISTICS INSIDE FLUIDIC CELLS DUE TO FLUID LEAKAGE AND WALL SLIP CONDITIONS**

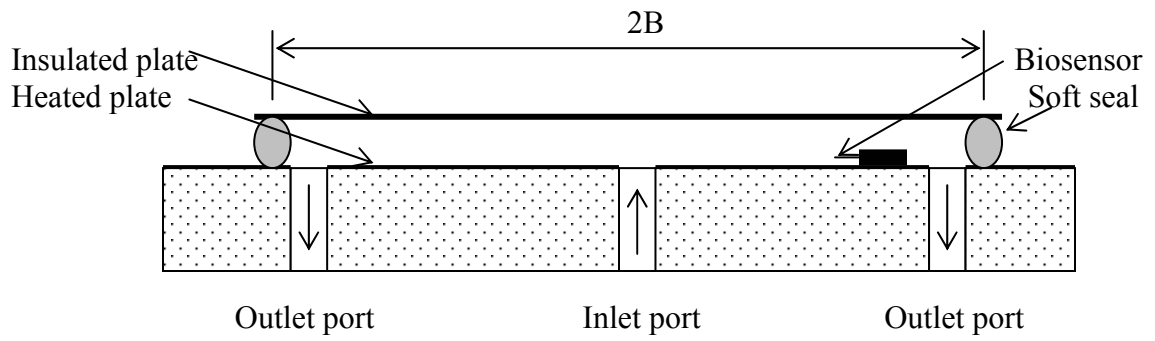
Flow disturbances in fluidic cells can be generated by many sources like external disturbance due to the presence of pulsations in external ambient pressure or due to internal pressure pulsations like irregularities in the pumping process. These disturbances can produce a noise in the sensor measurement especially the microcantilever (Fritz et. al., 2000). Part of the noise in the measurement is ascribed due to the fact that oscillations in the flow may produce an oscillatory drag force on the microcantilever surface causing it to vibrate. Meanwhile, flow oscillations may change the microcantilever temperature causing it to produce an additional noise as the microcantilever is composed of two layers (bimaterial) having different coefficients of the thermal expansion, Fritz et. al. (2000). The rate of receptor/analyte binding changes with the flow velocity, Pritchard et. al. (1995). As such, flow oscillations add an extra noise due to surface stresses. In order to minimize flow oscillations, a special concern is needed in designing fluidic cells so that they incubate minimum flow oscillations.

Another source for flow disturbance is the flow leakage which can seriously affect the operation of the microcantilever (Raiteri et. al., 2000)). Also, fluidic cells may encounter wall slip conditions and the literature lacks enough studies on their effects on

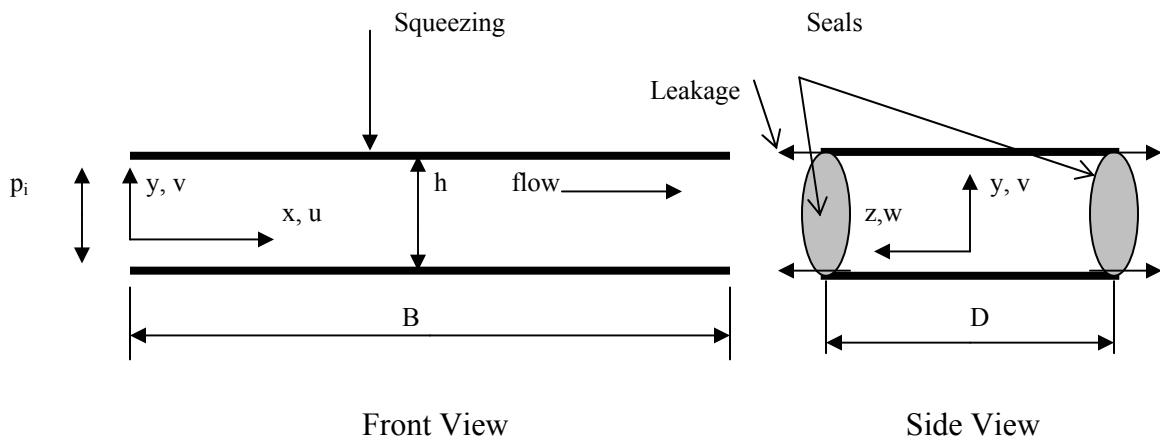
flow fluctuations. It is worth noting that wall slip conditions can be achieved either when the fluid contains suspensions or when the plates are coated with water repellent resins (Watanabe and Udagawa, 2001). Also, slip occur when the size of the thin film is so small that the Kundsens number, a ratio of the molecular mean free path to the characteristic length of the cell is between  $10^{-3}$  and  $10^{-1}$  (Shiping and Ameen, 2001). This chapter will analyze analytically and numerically the effects of side leakage, wall slip condition and non-Newtonian effects of flow fluctuations and heat transfer inside thin films supported by soft seals in the presence of pulsatile flows or external squeezing effects in order to better design fluidic cells.

### **11.1 Analysis**

A two-dimensional thin film fluidic cell that has a small thickness  $h$  compared to its length  $2B$  and its width  $D$  is considered. The inlet of this fluidic cell is taken to be at its center forming a symmetrical fluidic cell, Figure 11.1(a), in order to assure an almost uniform deformation in the seal along its length under pulsative flows. The analysis will be concerned with one half of the fluidic cell shown in Figure 11.1(b) due to the symmetry of the proposed cell. The x-axis is taken along the axial direction starting from the inlet while y-axis and z-axis are taken along its thickness and width, respectively, as shown in Figure 11.1(b).



(a)



(b)

Figure 11.1: Schematic diagram of (a) a symmetrical fluidic cell and, (b) corresponding coordinate systems with leakage directions

### 11.1.1 Fluid Leakage in the Presence of Internal Pressure Pulsations

The lower plate of the thin film is assumed to be fixed while the upper plate is attached to the lower plate by soft seals. The average dimensionless motion of the upper plate  $H$  is expressed according to the following relation:

$$H \equiv \frac{h}{h_o} = (1 + H_p) \quad (11.1)$$

where  $h$ ,  $h_o$  and  $H_p$  are the dimensional average thin film thickness, a reference thin film thickness and the average dimensionless change in the film thickness due to internal pressure forces, respectively.

The following dimensionless variables will be utilized in the analysis:

$$X = \frac{x}{B} \quad Y = \frac{y}{h_o} \quad Z = \frac{z}{B} \quad 11.2(a, b, c)$$

$$\tau = \omega t \quad 11.2(d)$$

$$U = \frac{u}{(\omega B + V_o)} \quad V = \frac{v}{h_o \omega} \quad W = \frac{w}{(\omega B + V_o)} \quad 11.2(e, f, g)$$

$$\Pi = \frac{p - p_e}{\mu \left( \omega + \frac{V_o}{B} \right) \varepsilon^{-2}} \quad 11.2(h)$$

$$\theta = \frac{T - T_1}{(qh_o)/k} \quad 11.2(i)$$

where  $\omega$ ,  $T_1$ ,  $p_e$ ,  $V_o$ ,  $\mu$ ,  $k$ , and  $\varepsilon$  are the reference frequency of internal pulsations, inlet temperature of the fluid, a constant representing the exit pressure, a constant representing a reference dimensional velocity, dynamic viscosity of the fluid, thermal conductivity of the fluid and the perturbation parameter ( $\varepsilon = h_o/B$ ), respectively. The pressure at the exit and the outside pressure are assumed to be at the exit pressure. The lower plate is maintained at a uniform wall heat flux condition  $q_o$ . The variables  $t$ ,  $u$ ,  $v$ ,  $w$ ,  $p$  and  $T$  are the time, axial velocity component, normal velocity component, lateral velocity component, pressure and the temperature, respectively. The dimensionless variables  $X$ ,

$Y, Z, \tau, U, V, W, \Pi$  and  $\theta$  are the dimensionless forms of  $x, y, z, t, u, v, w, p$  and  $T$  variables, respectively.

The average dimensionless change in the film thickness is related to the average dimensionless pressure inside the thin film fluidic cell  $\Pi_{AVG}$  through the theory of linear elasticity. It assumes that the pressure force on the upper plate is linearly proportional to the average change in the thin film thickness (Boresi et. al., 1978), by the following relation:

$$H_p = F_n \Pi_{AVG} \quad (11.3)$$

where  $F_n$  is named, the fixation parameter. A larger  $F_n$  value indicates softer seal-upper plate assembly. The inertia of the upper plate is negligible because the frequency of pulsations is usually small. The fixation parameter  $F_n$  is equal to

$$F_n = K^* \frac{\mu(V_o + \omega B)D}{2(B + 0.5D)E\varepsilon^2 h_s} \quad (11.4)$$

where  $E$  and  $h_s$  are the effective modulus of elasticity and the effective dimension of the seal ( $h_s=h_o$  for a square seal cross section), respectively. The factor  $K^*$  reflects the contribution of the elastic behavior of the upper plate. The parameter  $F_n$  becomes apparent when the thin film thickness is very small ( $h_o < 0.15\text{mm}$ ). The parameter  $F_n$  can have different forms depending on the type of the fixation of the thin film plates and loading conditions on the seal.

Most flows inside thin films are in the creep flow regime as in biological applications. Therefore, the application of the low Reynolds number flow model to continuity, momentum and energy equations for a flat thin film filled with Newtonian fluid results in the following reduced non-dimensionalized equations:

$$U = \frac{1}{2} \frac{\partial \Pi}{\partial X} H^2 \left( \frac{Y}{H} \right) \left( \frac{Y}{H} - 1 \right) \quad (11.5)$$

$$V = \frac{dH}{d\tau} \left( 3 \left( \frac{Y}{H} \right)^2 - 2 \left( \frac{Y}{H} \right)^3 \right) \quad (11.6)$$

$$W = -\frac{1}{2} M_L \Pi \frac{Z}{H} \left( \frac{Y}{H} \right) \left( \frac{Y}{H} - 1 \right) \quad (11.7)$$

$$\frac{\partial^2 \Pi}{\partial X^2} - \frac{M_L}{H^3} \Pi = \frac{\sigma}{H^3} \frac{dH}{d\tau} \quad (11.8)$$

$$P_s \left( \frac{\partial \theta}{\partial \tau} + \frac{12}{\sigma} U \frac{\partial \theta}{\partial X} + V \frac{\partial \theta}{\partial Y} \right) = \frac{\partial^2 \theta}{\partial Y^2} \quad (11.9)$$

According to Equation (11.7), the leakage inside the thin film is distributed equally on both sides of the thin film and it is relatively small thus linearization of the lateral pressure gradient is used. As seen in Equation (11.7), side leakage is proportional to the pressure difference between internal and external (at  $P_e$ ) pressures of the thin film. Equation (11.8) is the corresponding modified Reynolds equation of the problem. Equation (11.9) is applicable at the plane of symmetry at  $Z=0$ . The parameter  $M_L$  in Equation (11.7) is named the dimensionless leakage parameter. It is related to the total

leaked mass  $m_L$  through the following relation:  $m_L = \frac{1}{12} \int_0^1 M_L \Pi \rho D h_o (V_o + \omega B) dX$ . The

inlet pulsative pressure is considered to have the following relation:

$$\Pi_i = \Pi_o (1 + \beta_p \sin(\gamma \omega t)) \quad (11.10)$$

where  $\beta_p$ ,  $\gamma$ ,  $\Pi_i$  and  $\Pi_o$  are the dimensionless amplitude in the pressure, dimensionless frequency of the pressure pulsations, inlet dimensionless pressure and the mean dimensionless inlet pressure, respectively. The solution to Equation (11.8) is obtained as

$$\begin{aligned} \Pi(X, \tau) = & \left( \Pi_i + \frac{\sigma}{M_L} \frac{dH}{d\tau} \right) \cosh \left( \sqrt{\frac{M_L}{H^3}} X \right) - \frac{\sigma}{M_L} \frac{dH}{d\tau} \\ & + \left( \frac{\sigma}{M_L} \frac{dH}{d\tau} - \left[ \Pi_i + \frac{\sigma}{M_L} \frac{dH}{d\tau} \right] \cosh \left( \sqrt{\frac{M_L}{H^3}} \right) \right) \frac{\sinh \left( \sqrt{\frac{M_L}{H^3}} X \right)}{\sinh \left( \sqrt{\frac{M_L}{H^3}} \right)} \end{aligned} \quad (11.11)$$

The reference velocity  $V_o$  is taken to be the velocity inside the thin film in absence of any turbulence. Therefore, it can be related to  $\Pi_o$  according to following relation:

$$\Pi_o = 12 - \sigma \quad (11.12)$$

### 11.1.2 Slip Effects and non-Newtonian Effects in the Presence of External Squeezing

In this part, the effects of fluid slip at the boundaries and non-Newtonian effects in the presence of external turbulence are analyzed. The dimensionless oscillating upper plate oscillations are based on the following generic relationship:

$$H = 1 - \beta \cos(\gamma\tau) \quad (11.13)$$

where  $\beta$  and  $\gamma$  are the amplitude of the motion and a selected dimensionless frequency, respectively. The apparent viscosity  $\mu$  of a non-Newtonian fluid such as a biofluid at low flow rates can be expressed according to the following power-law formula:

$$\mu = \mu_o \left| \frac{\partial u}{\partial y} \right|^{n-1} \text{ where } n \text{ is a constant representing the power law index. As a result, axial}$$

momentum equation for creep flow reduces to the following,  $\mu_o$  replaces  $\mu$  in Equation

11.2(h):

$$\frac{\partial \Pi}{\partial X} = \left( \frac{V_o + \omega B}{h_o} \right)^{n-1} \frac{\partial}{\partial Y} \left( \left| \frac{\partial U}{\partial Y} \right|^{n-1} \frac{\partial U}{\partial Y} \right) \quad (11.14)$$

According to The slip velocity at the boundary is proportional to the shear rate through the slip parameter  $\beta_s$  (Navier, 1823) such that the dimensionless boundary conditions at the plates are:

$$\begin{aligned} U(0, \tau) - \frac{\beta_s}{h_o} \frac{\partial U(0, \tau)}{\partial Y} &= 0 \\ U(H, \tau) + \frac{\beta_s}{h_o} \frac{\partial U(H, \tau)}{\partial Y} &= 0 \end{aligned} \quad (11.15)$$

where  $\beta_s$  is the dimensional slip parameter. By solving Equation (11.15) and the continuity equation, the modified Reynolds equation is

$$\frac{\partial}{\partial X} \left[ \left( \frac{n}{(2n+1)} + 2 \left( \frac{\beta_s}{h_o} \right) \frac{1}{H} \right) \left( \frac{H}{2} \right)^{\frac{2n+1}{n}} \left( -\frac{\partial \Pi}{\partial X} \right)^{\frac{1}{n}} \right] = -\frac{\sigma}{24} \frac{dH}{d\tau} \left( \frac{V_o + \omega B}{h_o} \right)^{\frac{n-1}{n}} \quad (11.16)$$

For a constant average inlet velocity condition  $V_o$  during the oscillations, Equation (11.16) can be used for determining the velocity field,  $U$  and  $V$ , for the lower half of the thin film ( $Y/H < 0.5$ ). They are found to be

$$\begin{aligned} U(X, Y, \tau) &= \frac{[\sigma \beta \gamma \sin(\gamma \tau) X - (12 - \sigma) H(0, \tau)]}{12 \left( \frac{n}{2n+1} + 2 \left( \frac{\beta_s}{h_o} \right) \frac{1}{H} \right) H} \\ &\quad \times \left[ \frac{n}{n+1} \left\{ \left( 1 - 2 \left( \frac{Y}{H} \right) \right)^{\left( \frac{n+1}{n} \right)} - 1 \right\} - 2 \left( \frac{\beta_s}{h_o} \right) \frac{1}{H} \right] \end{aligned} \quad (11.17)$$

$$\begin{aligned} V(X, Y, \tau) &= \frac{\beta \gamma \sin(\gamma \tau)}{\left( \frac{n}{2n+1} + 2 \left( \frac{\beta_s}{h_o} \right) \frac{1}{H} \right)} \\ &\quad \times \left[ \frac{n}{n+1} \left\{ \left( \frac{n}{2n+1} \right) \left( \frac{1}{2} \right) \left\{ \left( 1 - 2 \left( \frac{Y}{H} \right) \right)^{\left( \frac{2n+1}{n} \right)} - 1 \right\} + \frac{Y}{H} \right\} + 2 \left( \frac{\beta_s}{h_o} \right) \left( \frac{1}{H} \right) \left( \frac{Y}{H} \right) \right] \end{aligned} \quad (11.18)$$

Accordingly, the fluid slip velocity at the wall is obtained as

$$U_{\text{slip}}(X, \tau) = \frac{-2\left(\frac{\beta_s}{h_o}\right)\frac{1}{H} [\sigma\beta\gamma \sin(\gamma\tau)X - (12 - \sigma)H(0, \tau)]}{12\left(\frac{n}{2n+1} + 2\left(\frac{\beta_s}{h_o}\right)\frac{1}{H}\right) H} \quad (11.19)$$

### 11.1.3 Thermal Boundary Conditions

It is assumed that the upper plate is insulated while the lower plate is maintained at a constant heat flux. Accordingly, the dimensionless thermal boundary and initial conditions are

$$\theta(X, Y, 0) = 0, \quad \theta(0, Y, \tau) = 0, \quad \frac{\partial\theta(X, 0, \tau)}{\partial Y} = -1, \quad \frac{\partial\theta(X, H, \tau)}{\partial Y} = 0 \quad (11.20)$$

## 11.2 Numerical Methods

The dimensionless thickness of the thin film for the leakage problem was determined by solving Equations (11.1) and (11.3) and the average of Equation (11.11), simultaneously, using the explicit formulation with respect to time. Accordingly, the velocity field  $U$ ,  $V$  and  $W$  was determined. The energy equation, Equation (11.9), was transferred to a problem with constant boundaries using the following transformations:

$\tau^* = \tau$ ,  $\xi = X$  and  $\eta = \frac{Y}{H}$ . It is then solved using a marching scheme in both the axial

direction and time. The values of 0.008, 0.03, 0.002 were chosen for  $\Delta\xi$ ,  $\Delta\eta$  and  $\Delta\tau^*$ .

## 11.3 Discussion of the Results

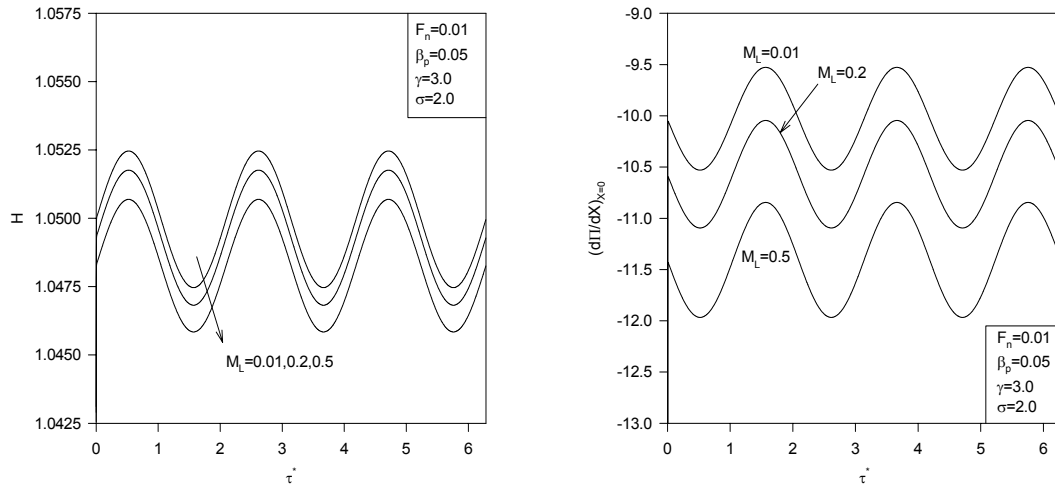
The used dimensionless parameters in the leakage problem were selected according to the following data from the literature: the estimated volume of the fluidic cell, Figure 11.1(b), is 50 $\mu$ l and the flow rate of the liquid is between 0.5-1.0 ml/min. The

thin film thickness was taken to be less than 0.2mm and the effective modulus of elasticity of the seal was considered to be of order  $10^5$ pa.

### **11.3.1 Leakage and Slippage Effects on Flow Dynamics inside Thin Films**

It is noticed from Figure 11.2(a) that the thin film thickness decreases as the dimensionless leakage parameter  $M_L$  increases. A relief in the average internal pressure is expected when the leakage rate increases at a constant inlet pressure. This reduced pressure results in a reduction in the force holding the upper plate thus the thickness decreases. Accordingly, the absolute values of the inlet pressure gradient increases as the leakage rate increases, Figure 11.2(b). This causes the inlet flow rate to increase.

According to Figure 11.2(a), the leakage rate has almost an insignificant effect on the fluctuation rate at the upper plate,  $dH/d\tau$ . However, the associated reduction in the film thickness increases fluctuations in axial and normal velocities at the sensor position which tend to magnify the noise in the sensor measurements especially if the sensor is placed near the disturbed plate. Induced lateral flow due to leakage may cause a lateral bending or twisting of the sensor (e.g. microcantilever). Both effects tend to reduce the accuracy of the measurement and may damage the microcantilever over a long period of time. The fluctuations due to mass leakage can be minimized if the fluidic cell width  $D$  is maximized.



(a) (b)  
 Figure 11.2: Effects of  $M_L$  on (a)  $H$ , and (b) Inlet Pressure Gradient

When the used seal-upper plate assembly is soft as for large  $F_n$  values, the film thickness will be more sensitive to internal pressure pulsations. As a result, an increase in the fixation parameter  $F_n$  causes an increase in the fluctuation rate at the upper plate (Figure 11.3) and consequently an increase in flow fluctuations is associated (Equations 11.5-11.7 and 11.12). Meanwhile, an increase in the squeezing number  $\sigma$  means a reduction in pressure pulsations levels thus a reduction in the fluctuation rate is noticed (Figure 11.4). As such, soft sealing assembly and large velocities produce large fluctuations in the flow within the fluidic cell. Similar trends can be extracted for the lateral fluctuations in view of Equation (11.7). Accordingly, the noise in the measurement with respect to a microcantilever sensor is magnified for relatively large values of the fixation parameter  $F_n$  especially at large pulsation rates.

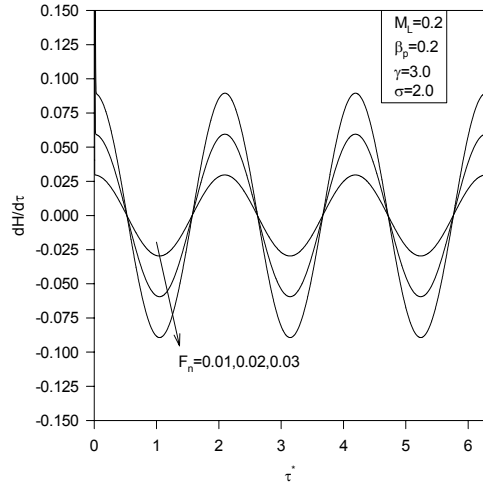


Figure 11.3: Effects of  $F_n$  on  $dH/d\tau$

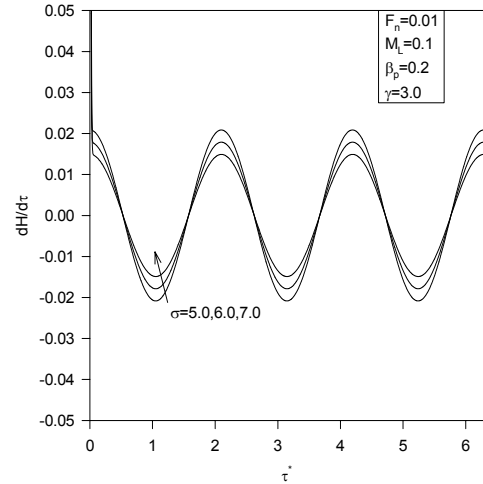


Figure 11.4: Effects of  $\sigma$  on  $dH/d\tau$

The resistance against the flow decreases as the dimensionless wall slip parameter  $\beta_s/h_0$  increases. Thus the slip velocity increases as  $\beta_s/h_0$  increases, Figure 11.5(a). This results in a reduction in the maximum axial velocity since the average flow velocity is kept constant for each case. The maximum slip velocity occurs during the squeezing stages. Due to the increase in the uniformity of the axial velocity profiles as  $\beta_s/h_0$  increases, flow fluctuations increase near the fixed plate, Figure 11.5(b). This causes enlargement in the noise with respect to microcantilever measurements.

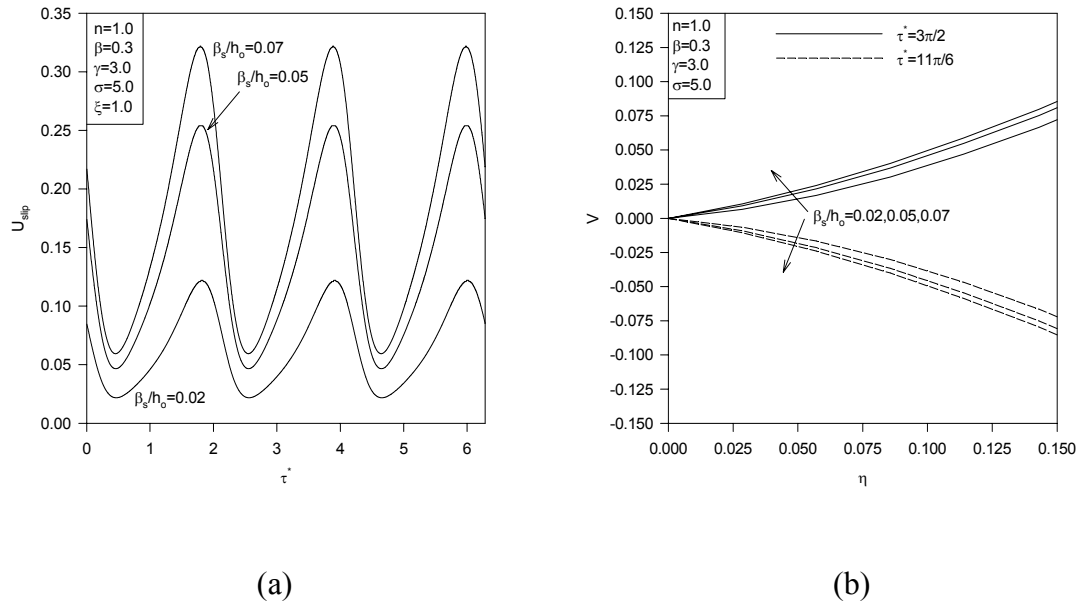


Figure 11.5: Effects of  $\beta_s/h_0$  on (a) wall slip velocity  $U_{slip}$ , and (b) normal velocity  $V$

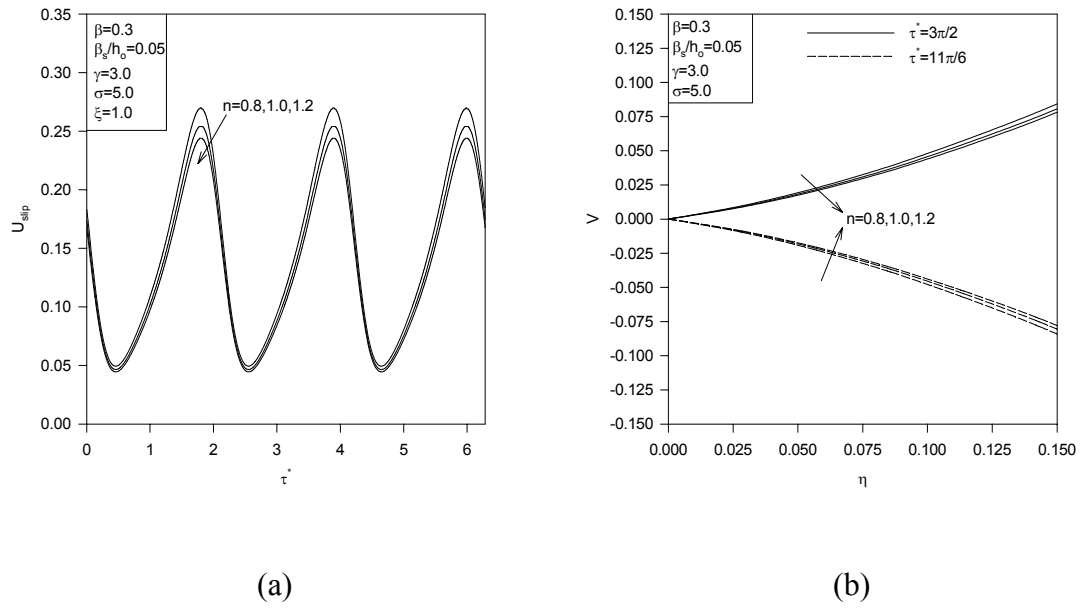


Figure 11.6: Effects of  $n$  on (a) wall slip velocity  $U_{slip}$ , and (b) normal velocity  $V$

Due to the expected increase in wall shear stresses for pseudoplastic ( $n < 1$ ) fluids as the power law index  $n$  decreases, the wall slip velocity increases as  $n$  decreases, Figure 11.6(a). The uniformity of the axial velocity profiles increases as  $n$  decreases. However, flow fluctuations increase near the fixed plate as  $n$  decreases, Figure 11.6(b). This indicates that dilute solutions of analytes are preferred over blood and many biofluids in biosensing applications as they produce minimal flow fluctuations near the undisturbed plate.

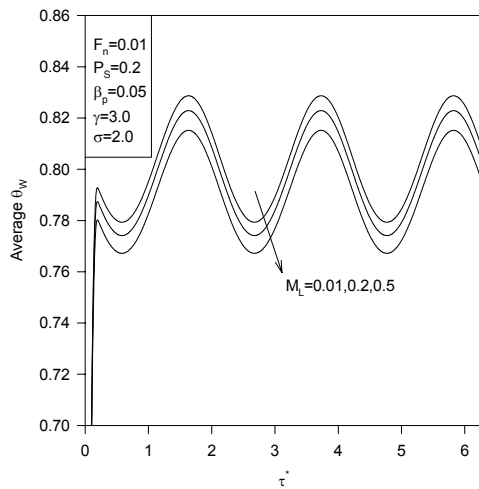


Figure 11.7: Effects of  $M_L$  on Average  $\theta_w$

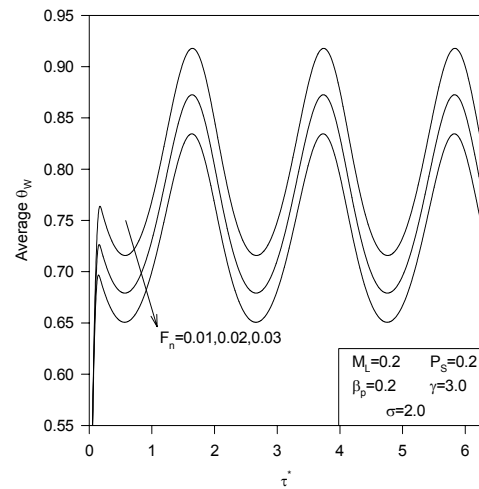


Figure 11.8: Effects of  $F_n$  on Average  $\theta_w$

### 11.3.2 Effects of Leakage on Thermal Characteristics of the Thin Film

The reduction in internal pressures associated with an increase in the leakage rate results in an increase in the inlet flow rate which reduces the average dimensionless lower plate temperature as seen in Figure 11.7. This causes the temperature levels around the microcantilever surface to be closer to the inlet temperature, Equation 11.2(i). These temperatures could be quite different from the original microcantilever temperature.

Thus, the deflection of the bimaterial microcantilever due to thermal effects is magnified when leakage is present. Similarly, thermal effects on bimaterial sensors can be magnified by an increase in  $F_n$  and a decrease in  $\sigma$  since both effects cause a reduction in the dimensionless average lower plate temperature (Figures 11.8 and 11.9). According to Figure 11.7, for the range of  $M_L$  used, thermal variations can be neglected when compared to variations in  $M_L$ .

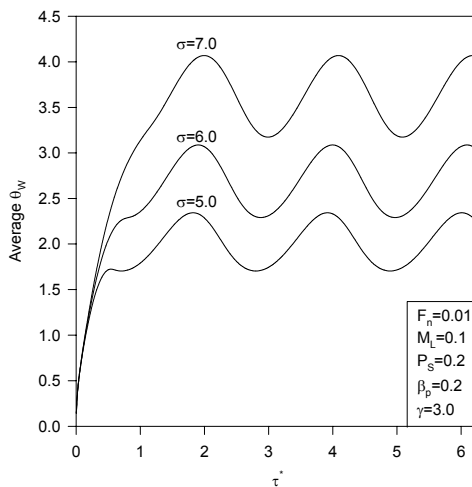


Figure 11.9: Effects of  $\sigma$  on Average  $\theta_w$

#### 11.4 Recommendations

It was established in this chapter that fluctuations inside the fluidic cell and consequently the noise in the measurement due to flow disturbances, can be minimized by considering the following effects:

- Minimizing the working velocities

- Maximizing the thickness of the upper plate
- Maximizing the thin film width if relatively large leakage rate is involved
- Minimizing the thin film width in the absence of leakage
- Maximizing the perturbation parameter
- Utilizing dilute working fluid
- Maximizing the thin film thickness

However, the last three effects may increase the microcantilever deflection due to thermal effects. As such, the problem of reducing flow oscillations was alleviated by considering a new suggested design for fluid cells so that reliable and accurate detections of biological agents can be achieved

## CHAPTER 12

### COOLING ENHANCEMENTS IN THIN FILMS SUPPORTED BY FLEXIBLE COMPLEX SEALS IN THE PRESENCE OF ULTRAFINE SUSPENSIONS

It is shown in chapter 9 that cooling achieved by having thin films supported by soft seals are more than when these seals are stiff. This is due to an increase in thickness resulting from pressure forces when soft seals are used. Soft sealing provides an excellent method of reducing fluid leakage from the thin film. Further, Additional cooling can be achieved if the thin film thickness is allowed to increase by an increase in the thermal load which will cause the coolant flow rate to increase. This task can be reached if the sealing assembly supporting the plates of the thin film is composed of the following: soft seals and voids of a stagnant fluid having a large value of the volumetric thermal expansion coefficient  $\beta_T$ . This proposed sealing assembly will be named a “flexible complex seal” and will be used regularly in the text. It is worth noting that the enhancement in the cooling when flexible complex seals are used is expected to be apparent at larger thermal loads for stagnant liquids while it is prominent at lower temperatures for stagnant gases, especially ideal gases. This is because the volumetric thermal expansion coefficient increases for liquids and decreases for gases as their temperatures increases.

## 12.1 Analysis

Figure 12.1 shows a thin film having a flexible complex seal. It is composed of the coolant flow, the working fluid, passage and the sealing assembly. This assembly contains closed voids filled with a stagnant fluid having relatively a large coefficient of volumetric thermal expansion. The sealing assembly contains also soft seals in order to allow the thin film to expand. A candidate for the soft seal is the closed cell rubber foam (Friis et. al., 1988). Any excessive heat increases the temperature of the hot plate thus the stagnant fluid becomes warmer and expands. The seals are soft enough so that the expansion results in an increase in the separation between the lower and the upper plates. Accordingly, the flow resistance of the working fluid passage decreases causing a flooding of the coolant. As a result, the excessive heating from the source is removed. It is worth noting that the soft seals can be placed between special guiders as shown in Figure 12.1(b). As such, side expansion of the seals can be minimized and the transverse thin film thickness expansion is maximized.

The analysis is concerned with a thin film that has a small thickness  $h$  compared to its length  $B$  and its width  $D$ . Therefore, a two-dimensional flow is assumed. The  $x$ -axis is taken along the axial direction of the thin film while  $y$ -axis is taken along its thickness as shown in Figure 12.1(a). Further, it is assumed in this work that the film thickness is independent of the axial coordinate. For example, this occurs in two main cases: symmetric thin films having a fluid injected from the center as shown in Figure 12.1(c) and in multiple passages thin films having alternating coolant flow directions.

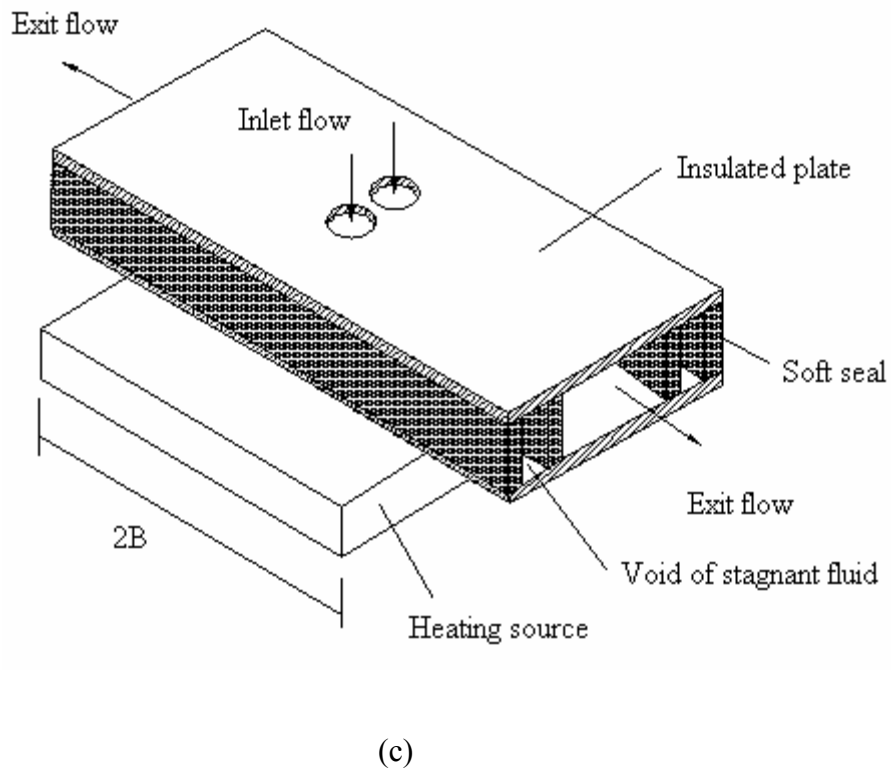
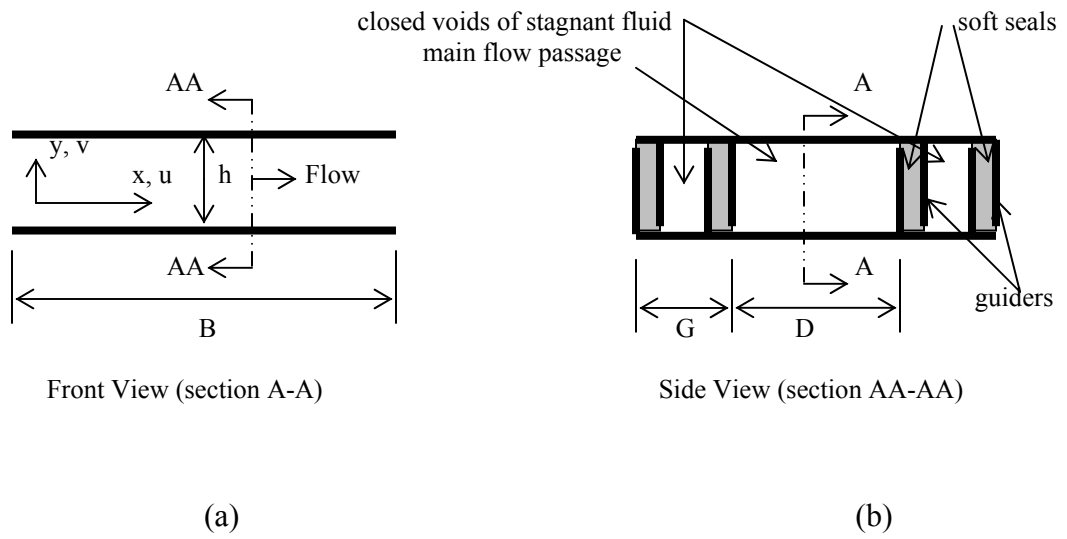


Figure 12.1: Schematic diagram for a thin film with flexible complex seal and the corresponding coordinate system: (a) front view, (b) side view, and (c) a three dimensional diagram

The lower plate of the thin film is assumed to be fixed to a heating source while the upper plate is attached to the lower plate by flexible complex seals allowing it to expand. The motion of the upper plate due to both internal variations in the stagnant fluid temperature and the induced internal pressure pulsations as a result of oscillating thermal loads is expressed according to the following relation:

$$H \equiv \frac{h}{h_o} = (1 + H_T + H_p) \quad (12.1)$$

where  $h$ ,  $h_o$  and  $H$  are the thin film thickness, a reference film thickness and the dimensionless thin film thickness, respectively. The variables  $H_T$  and  $H_p$  are the dimensionless motion of the upper plate due to the thermal expansion of the stagnant fluid and the dimensionless motion of the upper plate as a result of the deformation of seals due to the average internal pressure of the working fluid, respectively. It is assumed that the fluid is Newtonian having constant average properties except for the thermal conductivity. Also, it is assumed that the upper plate is insulated to simplify the analysis and that the lower plate is subjected to periodically varying wall heat flux  $q_L$  condition according to the following relation:

$$q_L = q_o (1 + \beta_q \sin(\gamma\omega t)) \quad (12.2)$$

where  $\beta_q$  and  $\gamma$  are the dimensionless amplitude of the lower plate's heat flux and a dimensionless frequency, respectively.

For the thin film shown in Figure 12.1(c), the displacement of the upper plate due to internal pressure variations is related to the average dimensionless pressure of the working fluid,  $\Pi_{AVG}$ , through the theory of linear elasticity by the following relation:

$$H_p = F_n \Pi_{AVG} \quad (12.1)$$

This is based on the fact that the upper plate is assumed to be rigid and that the applied force on an elastic material, the soft seal is assumed to behave as an elastic material is proportional to the elongation of this material (Norton, 1998). The parameter  $F_n$  is referred to as the fixation parameter and it is a measure of the softness of the seal, soft seals have large  $F_n$  values. It is equal to

$$F_n = \frac{\mu(V_o + \omega B)}{E \varepsilon^2 d_s} \quad (12.4)$$

where  $E$  and  $d_s$  are the effective modulus of elasticity for the complex seal and a characteristic parameter which depends on the seal's dimensions and the thin film width  $D$ , respectively. The quantity  $d_s$  is equal to the effective dimension of the seal's cross section times the ratio of the total length of the seal divided by the thin film width  $D$ . The seal is considered to have isotropic properties. Further, the effective dimension of the seals times their total length represents the contact area between the seals and the upper or lower plates when the seals have a rectangular cross section as shown in Figure 12.1. Other than this, the effective diameter requires a theoretical determination.

In this work, the analysis is performed for relatively small thermal load frequencies in order to ascertain that squeezing generated flows have relatively small Reynolds numbers. For these frequencies, Equation (12.3) is applicable and the inertia effect of the upper plate is negligible. Moreover, the increase in the thickness due to a pressure increase in the thin film causes a reduction in the stagnant fluid pressure. This action stiffens the sealing assembly. Therefore, the parameter  $E$  is considered to be the effective modulus of elasticity for the sealing assembly not for the seal itself. For ideal

gases, the effective  $E$  can be shown to be approximately equal to the following when the mass of the stagnant fluid is kept constant for the configuration shown in Figure 12.1(b):

$$E \cong E_{sm} \left[ 1 + \frac{mRT_1}{E_{sm} d_s Dh_o} \right] \quad (12.5)$$

where  $m$ ,  $R$  and  $E_{sm}$  are the mass of the ideal gas in the voids, gas constant and the modulus of elasticity for the pure seal material, respectively. In case where additional mass can be added to the voids when the pressure falls below the initial stagnant pressure as when check valves are used,  $E$  is expected to approach  $E_{sm}$ . Practically, the void width  $G$  is assumed to be large enough such that a small increase in the stagnant fluid pressure due to the expansion can support the associated increase in the elastic force on the seal. Moreover, the fixation parameter can be enhanced by replacing segments of the seals at different locations by elastic membranes especially the outermost ones so the effective length of the seal is reduced.

The dimensionless displacement of the upper plate due to thermal expansion is related to the dimensionless average temperature of the lower plate,  $(\theta_w)_{AVG}$ , by the following linearized model:

$$H_T = F_T (\theta_w)_{AVG} \quad (12.6)$$

where  $F_T$  is named the dimensionless thermal expansion coefficient. It is equal to

$$F_T = A^* \frac{\beta_T q_o h_o}{k_o} C_F \quad (12.7)$$

where  $A^*$  is a constant depending on voids dimensions (equal to unity for Fig. 12.1(b)).

The parameter  $\beta_T$  is the volumetric thermal expansion coefficient of the stagnant fluid in

its approximate form:  $\beta_T \approx (1/V_{s0})(V_s - V_{s1})/(T_s - T_1)_{p_{s1}}$  evaluated at the pressure  $p_{s1}$  corresponding to the stagnant fluid pressure at the inlet temperature  $T_1$  condition. The quantities  $V_{s1}$  and  $V_s$  represent the void volumes at the operating condition when the stagnant fluid is at temperature  $T_1$  and at the present stagnant fluid temperature  $T_s$ , respectively. The volume  $V_{s0}$  represents the void volume at the reference condition. The factor  $C_F$  represents an average volumetric thermal expansion correction factor. This factor is introduced in order to account for the increase in the stagnant pressure due to the increase in the elastic force in the seal during the expansion which tends to decrease the effective volumetric thermal expansion coefficient. Also, it accounts for the decrease in the stagnant pressure associated with elongation of the seal due flow pressure. For ideal gases and assembly shown in Figure 12.1(b), the parameter  $\beta_T$  times  $C_F$  is:

$$\beta_T C_F \cong \frac{1}{T_1 (h_o/h_{pm}) + (E_{sm} d_s D h_{pm}) / (mR)} \quad 12.8(a,b)$$

where  $h_{pm}$  is the mean value for the dimensional film thickness prior thermal effects.

The parameter  $F_T$  is enhanced at elevated temperatures for liquids and at lower temperature for gases because  $\beta_T$  increases for liquids and decreases for gases as the stagnant temperature increases. Dimensionless thermal expansion parameter is also enhanced by a decrease in  $k_o$ , an increase in  $q_o$ , an increase in  $F_n$  or by increases in  $h_o$ . It is worth noting that Equation (12.6) is based on the assumption that the stagnant fluid temperature is similar to the lower plate temperature since entire void surfaces are considered insulated except that facing the lower plate. It is worth noting that the heat flux of the heating source is considered to be applied on the portion of the lower plate that is facing the working fluid. The other portion which faces the seals is taken to be

isolated from the heating source and the environment to minimize the variation in the lower plate temperature along the width direction.

In the presence of suspended ultrafine particles in the working fluid, the thermal conductivity of the working fluid composed from the pure fluid and suspensions is expected to vary due to the thermal dispersion (Xuan and Roetzel, 2000). To account for these variations, the following model which is similar to Xuan and Roetzel (2000) model that linearly relates the effective thermal conductivity of the working fluid to the fluid speed is utilized:

$$k(X, Y, \tau) = k_o \left( 1 + \lambda \sqrt{U^2(X, Y, \tau) + \Lambda^2 V^2(X, Y, \tau)} \right) = k_o \phi(X, Y, \tau) \quad (12.9)$$

where  $\lambda$  and  $\Lambda$  are the dimensionless thermal dispersion coefficient and reference squeezing to lateral velocity ratio. They are

$$\lambda = C^* (\rho c_p)_f h_o (V_o + \omega B) \quad \Lambda = \frac{\varepsilon \sigma}{12} \quad 12.10 \text{ (a, b)}$$

where  $C^*$  is the coefficient of the thermal dispersion which depends on the diameter of the ultrafine particles, its volume fraction (ratio of the particles volume to the total thin film volume), and both fluid and ultrafine particles properties.

It is worth noting that the term ultrafine suspensions indicate that the particle is extremely small compared with the thickness of the thin film. The coefficient  $C^*$  is expected to increase by an increase in the diameter of the particles, their volume fraction, their surface roughness and the working fluid Prandtl number,  $Pr = (\rho c_p \nu) / k_o$ . On the other hand, the stagnant thermal conductivity  $k_o$  increases with an increase in both the volume fraction and the surface area of the particles (Xuan and Roetzel, 2000). In the work of Li and Xuan (2002), they showed experimentally that dilute mixture of ultrafine suspensions

and water produced no change in the pressure drop compared to pure water which reveals that the viscosity is a weak function of the fluid dispersion for a dilute mixture.

Generally, flows inside thin films are in laminar regime and could be creep flows as in lubrication. Therefore, the low Reynolds numbers (the modified lateral Reynolds number  $Re_L = (V_o h_o) \epsilon / \nu$  and the squeezing Reynolds number  $Re_s = (h_o^2 \omega) / \nu$ ) flow model is adopted here. This model neglects the transient and convective terms in momentum equations. These terms become incomparable to the pressure gradient and diffusive terms for small squeezing frequencies and reference velocities. Utilizing variables (2.7) in chapter 2, the outcome of the application of the low Reynolds number model to momentum equations along with the dimensionless energy equation will be:

$$U = \frac{1}{2} \frac{\partial \Pi}{\partial X} H^2 \left( \frac{Y}{H} \right) \left( \frac{Y}{H} - 1 \right) \quad (12.11)$$

$$V = \frac{dH}{d\tau} \left( 3 \left( \frac{Y}{H} \right)^2 - 2 \left( \frac{Y}{H} \right)^3 \right) \quad (12.12)$$

$$\frac{\partial}{\partial X} \left( H^3 \frac{\partial \Pi}{\partial X} \right) = \sigma \frac{\partial H}{\partial \tau} \quad (12.13)$$

$$P_s \left( \frac{\partial \theta}{\partial \tau} + \frac{12}{\sigma} U \frac{\partial \theta}{\partial X} + V \frac{\partial \theta}{\partial Y} \right) = \frac{\partial}{\partial Y} \left( \phi \frac{\partial \theta}{\partial Y} \right) \quad (12.14)$$

Note that Equation (12.14) is based on the assumption that the axial conduction is negligible when compared to the transverse conduction. The parameters  $\sigma$  and  $P_s$  are the squeezing number and the thermal squeezing parameter. They are previously defined. It should be noted that both inlet and exit dimensionless pressures are assumed constant and the following relationship is obtained between the inlet dimensionless pressure and the

squeezing number based on the assumption that the reference velocity  $V_o$  represents the average velocity in the thin film at zero values of  $F_T$  and  $F_n$ :

$$\Pi_i = 12 - \sigma \quad (12.15)$$

Accordingly, the dimensionless pressure gradient, the dimensionless pressure and the average dimensionless pressure  $\Pi_{AVG}$  inside the thin film are related to the squeezing number through the following equations:

$$\frac{\partial \Pi(X, \tau)}{\partial X} = \frac{\sigma}{H^3} \frac{dH}{d\tau} \left( X - \frac{1}{2} \right) - (12 - \sigma) \quad (12.16)$$

$$\Pi(X, \tau) = \frac{\sigma}{2H^3} \frac{dH}{d\tau} (X^2 - X) - (12 - \sigma)(X - 1) \quad (12.17)$$

$$\Pi_{AVG}(\tau) = -\frac{\sigma}{12H^3} \frac{dH}{d\tau} + \frac{(12 - \sigma)}{2} \quad (12.18)$$

### 12.1.1 Thermal Boundary Condition

The dimensionless thermal boundary conditions for the previously defined problem are taken as follows:

$$\theta(X, Y, 0) = 0, \quad \theta(0, Y, \tau) = 0, \quad \frac{\partial \theta(X, 0, \tau)}{\partial Y} = -(1 + \beta_q \sin(\gamma\tau)), \quad \frac{\partial \theta(X, H, \tau)}{\partial Y} = 0 \quad (12.19)$$

Based on the physical conditions, the Nusselt number is defined as

$$Nu_1(X, \tau) \equiv \frac{h_c h_o}{k} = \frac{1}{\theta(X, 0, \tau) - \theta_m(X, \tau)} = \frac{1}{\theta_w(X, \tau) - \theta_m(X, \tau)} \quad (12.20)$$

The parameter  $\theta_m$  is the dimensionless mean bulk temperature. It is given as

### 12.2 Numerical Procedure

The procedure for the numerical solution is summarized as follows:

1. Initially, a value for  $H_T$  is assumed.

2. At the present time, the dimensionless thickness of the thin film  $H$  is determined by solving Equations (12.1), (12.3), (12.6) and (12.8), simultaneously, using an explicit formulation. The velocity field,  $U$  and  $V$ , is then determined from Equations (12.11), (12.12) and (12.16).
3. At the present time, The reduced energy equation, Equation (12.14) is transferred into one with constant boundaries using the following transformations:  $\tau^* = \tau$ ,  $\xi = X$  and  $\eta = Y/H$ . A tri-diagonal solution (Blottner, 1971) was implemented along with a marching scheme. Backward differencing was chosen for the axial convective and transient terms and central differencing was selected for the derivatives with respect to  $\eta$ . The values of 0.008, 0.03, 0.001 were chosen for  $\Delta\xi$ ,  $\Delta\eta$  and  $\Delta\tau^*$ , respectively.
4.  $H_T$  is updated from Equation (12.6) and steps (2)– (4) are repeated until
 
$$\left| \frac{(H_T)_{\text{new}} - (H_T)_{\text{old}}}{(H_T)_{\text{new}}} \right| < 10^{-6} \quad (12.21)$$
5. The converged solution for the flow and heat transfer inside the thin film is determined at the present time.
6. Time is advanced by  $\Delta\tau^*$  and steps (1)-(5) are repeated.

Numerical investigations were performed using different mesh sizes and time steps to assess and ascertain grid and time step independent results. It was found that any reduction in the values of  $\Delta\xi$ ,  $\Delta\eta$  and  $\Delta\tau^*$  below  $\Delta\xi=0.008$ ,  $\Delta\eta=0.03$  and  $\Delta\tau^*=0.001$  results in less than 0.2 percent error in the results.

In the results, the maximum value of the parameters  $P_S$  is chosen to be 1.0. Beyond this value, the error associated with the low Reynolds number model will increase for moderate values of the dimensionless thermal expansion parameter, fixation parameter, and the Prandtl number. As an example, the order of transient and convective terms in the momentum equations were found to be less 1.0 percent that of the diffusive terms for  $P_S=1.0$ ,  $Pr=6.0$ ,  $F_n=0.05$ ,  $F_T=0.25$ ,  $\beta_q=0.1$  and  $\sigma=6.0$ . The parameters correspond, for example, to a thin film filled with water and having  $B=D=60\text{mm}$ ,  $h_o=0.3\text{mm}$ ,  $d_s=1.0\text{mm}$ ,  $\omega=2.0\text{s}^{-1}$ ,  $V_o=0.12\text{m/s}$  and  $E=1.6 (10^5)\text{pa}$ .

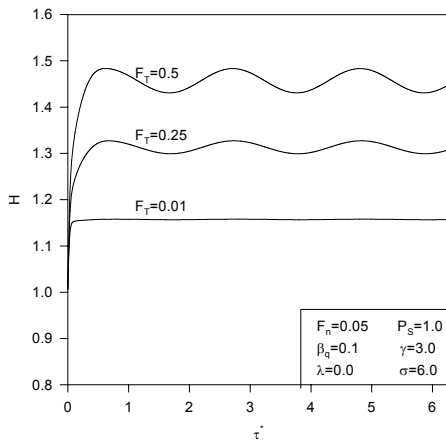
### **12.3 Discussions of the Results**

Ideal gases produce a 15 percent increase in the void volume at room conditions for a  $45^\circ\text{C}$  maximum temperature difference. Further, Li and Xuan (2002) reported a 60 percent increase in the convective heat transfer coefficient for a volume fraction of copper ultrafine particles of 2.0 percent. Accordingly, the parameters  $F_T$  and  $\lambda$  were varied until comparable changes have been attained in the dimensionless thin film thickness and the Nusselt number.

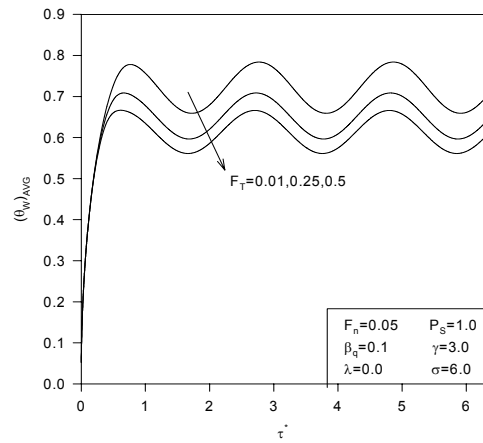
#### **12.3.1 Effects of Dimensionless Coefficient of Thermal Expansion**

Figure 12.2(a) illustrates the effects of the dimensionless thermal expansion parameter  $F_T$  on the dimensionless thickness  $H$  of the thin film. The parameter  $F_T$  can be increased either by an increase in the volumetric thermal expansion coefficient of the stagnant fluid or by an increase in dimensional reference temperature  $(q_o h_o)/k_o$ . Both factors make the flexible complex seal softer thus dimensionless thickness  $H$  is increased as  $F_T$  increases as shown in Figure 12.2(a). This allows more coolant to flow causing

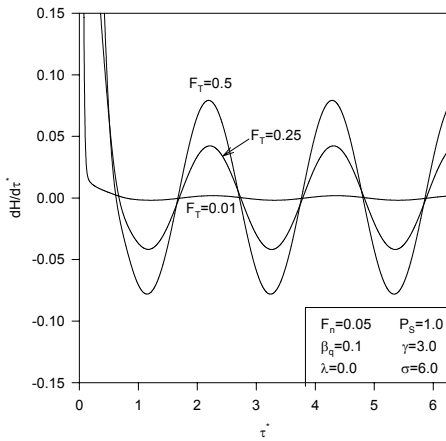
reductions in the average dimensionless lower plate's temperature  $(\theta_W)_{AVG}$  as clearly seen in Figure 12.2(b) which can provide additional cooling to any heated surface such as surfaces of electronic components.



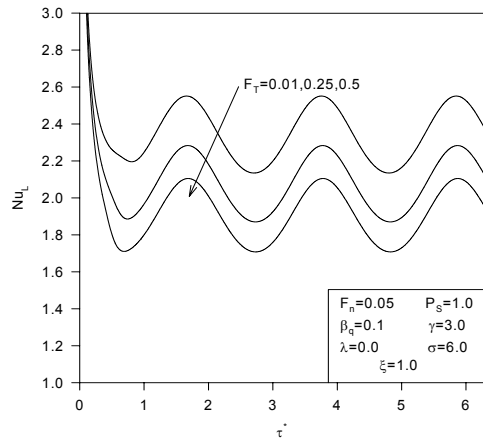
(a)



(b)



(c)



(d)

Figure 12.2: Effects of the dimensionless thermal expansion parameter  $F_T$  on (a) dimensionless thin film thickness  $H$ , (b) dimensionless average lower plate temperature  $(\theta_W)_{AVG}$ , (c)  $dH/d\tau$ , and (d) exit Nusselt number  $Nu_L$

Figure 12.2(b) can be also read as follows: as thermal load increases, the average lower plate's temperature increases however this increase can be reduced by using a flexible complex seal. This additional cooling is obtained with no need for external controlling devices which provides extra safety for an electronic component, as an example for a heated surface, when their thermal loads increase over the projected capacity. The fluctuation rate at the upper plate,  $|dH/d\tau|$ , is noticed to increase as  $F_T$  increases as shown in Figure 12.2(c). This could be an advantage for the cooling process especially at high levels of fluctuation rates since it will enhance the thermal dispersion in the coolant when suspended ultrafine particles are present.

The Nusselt number is decreased as  $F_T$  increases as shown in Figure 12.2(d) because it is inversely proportional to  $H$ . This is the reason for the fact that the percentage decrease in lower plate temperatures is lower than the percentage increase in the thin film thickness as  $F_T$  increases.

### **12.3.2 Effects of Dimensionless Thermal Dispersion Parameter**

Figure 12.3(a) describes the effects of the dimensionless thermal dispersion parameter  $\lambda$  of the coolant fluid on the average lower plate's temperature of the thin film. This parameter can be increased either by increasing the diameter of the ultrafine particles or increasing the roughness of these particles while keeping a fixed volume fraction inside the coolant. This insures that thermal squeezing parameter remains constant. Figure 12.3(a) physically shows that the thermal dispersion can provide additional cooling to a heated element, thus it causes an additional reduction in the average dimensionless lower plate temperature  $(\theta_w)_{AVG}$ . Part of this cooling is due to the expansion process since it results in flooding of the working fluid which increases the

irregularity and the random motion of the particles. This causes additional enhancements in the energy exchange rate. Another part for the enhancement in the cooling is attributed to the fact that the noise in the thermal load, especially those having heterogeneous fluctuation rates, produces additional squeezing due to the velocities that appear in Equation (12.9).

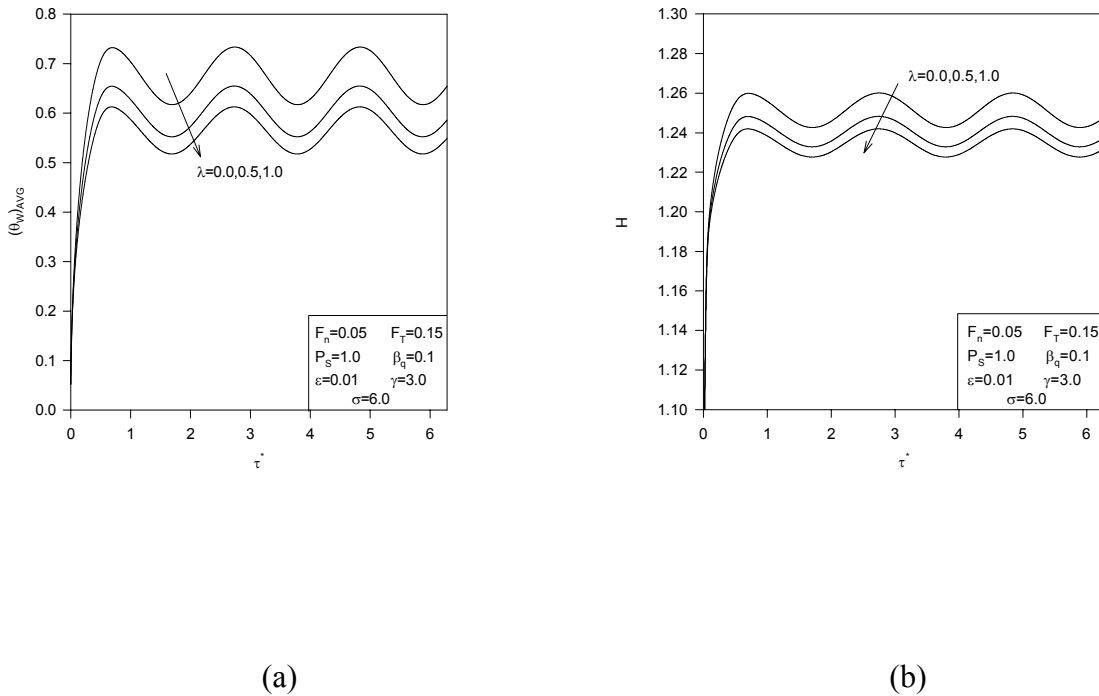
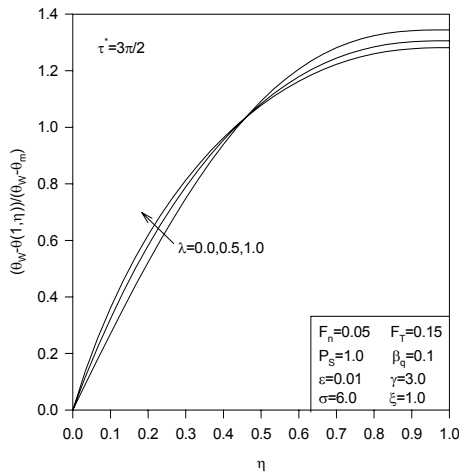
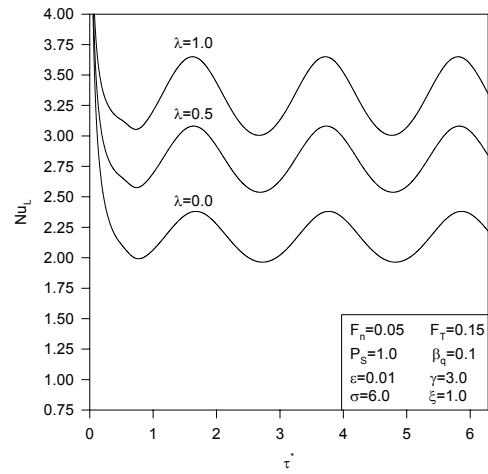


Figure 12.3: Effects of the dimensionless thermal dispersion parameter  $\lambda$  on (a) dimensionless average lower plate temperature  $(\theta_w)_{AVG}$ , (b) dimensionless thickness  $H$ , (c) temperature Profile, and (d) exit Nusselt number  $Nu_L$



(c)



(d)

Figure 12.3: Effects of the dimensionless thermal dispersion parameter  $\lambda$  on (a) dimensionless average lower plate temperature  $(\theta_w)_{AVG}$ , (b) dimensionless thickness  $H$ , (c) temperature Profile, and (d) exit Nusselt number  $Nu_L$  .....Continued

Due to the reduction in the lower plates temperatures as  $\lambda$  increases, the dimensionless thin film thickness decreases as  $\lambda$  increases as depicted in Figure 12.3(b). It is worth noting that additional enhancements in the thermal dispersion effect are expected as both the perturbation parameter and the squeezing number increase as suggested by Equations (12.7) and (12.8). Both effects result in a magnification in the fluctuation rates in the flow which causes additional increases in the cooling process. In our example, the perturbation parameter and the fluctuation rates are small and their effects are not noticeable.

The reduction in thermal resistance across the transverse direction when  $\lambda$  increases causes the temperature profiles to be more flattened as  $\lambda$  increases as seen in

Figure 12.3(c). Accordingly, the Nusselt number increases as  $\lambda$  increases as seen in Figure 12.3(d). It can be seen in Figure 12.4 that the fluctuation rate at the upper plate,  $|dH/d\tau|$ , decreases as  $\lambda$  increases. As a result, ultrafine particle suspensions inside thin films supported by flexible complex seals not only cause enhancements in heat transfer but also make these thin films dynamically more stable. In this example, an increase in  $\lambda$  between zero and unity cause a reduction in the average lower temperature by dimensionless temperature of 0.12 and an increase in the Nusselt number by 50 percent.

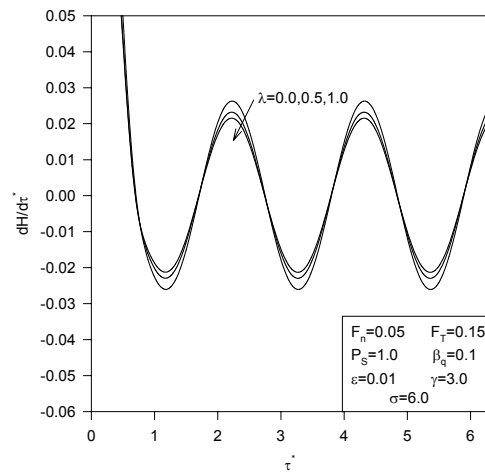


Figure 12.4: Effects of the dimensionless dispersion parameter  $\lambda$  on the time variation of the dimensionless thin film thickness  $dH/d\tau$

### 12.3.3 Effects of Thermal Squeezing Parameter and the Squeezing Number

Figure 12.5(a) shows the effects of the thermal squeezing parameter  $P_S$  and the squeezing number  $\sigma$  on the average dimensionless lower plate temperature  $(\theta_W)_{AVG}$ . It is clearly seen that the lower plate temperature decreases as  $P_S$  increases and as  $\sigma$  decreases.

Both effects tend to increase thermal convection which decreases the lower plate temperature. The increase in  $P_S$  means an increase in the thermal capacitance of the working fluid and a decrease in  $\sigma$  indicates an increase in the reference velocity. Accordingly, the dimensionless thickness  $H$  decreases as  $P_S$  increases as shown in Figure 12.5(b). In addition, the pressure force inside the thin film increases as  $\sigma$  decreases causing an increase in  $H_p$  while  $H_T$  decreases as  $\sigma$  decreases due to the enhancement in the cooling. As a result, the thin film thickness is noticed to vary slightly when  $\sigma$  decreases as illustrated in Figure 12.5(b). As seen in Figure 12.5(c), the fluctuation rate at the upper plate is found to increase as  $\sigma$  increases while it decreases as  $P_S$  increases. Also, the fluctuation rate at the upper plate is shown to more pronounced to  $P_S$  more than to  $\sigma$ .

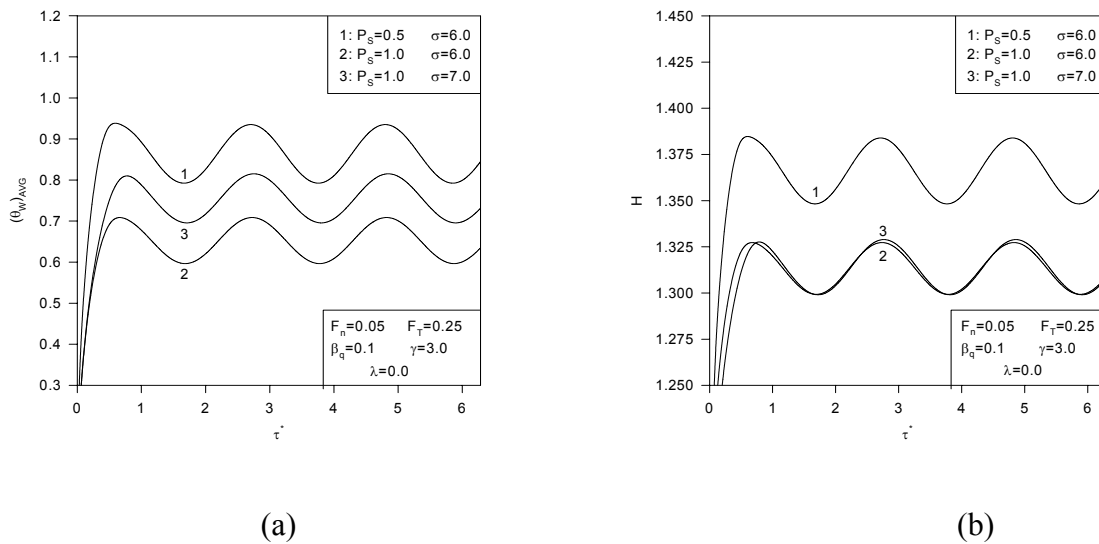
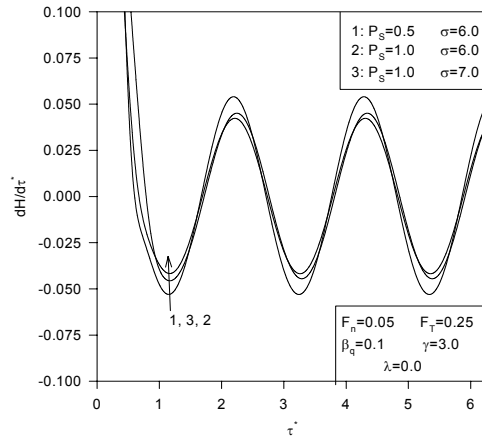


Figure 12.5: Effects of the thermal squeezing parameter  $P_S$  and the squeezing number  $\sigma$  on (a) dimensionless average lower plate temperature  $(\theta_w)_{AVG}$ , (b) dimensionless thin film thickness  $H$ , and (c)  $dH/dt$



(c)

Figure 12.5: Effects of the thermal squeezing parameter  $P_S$  and the squeezing number  $\sigma$  on (a) dimensionless average lower plate temperature  $(\theta_W)_{AVG}$ , (b) dimensionless thin film thickness  $H$ , and (c)  $dH/d\tau$  .....Continued

### 12.3.4 Effects of the Fixation Parameter and the Amplitude of the Thermal Load

Figure 12.6(a) shows the effects of the fixation parameter  $F_n$  and the dimensionless amplitude of the thermal load  $\beta_q$  on the average dimensionless lower plate temperature  $(\theta_W)_{AVG}$ . Since soft seals possess large  $F_n$  values,  $H$  increases and lower plate temperature decreases as  $F_n$  increases as shown in Figures 12.6(a) and 12.6(b). Further, these figures show that an increase in the amplitude of the heat flux results in an increase in the fluctuation rate at the upper plate and the lower plate temperature but their mean values are almost unaffected.

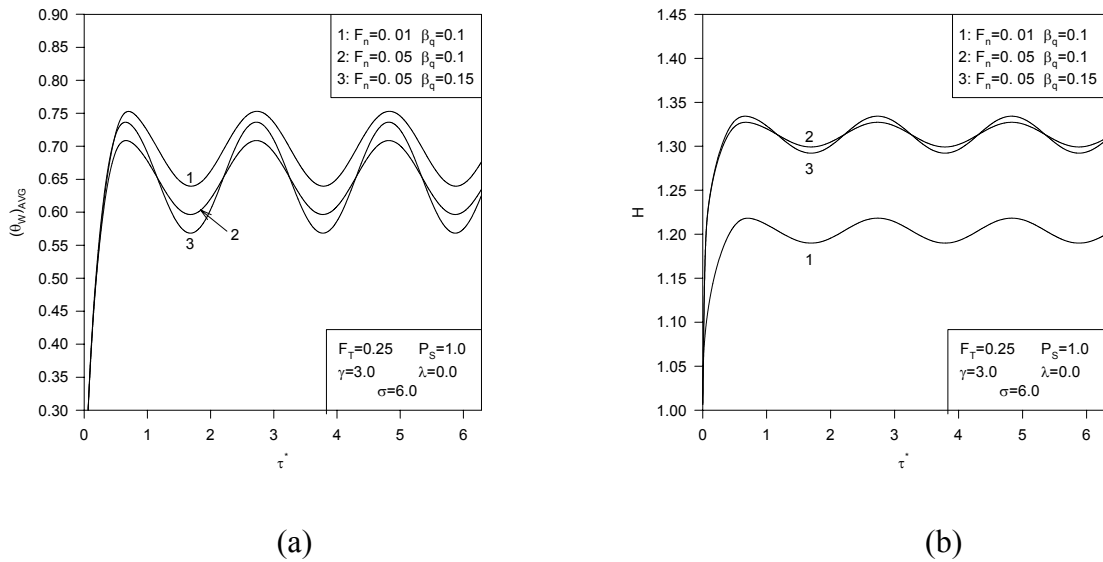


Figure 12.6: Effects of the fixation parameter  $F_n$  and the dimensionless thermal load amplitude  $\beta_q$  on (a) dimensionless average lower plate temperature  $(\theta_w)_{AVG}$ , and (b) dimensionless thin film thickness  $H$

### 12.3.5 Effects of Coefficient of Thermal Expansion on Average Pressure

Figure 12.7 shows the effects of  $F_T$  on the average dimensionless pressure inside a thin film supported by a flexible complex seal. The periodic behavior of the heat flux results in a periodic variation in the average pressure inside the thin film. The fluctuation in the pressure increases as  $F_T$  increases as seen in Figure 12.7. Further, it is noticed that the thermal load exceeding the internal pressure by a phase shift approximately equal to  $\pi/(2\gamma)$ . According to Figure 12.7, the induced pressure pulsation can be used as a

measurable quantity in order to read, diagnose or for feedback to control the heating source.

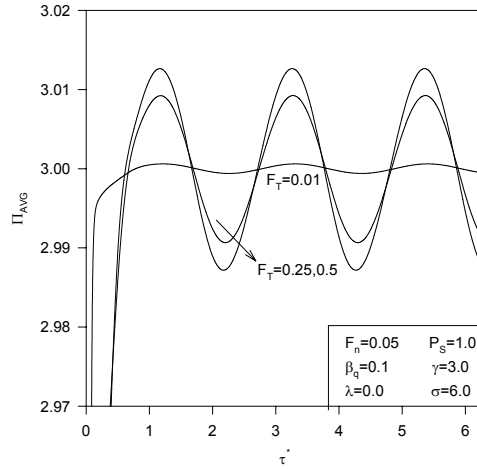


Figure 12.7: Effects of the dimensionless thermal expansion parameter  $F_T$  on the average dimensionless pressure inside the thin film  $\Pi_{AVG}$

## CHAPTER 13

### CONCLUSIONS

The flow and heat transfer inside incompressible thin films have been considered in this work in the presence of pressure squeezing of the plates. Although flow inside thin films have been studied in the past, the heat transfer characteristics of thin films having a boundary moving under oscillatory motion have not been studied. The proper energy equation and its limiting cases were obtained. Energy and momentum equations have been non-dimensionalized and properly set to model two regimes: low and large flow Reynolds number models. Special cases for the squeezed problem have been solved analytically and numerically and excellent agreement was found between both results. It was found that the oscillating dynamic behavior of the thin film also results in a corresponding oscillatory thermal behavior.

It was found that heat transfer increases by an increase in the thermal squeezing parameter, presence of suspended ultrafine particles in the fluid and the perturbation parameter of the thin film, while it decreases as both the Eckert number and amplitude motion parameter are increased for viscous fluids.

Flow instabilities and flow separation were found to occur at lower squeezing Reynolds number for divergent thin films in contrast to convergent thin films. However, wall shear stress and the fluctuation in the axial and normal velocities were found to be

greater for convergent thin films as compared to divergent thin films especially at higher squeezing numbers. Further, Nusselt numbers and their amplitudes were found to decrease when the dimensionless slope of the upper plate was increased. Convergent thin films were found to be thermally more stable as lubricating thin films, for microchannels or fluidic cells of chemical or biological nano-sensors.

In the presence of a magnetic field normal to the flow, flow instabilities were found to decrease as the Hartmann number increases. The Nusselt number was found to be affected by variations in the squeezing Reynolds number and also the Nusselt number was found to increase as the Hartmann number increases for similar inlet flow conditions. In the presence of internal pressure pulsations, the disturbance level at the upper plate was found to increase by an increase in both the Fixation parameter of the supporting seal and the frequency of the internal pressure pulsations. However, an increase in the squeezing number decreases the disturbance level at the upper plate. The fluid temperatures and the corresponding fluctuations were found to decrease when the Fixation parameter and the thermal squeezing parameter were increased for both CWT and UHF conditions. Also, fluctuations in the heat transfer and the fluid temperatures are more pronounced at relatively lower frequencies of internal pressure pulsations.

For flow inside thin films induced by both natural convection and boundary squeezing effects as in vertical channel with one open-end from the top, oscillatory vibration at one wall may result in a separated cell inside the vertical channel at low Grashof numbers. Mean values for average Nusselt numbers at the vibrated wall were found to be mainly affected by the Grashof number and the amplitude of horizontal vibrations. The amplitude of Nusselt numbers was found to increase with an increase in

the amplitude of vibrations. However, it decreases at the vibrated wall with an increase in the Grashof number.

In the presence of lateral flow leakage and wall slip conditions inside thin films supported by soft seals, flow fluctuations within a fluidic cell increase with an increase in the fixation parameter, the leakage rate and the wall slip condition while it decreases as the squeezing number and the power index  $n$  of the fluid increase. Slip velocity was found to increase as the power index  $n$  decreases. The cooling was enhanced by an increase in the fixation parameter and leakage rate. Moreover, hydromagnetic effects and suction wall velocity effects were found to enhance heat and mass transfer over a surface under squeezed conditions

Enhancements in the cooling can be achieved when the supporting seals contain voids of fluids having large coefficient of thermal expansion, these enhancements were found to increase by an increase in the coefficient of thermal expansion, dispersion parameter, fixation parameter and the thermal squeezing parameter. Finally, the thermal dispersion parameter was found to increase the stability of the thin film by reducing the fluctuation rate at the moving plate.

## LIST OF REFERENCES

- Adams, T. M., Ghiaasiaan, S. M. and Abdel-Khalik, S. I., Enhancement of Liquid Forced Convection Heat Transfer Microchannels due to the Release of Dissolved Noncondensables, *Int. J. Heat & Mass Transfer*, vol. 42, pp. 3563-3573, 1999.
- Barozzi, G. S. and Corticelli, M. A., Natural Convection in Cavities Containing Internal Sources, *Heat and Mass Transfer*, vol. 36, pp. 473-480, 2000.
- Bessaih, R. and Kadja, M., Turbulent natural convection cooling of electronic components mounted on a vertical channel, *Applied Thermal Engineering*, vol. 20, pp. 141-154, 2000.
- Bhattacharyya, S. and Pal, A., Unsteady MHD Squeezing Flow between Two Rotating Discs, *Mechanics Research Communications*, vol. 24, pp. 615-623, 1997.
- Bhattacharyya, S., Pal, A., and Nath, G., Unsteady Flow and Heat Transfer between Rotating Coaxial Disks, *Numerical Heat Transfer, Part A*, vol. 30, pp. 519-532, 1996.
- Blottner, F. G., Finite-Difference Methods of Solution of the Boundary-Layer Equations, *AIAA Journal*, vol. 8, pp. 193-205, 1970.
- Boresi, A. P., Sidebottom, O. M., Seely, A. B., and Smith J. O., *Advanced Mechanics of Materials*. Wiley, New York, 1978.
- Brown, J. W. and Churchill, R. V., *Complex Variables and Applications*, Sixth ed., McGraw-Hill, New York, 1996.
- Chamkha, A. J., Unsteady Laminar Hydromagnetic Flow and Heat Transfer in Porous Channels with Temperature-dependent Properties, *International Journal of Numerical Methods for Heat & Fluid Flow*, vol. 11, pp. 430-448, 2001.
- Dalal, D. C., Datta, N. and Mukherjea, S. K., Unsteady Natural Convection of a Dusty Fluid in an Infinite Rectangular Channel, *International Journal of Heat and Mass Transfer*, vol. 41, pp. 547-562, 1998.
- Derek, C., Tretheway, D. C. and Meinhart, C. D., Apparent fluid slip at hydrophobic microchannel walls, *Physics of Fluids*, vol. 14, L9-L12, 2002.

Dyko, M. P., Vafai, K. and Mojtabi, A. K., Numerical and Experimental Investigation of Stability of Natural Convective Flows Within a Horizontal Annulus, *Journal of Fluid Mechanics*, vol. 381, pp. 27-61, 1999.

Dyko, M. P., and Vafai, K., On the Presence of Odd Transverse Convection Rolls in Narrow-Gap Horizontal Annuli, *Physics of Fluids*, vol. 14, pp. 1291-1294, 2002.

Eastman, J. A., Choi, S. U. S., Li, S., Yu, W. and Thompson, L. J., Anomalously Increased Effective Thermal Conductivities of Ethylene Glycol-based Nanofluids Containing Copper Nanoparticles, *Applied Physics Letters*, vol. 78, pp. 718-720, 2001.

Eckmann, D. M., Bowers, S., Stecker, M. and Cheung, A. T., Hematocrit, Volume Expander, Temperature, and Shear Rate Effects on Blood viscosity, *Anesth. Analg.*, vol. 91, pp. 539-545, 2000.

Erdogan M. E., A note on unsteady flow of a viscous fluid due to an oscillating plane wall, *Int. J. of Non-Linear Mech.*, vol. 35, pp. 1-6, 2000.

Ettefaqh, J., Vafai, K. and Kim, S. J., Non-Darcian Effects in Open-Ended Cavities filled with a Porous Medium, *Journal of Heat Transfer.*, vol. 113, pp. 747-756, 1991.

Friis, E. A., Lakes, R. S., and Park, J. B., "Negative Poisson's Ratio Polymeric and Metallic Materials", *Journal of Materials Science*, vol. 23, pp. 4406-4414, 1988.

Fedorov, A. G. and Viskanta, R., Three-dimensional conjugate heat transfer in the microchannel heat sink for electronic packaging, *International Journal of Heat and Mass Transfer*, vol 43, pp. 399-415, 2000.

Fritz, J., Baller, M. K., Lang, H. P., Rothuizen, H., Vettiger, P., Meyer, E., Güntherodt, H. -J., Gerber, Ch. and Gimzewski, J. K., Translating Biomolecular Recognition into Nanomechanics, *Science*, vol 288, pp. 316-318, 2001.

Fu, W. S. and Shieh, W. J., Transient Thermal-Convection in an Enclosure Induced Simultaneously by Gravity and Vibration, *International Journal of Heat and Mass Transfer*, vol. 36, pp. 437-452, 1993.

Gross, W. A., Matsch, L. A., Castelli, V., Eshel, A., Vohr, J. H. and Wildmann, M., *Fluid Film Lubrication*, pp. 427-461, Wiley, New York, 1980.

Hall, D. A., Vliet, G. C., Bergman, T. L., Natural Convection Cooling of Vertical Rectangular Channels in Air Considering Radiation and Wall Conduction, *Transactions of the ASME. Journal of Electronic Packaging*, vol. 121, pp. 75-84, 1999.

Hamza, E. A., Unsteady Flow between Two Disks with Heat Transfer in the Presence of a Magnetic Field, *J. Phys. D: Appl. Phys.*, vol. 25, pp. 1425-1431, 1992.

Hoffmann, K. A., and Chiang, S. T., Computational Fluid Dynamics: Volume I, pp. 337-352, Third Edition, Wichita, Kansas: Engineering Education System, 1998.

Huang, P. C., and Vafai, K., Flow and Heat transfer Control using a Porous Block Array Arrangement, International Journal of Heat and Mass Transfer, vol. 36, pp. 4019-4062, 1993.

Huang, P. C., and Vafai, K., Analysis of Forced Convection Enhancements in a Channel Using Porous Blocks, AIAA Journal of Thermophysics and Heat Transfer, vol. 8, pp. 563-573, 1994.

Jha B. K., Natural Convection in Unsteady MHD Couette Flow, Heat & Mass Transfer, vol. 37, pp. 329-331, 2001.

Khaled, A. –R. A. and Vafai, K., Non-Isothermal Characterization of Thin Film Oscillating Bearings, Numerical Heat Transfer: Part A, vol. 41, pp. 451-467, 2002.

Kuan-Tzong, L., Laminar Natural Convection Heat and Mass Transfer in Vertical Rectangular Duct, International Journal of Heat and Mass Transfer, vol. 42, pp. 4523-4534, 1999.

Kwak, H. S., Kuwahara, K. and Hyun, J. M., Resonant Enhancement of Natural Convection Heat Transfer in a Square Enclosure, International Journal of Heat and Mass Transfer, vol. 41, pp. 2837-2846, 1998.

Langlois, W. E., Isothermal Squeeze Films, Quarterly of Applied Math., vol. XX, pp. 131-150, 1962.

Lavrik, N. V., Tipple, C. A., Sepaniak, M. J., and Datskos, D., Gold Nano-Structure for Transduction of Biomolecular Interactions into Micrometer Scale Movements, Biomedical Microdevices, vol 3:1, pp. 35-44, 2001.

Lee, D.Y., and Vafai, K., Analytical Characterization and Conceptual Assessment of Solid and Fluid Temperature Differentials in Porous Media, International Journal of Heat and Mass Transfer, vol. 42, pp. 423-435, 1999.

Li, Q. and Xuan, Y., Convective Heat Transfer and Flow Characteristics of Cu-water Nanofluid, Science in China (Series E), vol. 45, pp. 408-416, 2002.

Marques W. Jr., Kremer G. M. and Sharipov, F. M., Couette flow with slip and jump boundary conditions, Continuum Mechanics and Thermodynamics, vol. 12, pp. 379-386, 2000.

- Moon, S. H., Yun, H. G., Hwang, G. and Choy, T. G., Investigation of packaged miniature heat pipe for notebook PC cooling, *International Journal of Microcircuits and Electronic Packaging*, vol 23, pp.488-93, 2000.
- Morrone, B., Natural Convection between Parallel Plates with Conjugate Conductive Effects, *Numerical Heat Transfer, Part A-Applications*, vol. 40, pp. 873-886, 2001
- Navier, C.L. M. H. *Mem. Acad. Sci. Inst. France*, vol. 1, pp. 414-416, 1823.
- Norton, R. L., *Machine Design; An Integrated Approach*, Prentice-Hall, New Jersey, 1998.
- Paul, T., Singh, A. K. and Thorpe, G. R., Transient Natural Convection in a Vertical Channel Partially Filled with a Porous Medium, *Mathematical Engineering in Industry*, vol. 7, pp. 441-455, 1999.
- Radakovic, D. J. and Khonsari, M. M., Heat transfer in a Thin-Film Flow in the Presence of Squeeze and Shear Thinning: Application to Piston Rings, *J. of Heat Transfer*, vol. 119, pp. 249-257, 1997.
- Raiteri, R., Butt, H. -J. and Grattarola, M., Changes in Surface Stress at the Liquid/Solid Interface Measured with a Microcantilever, *Electrochimica Acta*, 46, 157-163, 2000.
- Reynolds, O., On the Theory of Lubrication and its Application to Mr. Beauchamp Tower's Experiments, Including an Experimental Determination of the Viscosity of Olive Oil, *Philos. Trans. R. Soc. Lond.*, vol. 177, pp. 157-237, 1886.
- Saundres, D. K. and Patel, K. H., Comparison between Blood Viscosity in Red-Eared Sliders (*Trachemys Scripta*) Adapted to Cold and Room Temperature, *The Journal of Experimental Zoology*, vol. 28, pp. 157-163, 1998.
- Schlichting H., *Boundary Layer Theory*, Sixth ed., McGraw-Hill, New York, 1968.
- Sezai, I. and Mohammad, A. A., Natural Convection in a Rectangular Cavity Heated from Below and Cooled from Top as well as the Side Walls, *Physics of Fluid*, vol. 12, pp. 432-443, 2000.
- Sezri, A. Z., *Tribology*, Hemisphere, pp. 10-12, New York, 1980.
- Shiping Y. and Ameel, T. A., Slip-flow Heat Transfer in Rectangular Microchannels, *Int. J. Heat Mass Transfer*, vol. 44, pp. 4225-4234.
- Soltani, F. and Yilmazer, U., Slip Velocity and Slip Layer Thickness in Flow of Concentrated Suspensions, *Journal of Applied Polymer Science*, vol. 70, pp. 515-522, 1998.

Tashtoush, B., Tahat, M. and Probert, D., Heat Transfers and Radial Flows Via a Viscous Fluid squeezed between Two Parallel Disks, *Applied Energy*, vol. 68, pp. 275-288, 2001.

Tretheway, D. C. and Meinhart, C. D., Apparent fluid slip at hydrophobic microchannel walls, *Physics of Fluids*, vol. 14, L9-L12, 2002.

Wang, X., Zhu, K., and Wen, S., Thermodynamic Analysis of Journal Bearings Lubricated with Couple Stress Fluids, *Tribology International*, vol. 34, pp. 335-343, 2001.

Wasp, F. J., *Solid-Liquid Slurry Pipe Line Transportation*, Trans. Tech, Berlin, 1977.  
Xuan, Y. and Li, Q., Heat Transfer Enhancement of Nanofluids, *Int. J. of Heat and Fluid Flow*, vol. 21, pp. 58-64, 2000.

Watanabe, K. and Udagawa, H., Drag Reduction of non-Newtonian Fluid in a circular pipe with a highly-water repellent wall, *AIChE Journal*, vol. 47, pp. 256-262, 2001.

Xuan, Y. and Roetzel, W., Conceptions for Heat Transfer Correlation of Nanofluids, *Int. J. Heat and Mass Transfer*, vol. 43, pp. 3701-3707, 2000.

Zamora, B. and Hernandez, J., Influence of Variable Property Effects on Natural Convection Flows in Asymmetrically-heated Vertical Channels, *International Communications in Heat and Mass Transfer*, vol. 24, pp. 1153-1162, 1997.